China Geology 6 (2023) 100−136

China Geology

Journal homepage: http://chinageology.cgs.cn
https://www.sciencedirect.com/journal/china-geology

Geology and mineralization of the Duobaoshan supergiant porphyry Cu-Au-Mo-Ag deposit (2.36 Mt) in Heilongjiang Province, China: A review

Sen Zhang[a], Nan Ju[b,*], Guo-bin Zhang[c], Yuan-dong Zhao[d], Yun-sheng Ren[e, f], Bao-shan Liu[b], Hui Wang[g], Rong-rong Guo[h], Qun Yang[f], Zhen-ming Sun[i], Feng-ming Xu[b], Ke-yong Wang[f], Yu-jie Hao[f]

[a] *Cores and Samples Centre of Natural Resources, China Geological Survey, Ministry of Natural Resources, Langfang* 065200, *China*
[b] *Shenyang Center, China Geological Survey, Ministry of Natural Resources (Northeast Geological S&T Innovation Center), Shenyang* 110034, *China*
[c] *Mining College, Liaoning Technical University, Fuxin* 123000, *China*
[d] *Mudanjiang Natural Resources Survey Center, China Geological Survey, Ministry of Natural Resources, Mudanjiang* 157021, *China*
[e] *Institute of Disaster Prevention, Langfang* 065200, *China*
[f] *College of Earth Sciences, Jilin University, Changchun* 130000, *China*
[g] *School of Earth Science and Resources, Chang'an University, Xi'an* 710000, *China*
[h] *School of Resources and Civil Engineering, Northeastern University, Shenyang* 110031, *China*
[i] *School of Prospecting & Surveying Engineering, Changchun Institute of Technology, Changchun* 130000, *China*

ARTICLE INFO

Article history:
Received 5 December 2022
Received in revised form 9 January 2023
Accepted 16 January 2023
Available online 18 January 2023

Keywords:
Cu-Au-Mo-Ag deposit
Porphyry
Mineralization
Mineralization model
Mineral exploration engineering
Prospecting modle
Duobaoshan
Heilongjiang
China

ABSTRACT

The reserves of the Duobaoshan porphyry Cu-Au-Mo-Ag deposit (also referred to as the Duobaoshan porphyry Cu deposit) ranks first among the copper deposits in China and 33rd among the porphyry copper deposits in the world. It has proven resources of copper (Cu), molybdenum (Mo), gold (Au), and silver (Ag) of 2.28×10^6 t, 80×10^3 t, 73 t, and 1046 t, respectively. The major characteristics of the Duobaoshan porphyry Cu deposit are as follows. It is located in a zone sandwiched by the Siberian, North China, and paleo-Pacific plates in an island arc tectonic setting and was formed by the Paleozoic mineralization and the Mesozoic mineralization induced by superposition and transformation. The metallogenic porphyries are the Middle Hercynian granodiorite porphyries. The alterations of surrounding rocks are distributed in a ring form. With silicified porphyries at the center, the alteration zones of K-feldspar, biotite, sericite, and propylite occur from inside to outside. This deposit is composed of 215 ore bodies (including 14 major ore bodies) in four mineralized zones. Ore body No. X in the No. 3 mineralized zone has the largest resource reserves, accounting for more than 78% of the total reserves of the deposit. Major ore components include Cu, Mo, Au, Ag, Se, and Ga, which have an average content of 0.46%, 0.015%, 0.16 g/t, 1.22 g/t, 0.0003%, and 0.001%–0.003%, respectively. The ore minerals of this deposit primarily include pyrite, chalcopyrite, bornite, and molybdenite, followed by magnetite, hematite, rutile, gelenite, and sphalerite. The ore-forming fluids of this deposit were magmatic water in the early metallogenic stage and then the mixture of meteoric water and magmatic water at the late metallogenic stage. The ore-forming fluids experienced three stages. The ore-forming fluids of stage I had a hydrochemical type of H_2O-CO_2-NaCl, an ore-forming temperature of 375–650°C, and ore-forming pressure of 110–160 MPa. The ore-forming fluids of stage II had a hydrochemical type of H_2O-CO_2-NaCl, an ore-forming temperature of 310–350°C, and ore-forming pressure of 58–80 MPa. The ore-forming fluids of stage III had a hydrochemical type of NaCl-H_2O, an ore-forming temperature of 210–290°C, and ore-forming pressure of 5–12 MPa. The Cu-Au-Mo-Ag mineralization mainly occurred at stages I and II, with the ore-forming materials having a mixed crust-mantle source. The Duobaoshan porphyry Cu deposit was formed in the initial subduction environment of the Paleo-Asian Ocean Plate during the Early Ordovician. Then, due to the closure of the Mongol-Okhotsk Ocean and the subduction and compression of the Paleo-Pacific Ocean, a composite orogenic metallogenic model of the deposit was formed. In other words, it is a porphyry - epithermal copper-gold polymetallic mineralization system of composite orogeny consisting of Paleozoic island arcs and Mesozoic orogeny and extension.

First author: *E-mail address*: zhangsen556@163.com (Sen Zhang).

* Corresponding author: *E-mail address*: junan-cgs@qq.com (Nan Ju).

Literary editor: Li-qiong Jia
doi:10.31035/cg2023006
2096-5192/© 2023 China Geology Editorial Office.

1. Introduction

The Duobaoshan porphyry Cu deposit is located in the superposed area of the Paleo-Asian Ocean and the Paleo-Pacific Ocean. This area experienced long-term complex tectonic evolution and frequent tectonic and magmatic processes. The multi-stage magmatic processes and numerous faults and folds created favorable metallogenic conditions for the formation of deposits. The Duobaoshan porphyry Cu deposit was discovered by the geological survey team of the Xiao Hinggan Mountains, Heilongjiang in 1958 and experienced two stages of exploration. In the first stage (1958–1962), the geological survey team submitted the first geological exploration report in 1962. The report stated that the gold-bearing Duobaoshan porphyry copper deposit contained 0.2×10^6 t of Cu and 13×10^3 t of Mo and that the Tongshan porphyry copper deposit existed about 3.5 km southeast of the Duobaoshan deposit. In the second stage (1972–1983), through further exploration, the No. 4 geological team of Heilongjiang Province finally revealed that the Cu and Mo reserves in the Duobaoshan deposit increased from 0.2×10^6 t to 2.37×10^6 t and from 13×10^3 t to 79.991×10^3 t, respectively. Moreover, they newly determined 73.4 t of associated Au and more than 1000 t of Ag in the Duobaoshan porphyry Cu deposit and found that the Duobaoshan porphyry Cu deposit also hosts Re, Se, PGE, and other associated beneficial components. The explorations mentioned above roughly determined the occurrence state of the ore bodies and the Cu resources. At present, the Duobaoshan mining area has proven resources of Cu, Mo, Au, and Ag of 2.28×10^6 t, 80×10^3 t, 73 t, and 1046 t, respectively. In terms of resource reserves, this deposit ranks first among the copper deposits in China and 33rd among the porphyry copper deposits in the world (Du Q et al., 1988; Bai LA, 2013; Hu XL et al., 2017; Liu J et al., 2017; Li ZT et al., 2008; Deng K et al., 2018; Gao RZ et al., 2017; Song GX et al., 2019, 2015).

Since 1958, many studies have been carried out on the Duobaoshan porphyry Cu deposit, achieving fruitful results. Significant progress has been made in geological characteristics (Du Q et al., 1988; Tan CY et al., 2010; Zeng QD et al., 2014), geochronology (Ge WC et al., 2007; Cui G et al., 2008; Xiang AP et al., 2012; She HQ et al., 2012; Zhao HL et al., 2012; Bai LA, 2013; Zeng QD et al., 2014; Wu G et al., 2015; Liu J et al., 2012, 2017; Hao YJ et al., 2014, 2015, 2016, 2017; Che HW et al., 2015; Song GX et al., 2015; Li Y et al., 2016a, 2016b; Gao RZ et al., 2017; Zhao C et al., 2018, 2019a, 2019b; Deng K et al., 2018; Wang L et al., 2018; Chu XL et al., 2019), geochemistry (Zhao YY et al., 1997) and deposit genesis (Wu G et al., 2009; Chu SX et al., 2012; Wei H et al., 2014; Liu J et al., 2010, 2012). However, the genesis of the Duobaoshan porphyry Cu deposit is still controversial: (1) Du Q et al. (1988) and Zhao YY and Zhao GJ (1995) put forward the metallogenic model of pumping and drainage and the metallogenic model of n+1 activities of porphyry fluids, respectively. (2) Hao YJ et al. (2016), Liu J et al. (2012), Zeng QD et al. (2014), Du Q et al. 1988, She HQ et al. (2012), Yu JJ et al. (1996), and Zhao YY and Zhao GJ (1995) believed that the Duobaoshan porphyry Cu deposit was formed in a subduction-related volcanic arc environment. (3) Ge W et al. (2007a), Hu XL et al. (2017), and Wu G et al. (2015) believed that the formation of the Duobaoshan porphyry Cu deposit is related to the collision between the Eerguna and the Xing'an blocks. (4) Bai LA (2013), Bai LA et al. (2012), and Yin BC and Ran QC (1997) believed that the Duobaoshan porphyry Cu deposit was formed in the tectonic setting of the collision between the Eerguna-Xing'an and Songnen blocks.

In 2017, the Shenyang Center, China Geological Survey led the implementation of the key R&D program of the Ministry of Science and Technology entitled the "Three-Dimensional Geological Structures and Ore Body Positioning of Typical Ore Concentration Areas", obtaining the following results. (1) It reconstructed the Paleozoic trench-arc-basin system of the Duobaoshan area and proposed the metallogenic mechanisms of Paleozoic mineralization - Mesozoic mineralization induced by superposition and transformation of the Duobaoshan porphyry Cu deposit; (2) it established a composite orogenic metallogenic model of the deposit, i.e., a porphyry-epithermal copper-gold polymetallic mineralization system of composite orogeny consisting of Paleozoic island arcs and Mesozoic orogeny-extension; (3) it built a three-dimensional geological structure model, depicted the geological structures and ore-bearing geological bodies of the mining area, and accurately described the listric spatial distribution of the Tongshan Fault, which destroys and transforms the Tongshan deposit; (4) it presented clear geological structure and ore-bearing geological bodies at a depth of 3000 m and less, built prospecting and prediction models, and delineated four deep prospecting targets; (5) it verified the predicted target No. IV in the Duobaoshan mining area from the deep part. As a result, large thick Cu-Mo ore bodies were discovered through single-well drilling, and they have an ore-penetrating thickness of 521.59 m and a highest Cu grade of 4.328%. It is estimated that the newly discovered Cu-Mo ore bodies have 1.98×10^6 t of Cu reserves, making a breakthrough in deep prospecting. The Tongshan copper deposit is expected to have a supergiant scale. This study will guide the further understanding of the metallogenic rule and genetic mechanism of porphyry Cu-Au-Mo-Ag deposits and guide the prospecting and exploration of the deep and edge parts of these deposits.

2. Regional geological setting

The Duobaoshan porphyry Cu deposit is located in the north of Nenjiang County, Heilongjiang Province, China. In terms of geotectonic position, it lies in the superposed area of the Xingmeng Orogenic Belt and the circum-Western Pacific active continental margin tectonic belt (Fig. 1). During the Paleozoic, the evolution and subduction of the Paleo-Asian Ocean caused frequent collisions among the Eerguna, Xing'an, Songnen, and Jiamusi blocks, resulting in multi-stage

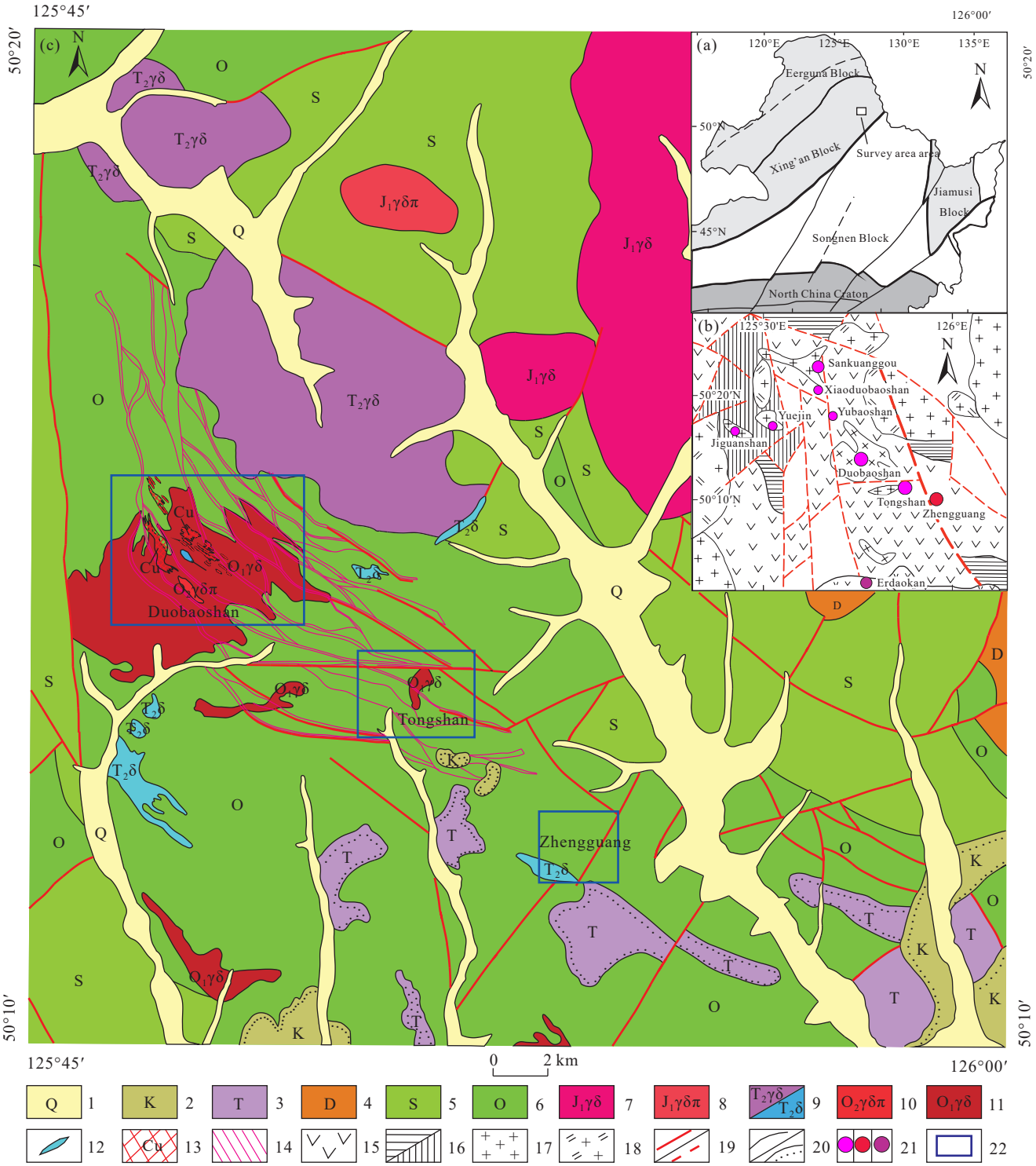

Fig. 1. Geotectonic location map of the study area (a, b) and the regional geological map of the Duobaoshan area (c; modified from Liu J. et al., 2015). 1–Quaternary; 2–Cretaceous; 3–Triassic; 4–Devonian; 5–Silurian; 6–Ordovician; 7–Early Jurassic granodiorite; 8–Early Jurassic granodiorite porphyry; 9–Late Triassic granodiorite/diorite; 10–Middle Ordovician granodiorite porphyry; 11–Early Ordovician granodiorite; 12–diorite; 13–copper ore body; 14–ductile shear zone; 15–volcanic rock; 16–Paleozoic/Cenozoic strata; 17–granite; 18–monzogranite; 19–fault; 20–geological boundary; 21–copper/gold/silver deposit; 22–mining area.

magmatic processes in the area (Bai LA, 2013; Xu WL et al., 2013; Wei H, 2014; Cai WY, 2020; Tang WH, 2020). During the Mesozoic, the superposition of the tectonic systems of the Mongol-Okhotsk Ocean and the Paleo-Pacific Ocean brought a new round of geological environment transformation of the Duobaoshan mining area. Meanwhile, the eruption of large quantities of intermediate-acid volcanic rocks such as granitic rocks provided favorable geological conditions and material sources for the mineralization in the mining area.

In terms of regional strata (Table 1), the Paleozoic, Mesozoic, and Cenozoic strata are exposed in the study area. Among them, the Paleozoic Ordovician and Silurian strata are

Table 1. Stratigraphic division of the study area (after Wei H, 2014; Cai WY, 2020).

Chronostratigraphic unit			Lithostratigraphic unit				
Erathem	System	Series	Formation	Member	Code	Thickness /m	Lithology
Cenozoic	Quaternary	Holocene	Low floodplain sediments		Q_4^2	<10	Gravel, sandy gravel, clay, and sandy clay
			High floodplain alluvium		Q_4^1	10-20	Loam and sandy gravel
Mesozoic	Cretaceous	Lower	Ganhe Formation		K_1g	>10	Tight or amygdaloidal basalt
			Jiufengshan Formation		K_1j	>100	Hoary conglomerate, sandstone, and siltstone
			Guanghua Formation		K_1gh	>80	Rhyolite, dacite, rhyolitic-dacitic tuff
	Triassic	Lower	Bazhan Formation		T_1b	>1254	Carbonaceous siltstone and sandy slate
Late Paleozoic	Permian	Middle	Huaduoshan Formation		P_2h	>450	Andesite, silty slate, and andesitic tuff
	Carboniferous	Upper	Xinghuo Formation		C_3x	>300	Rhyolite, dacite, and tuff
	Devonian	Middle	Genlihe Formation		D_2g	127	Arkose and silty slate interbedded with tuff
			De'an Formation		D_2d	491	Sandstone, tuffaceous slate, and limestone
			Huolongmen Formation		D_2hl	63–405	Sandstone, intermediate-acid tuff, and slate interbedded with limestone lens
		Lower	Nichouhe Formation		D_1n	273	Crystalline limestone, siltstone, and argillite
Early Paleozoic	Silurian	Upper	Woduhe Formation		S_3w	216	Sandstone, siltstone, and silty slate
		Middle	Bashilixiaohe Formation		S_2b	731	Mixed sandstone, silt to fine-grained sandstone, and metamorphic siltstone
		Lower	Huanghuagou Formation		S_1h	650	Siltstone, silty slate, and metamorphic fine-grained sandstone
	Ordovician	Upper	Aihui Formation		Q_3a	>273	Sericite-chlorite slate, metamorphic siltstone, and black slate
			Luohe Formation		Q_3l	>284	Tuffaceous silt to fine-grained sandstone and metamorphic siltstone
		Middle	Duobaoshan Formation	Third member	Q_2d^3	1323	Tuffaceous silt to fine-grained sandstone
				Second member	Q_2d^2	1653	Tuff and volcanic breccia
				First member	Q_2d^1	1888	Tuffaceous sandstone and andesite
			Tongshan Formation	Third member	Q_2t^1	836	Andesitic breccia tuff
				Second member	Q_2t^2	394	Silt to fine-grained sandstone interbedded with andesitic tuff
				First member	Q_2t^1	321	Tuffaceous silt to fine-grained sandstone

the best developed, and the Ordovician Tongshan and Duobaoshan formations are most closely related to mineralization. In terms of geotectonic position, the Duobaoshan area is located in the NW-trending arcuate tectonic belt sandwiched by the NNE-trending Nenjiang Fault and the NE-trending Xinkailing Fault. This area experienced multi-stage tectonic movements during the Phanerozoic, leading to strong tectonic deformation, complex tectonic patterns, and well-developed folds, faults, and ductile shear zones in the mining area. The NW- and NE-trending structures were mainly formed by the intense tectonic movements during the Caledonian and the Hercynian, which, along with Indosinian-Yanshanian tectonic processes, formed the magma intrusion-related annular structures, such as the typical Huaduoshan structure (Li DR, 2011; Wei H, 2014).

In terms of magmatic rocks (Table 2), the Duobaoshan area features well-developed intrusions and intense magmatism. Cai WY (2020) divided the intrusion epochs in the area into Early Cambrian–Early Silurian (539–436 Ma), Late Carboniferous–Early Permian (320–292 Ma), Middle-Late Triassic (244–214 Ma), Early-Late Jurassic (177–151 Ma), and Early Cretaceous (128–127 Ma). The Early Cambrian–Early Silurian intrusions are closely related to the formation of the Duobaoshan and Tongshan deposits. In the Duobaoshan area, mafic intrusions are dominated by the peridotites (530–520 Ma) in the Yubaoshan deposit and occur as dykes; intermediate intrusions mainly include medium-grained diorite (543–533 Ma) in the Zhengguang deposit (Hao YJ, 2015), and acid intrusions mostly include the granodiorites (granodiorite porphyries) (478–474 Ma) in the Duobaoshan deposit (Ge WC et al., 2007; Cui G et al., 2008; Tang WH, 2020) and the granodiorites (478–474 Ma) in the Tongshan deposit (Hao YJ et al., 2015; Liu J et al., 2017, 2015). A few Late Carboniferous–Early Permian magmatic rocks are exposed in the Duobaoshan area. They are dominated by granodiorites (315–310 Ma) in the Jiguanshan deposit (Li Y, 2016) in the west of the mining area and exhibit intense Cu-Mo mineralization (Zhao GJ et al, 2007).

Table 2. Magma stages and magmatic rock formation sequence in the study area (after Cai WY, 2020).

Epoch	Magmatism		Age/Ma	Intrusions		Volcanic rocks
Era	Period	Stage		Lithology	Typical pluton	Lithology
Cenozoic	Himalayan		70			Basalt
Mesozoic	Yanshanian	III	137	Granite porphyry	Southwestern Jiguanshan	Basalt and andesite
				Alaskite granite	Xinsheng	
				Alaskite granite	Wushideji	
		II		Diorite porphyrite	184 km	Intermediate, intermediate-acid, and acid volcanic rocks
				Granodiorite	Dulishan	
		I	195	Granodiorite	Alongshan	
				Quartz diorite	Luohe (182 Ma)	
				Quartz diorite	Xigulanhe Dingzi	
Paleozoic	Hercynian	III		Alkaline granite	Gongbiela	Intermediate, intermediate-acid and acid volcanic rocks
				Alaskite granite	Sandaogou	
				Alaskite granite	Highland (elevation: 762.2 m)	
				Alaskite granite	Guguhe	
		II	230	Biotite granite	Yangnaiqigou	
				Biotite granite	Piergelihe	
				Granite	Erzhan	
				Plagiogranite	Quanhuhe	
				Granodiorite	Jiguanshan	
				Muscovite oligoclase granite	Highland (elevation: 568.3 m)	
				Plagiogranite	Sankuanggou	
				Plagiogranite	Wolihe	
				Plagiogranite	Wengeshan	
		I	285	Diorite	Laogongsi	
				Gabbro peridotite	Fudiyingzi	
		III		Alkaline granite	Daheishan	Intermediate, intermediate-acid, and acid volcanic rocks
				Moyite	Wangfeng	
				Granodiorite porphyry	Duobaoshan	
		II	350–400	Granodiorite	Yuejin	
				Granodiorite	Duobaoshan	
				Subandesite	East bank of the top reaches of the Luohe River	
				Plagiogranite	Lengchuan	
				Plagiogranite	Chengzhongshan	Mafic and intermediate-mafic lava
				Granite	Woduhe	
		I		Pyroxene peridotite	Erdaohezi	
				Diorite	Menluhedingzi	Intermediate, intermediate-acid, and intermediate-mafic to intermediate-acid volcanic rocks
	Caledonian		450	Subpyroxene andesite	Two banks of the Luohe River	
			500	Andesite	Two banks of the Luohe River	

Moreover, a small number of diorite porphyrites (292–286 Ma) in the Zhengguang deposit are exposed in the metallogenic belt (Song GX et al., 2015). The Middle-Late Triassic magmas are exposed in a large area in the Duobaoshan area. They are dominated by acid rocks and occur as dykes, including the diorites and granodiorites (240–236 Ma) in the Zhengguang deposit, the granodiorites (226–220 Ma) in the Tongshan deposit, and the granodiorites (240–235 Ma) in the Wolihedingzi deposit (Li Y, 2016; Hao YJ, 2015; Fan SW, 2020). Early-Late Jurassic intrusions are widely distributed in the Duobaoshan area and are mainly controlled by NW-trending fold belts in the Sankuanggou and Duobaoshan areas. They are mainly intermediate-acid and consist of the granodiorites (177–175 Ma) in the Sankuanggou deposit and those (176–171 Ma) in the Xiaoduobaoshan deposit (Fan SW, 2020). A small quantity of Early Cretaceous magmatic rocks are exposed in the Duobaoshan area and consist only of granodiorites (129–127 Ma) and andesites (128–126 Ma) (Cai WY, 2020; She HQ, 2012). Among these rocks, Hercynian granodiorites and granodiorite porphyries, and Yanshanian granodiorites are related to regional mineralization.

3. Geological characteristics of the Duobaoshan mining area

3.1. Strata

The strata in the mining area include the Middle

Ordovician Tongshan, Duobaoshan, and Niqiuhe formations, the Upper Ordovician Luohe and Aihui formations, the Lower Silurian Huanghuagou Formation, and the Middle Silurian Bashilihe Formation (Fig. 2). The most important rocks in the mining area include the volcanic-terrigenous clastics and sandy argillaceous rocks of the Tongshan and Duobaoshan formations. The Middle Ordovician Duobaoshan Formation constitutes the surrounding rocks at the top of the ore bodies in the mining area, while the middle and bottom parts of the ore bodies occur in granodiorites (Bureau of Geology and Mineral Resources of Heilongjiang Province, 1993).

3.1.1. Duobaoshan Formation

The Duobaoshan Formation is a marine volcanic rock formation and is composed mainly of intermediate volcanic rocks, interbedded with a small quantity of intermediate-acid volcanic rocks and volcanic-sedimentary rocks. It conformably overlies the third member of the Tongshan Formation. Based on rock associations, this formation can be divided into three members and seven sub-members.

The first member of the Duobaoshan Formation can be divided into three sub-members. The first sub-member has a thickness of 440 m and is distributed in the southwest of the Tongshan-Duobaoshan baseline. It consists mainly of intermediate tuffs, grayish-green andesites, tuffaceous glutenites, and siltstones. Ore bodies at the top of the No.3 mineralized zone in the Duobaoshan deposit mostly occur in andesites and tuffs of this sub-member. The second sub-member is distributed in the NW direction in the southwest of the Tongshan-Duobaoshan baseline. The lower part occurs as interbeds consisting of grayish-green intermediate tuffs and intermediate breccia tuffs. The middle part is largely composed of grayish-green intermediate tuffs and is interbedded with grayish-green porphyroclastic andesites. The upper part is composed of grayish-green - grayish-purple tuffaceous sandstones, glutenites, and argillaceous siltstones and are interbedded with crystalline limestone lenses. The third sub-member is distributed in the NW direction on both sides of the Tongshan-Duobaoshan baseline. The lower part is composed of grayish-green intermediate tuffs and a small quantity of purple-gray tuff breccias. The middle part is composed of grayish-green andesites and schistous andesites. The upper part is composed of grayish-green tuffaceous siltstones, tuffaceous fine sandstones, dark green andesites, and intermediate-acid tuff breccias and is interbedded with limestone lenses.

The second member of the Duobaoshan Formation can be divided into two sub-members. The first sub-member is primarily distributed in the NW direction on both sides of the Tongshan-Duobaoshan baseline. The lower part is composed of grayish-green intermediate tuffs. The middle part is mostly composed of gray andesites and is interbedded with a small number of tuffaceous sandstones and glutenites. The upper part is composed of grayish-green tuffaceous siltstones. The second sub-member is mainly distributed on both sides of the Tongshan-Duobaoshan baseline. It consists mainly of grayish-green intermediate-acid tuffs interbedded with thin tuff sandstones.

The third member of the Duobaoshan Formation can be divided into two sub-members. The first sub-member is mainly distributed on both sides of the Tongshan-Duobaoshan baseline. The lower part is composed mainly of hoary intermediate-acid tuffs. The middle part is composed of light-gray intermediate-acid tuff lavas. The upper part is composed of grayish-green andesites and intermediate tuffs. The second sub-member is mostly distributed on both sides of the

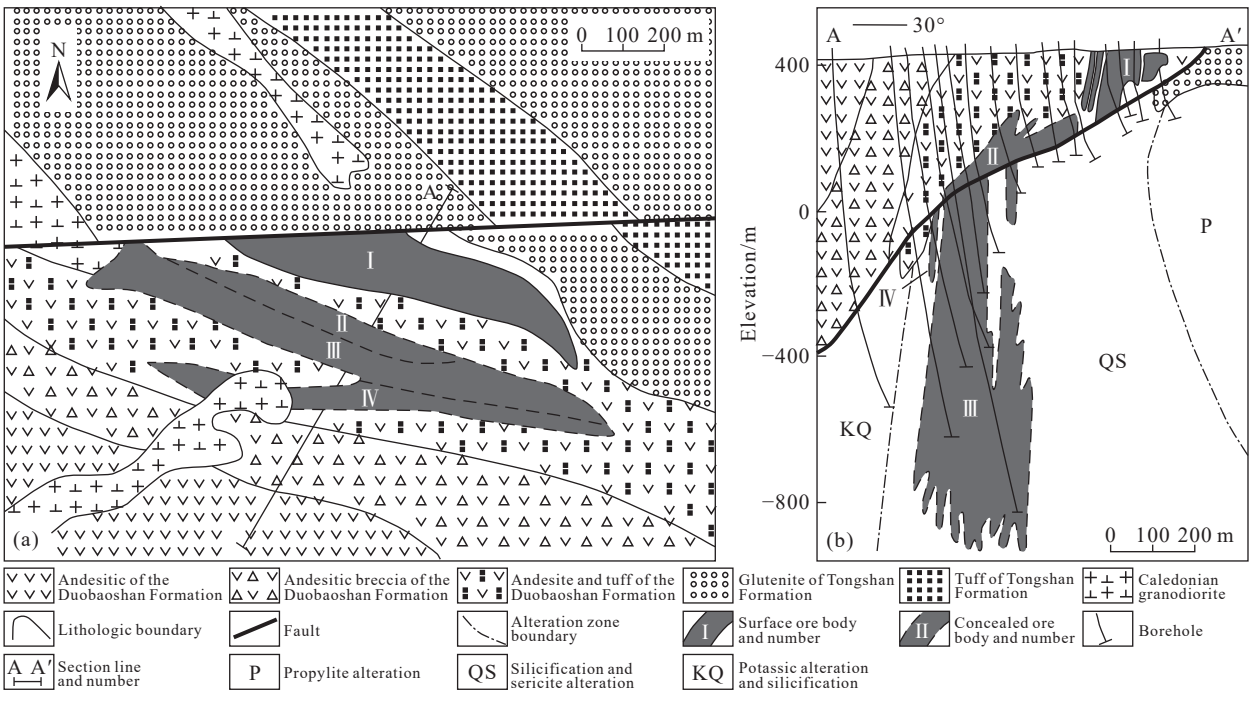

Fig. 2. Geological map (a) and an exploration line profile (b) of the Duobaoshan porphyry Cu deposit (after Wei H, 2014).

Tongshan-Duobaoshan baseline. It is composed mainly of hoary intermediate tuffs, intermediate-acid tuffs, light-gray to green dacites, andesites, hoary intermediate-acid breccia-bearing tuffs, and hoary intermediate-acid tuffs from bottom to top.

3.1.2. Tongshan Formation

Only the second and third members of the Tongshan Formation can be observed in the study area. The second member is distributed in the NW direction on the north and south sides of the Tongshan Fault. The lower part is composed of intermediate-acid tuff lavas and intermediate-acid breccia-bearing tuffs. The upper part is composed of tuffaceous siltstones and tuffaceous glutenites. The third member is distributed in the NW direction near the Tongshan Fault. The lower part is composed of intermediate-acid tuffs and andesites. The middle part consists mainly of hoary to grayish-purple tuffaceous glutenites and is interbedded with tuffaceous sandstones and crystalline limestone lenses. The upper part is mostly composed of purplish-gray to grayish-purple glutenites, arkoses, coarse sandstones, and calcareous fine sandstones.

3.1.3. Niqiuhe Formation

The Niqiuhe Formation has a thickness of about 273 m. It is mainly exposed in the Sankuanggou area and conformably overlies the Woduhe Formation. It is composed mainly of crystalline limestones, siltstones, and argillaceous slates and contains fossils of Pacificocoeliasinica brachiopods and Syringaxombohemicum tetracorallas. This formation is a set of neritic volcanic rock - sedimentary clastic rock - carbonate rock suites.

3.2. Structures

The Duobaoshan mining area mainly hosts three sets of ore-controlling structures, namely the NW-trending structure, the NW-trending arcuate tectonic belt, and the NE-NNE-trending structures, reflecting regional evolution and transformation (Figs. 2, 3). The NW-trending structure was formed during the Pre-Ordovician and remained active until the Late Hercynian, with the end of the Early Carboniferous acting as the main active stage. It occurs mainly as NW-trending folds and faults, including the Duobaoshan overturned anticlinorium. The fold structures are extremely developed and are tight steep-dipping folds of the trap type.

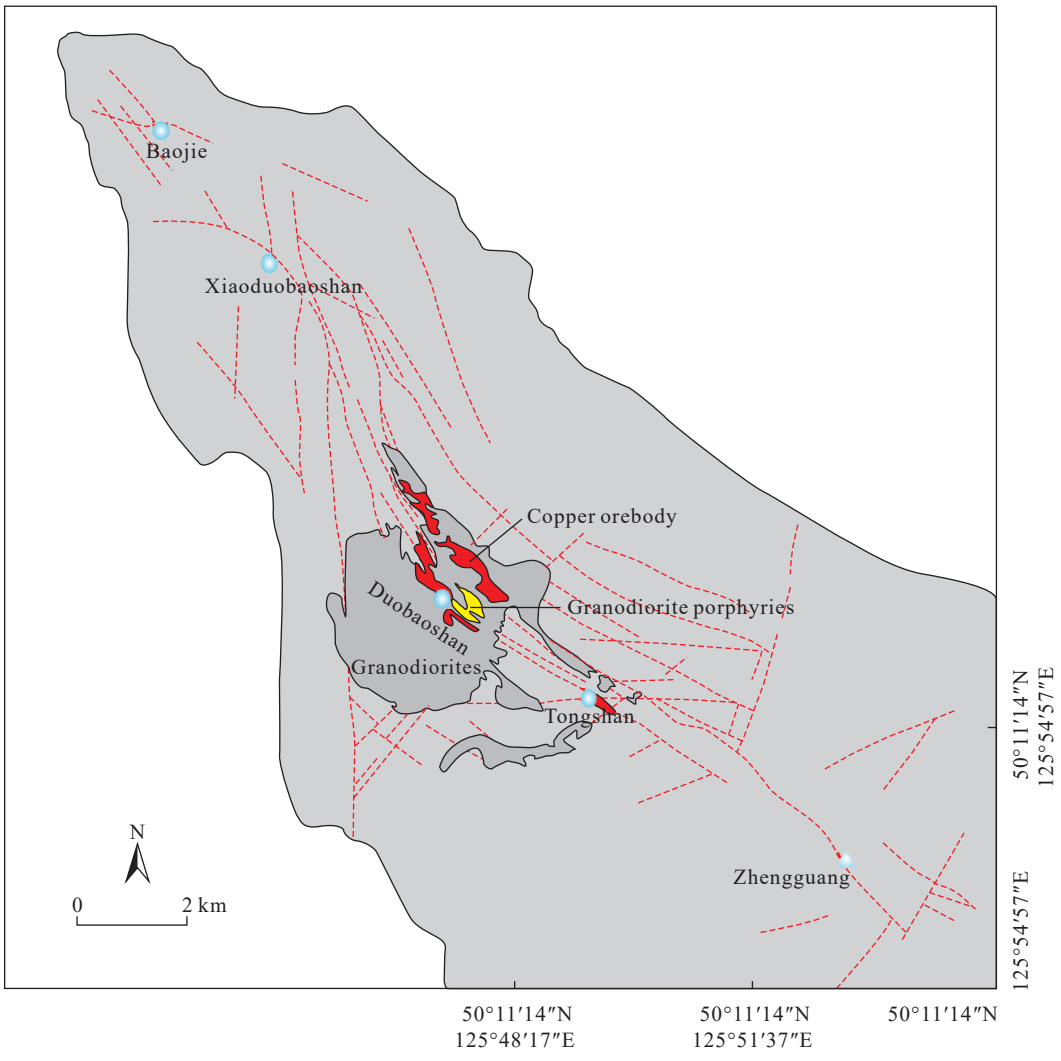

Fig. 3. Structure outline map of the Duobaoshan porphyry Cu deposit (after Zhao C, 2019).

The Duobaoshan anticlinorium hinge generally plunges northwestward. The exposed strata gradually widen from the NW direction to the SE direction. The NW-trending arcuate tectonic belt was formed from the superposition on a NW-trending tectonic belt. Specifically, the stratigraphic strike and fold axial direction in the Duobaoshan mining area shift from the NNW direction in the northwest section of the NW-trending tectonic belt into the NW-NWW direction in the southeast section of the tectonic belt, generally presenting a reversed-S-shaped arcuate structure. The major faults, NW-trending schistosity zone, porphyry plutons, alteration zones, and mineralized zones in the mining area are all distributed along the NW-trending arcuate tectonic belt. The distribution of ore bodies in the area is closely related to the NW-trending arcuate schistosity zone. The schistosity zone provides ore-transmitting and -hosting spaces for ore-forming fluids and converges northwestward. The schistosity zone controls most ore bodies, especially large and thick ones. The ore bodies in the mining area are mostly distributed in a lenticular or zonal form. Their occurrence is consistent with that of the schistosity zone, with strikes of 310°–330° and dip angles of 70°–80°. The ore bodies generally have a thickness of several to tens of meters (300 m to 400 m at most) and a depth of 400 m to 500 m (nearly 1000 m at most). However, the thick and large parts of the ore bodies mostly occur at a depth of 100–400 m, where the ore bodies are the richest and have the highest ore grades. Nevertheless, ore bodies do not occur throughout the arcuate schistosity zone, and they can be formed only in areas where strong schistosity is superposed on the copper-bearing mineralized zones. The NE-NNE-trending structures were mainly active from the Late Carboniferous to the Triassic. Despite small scales, they host widely developed small faults and joints and have the characteristics of secondary structures or late transformation. In summary, the Early Paleozoic sedimentation and magmatism formed the basic tectonic framework of the mining area, the Ordovician tectonic and magmatic processes laid a material foundation for the formation of the Duobaoshan porphyry Cu deposit, and the Caledonian and Hercynian tectonic movements provided the main metallogenic space. The NW-trending structure is a fundamental structure in the Duobaoshan ore field. It is a repeatedly active tectonic belt formed during the Early Ordovician and intersects with the regional NE-trending structure, forming huge-scale faults and fissures. The formed folds and faults of both structures are mostly long-term active deep-rooted faults or basement faults and serve as the main ore-controlling and -hosting structural systems. The formation of the Duobaoshan porphyry Cu deposit is also the result of the superposition of various favorable geological factors in the Middle Hercynian tectonic and magmatic events. The Late Yanshanian movement mainly formed EW-trending fault structures in the Duobaoshan ore field. It both destroyed and protected the Duobaoshan porphyry Cu deposit and was the dominant tectonic movement after the mineralization epoch (Du Q et al., 1988; Zhao YY et al., 1994; Wang XC et al., 2007).

In addition, the fact that the Duobaoshan porphyry Cu deposit was transformed by the Yanshanian movement reflects that the early porphyry system was transformed and destroyed by the late orogenic events. The Yanshanian movement can be divided into two stages. In the early stage, the tectonic line was in the NEE direction, and it started with the development and collapse of intracontinental orogenic belts. In the late stage, the direction of the tectonic movement shifted to the NE direction, and sinistral strike-slip motion also occurred. The Tongshan Fault, located in the south of the Duobaoshan ore field, is a transform fault formed after the mineralization epoch. It has an engineering-controlled length of more than 10 km and extends beyond the Duobaoshan mining area. It is 10 m wide (or wider) and cuts off geological bodies, ore bodies, and porphyry mineralized alteration zones in the nearly EW direction. Meanwhile, the Tongshan Fault protects the ore bodies at the footwall from denudation. The Tongshan Fault zone inclines southward, with a dip angle of 30°–40°. The tectonic breccias in the fault zone consist of tectonic angular pieces and sandy argillaceous materials, exhibiting roughly the same components as the surrounding rocks on both sides of the fault. The tectonic angular pieces are generally wrapped by graphitized coating and are lentil-shaped or lenticular mostly and tend to be rounded. They mostly show schistosity, which occurs in a certain preferred orientation, and have significant characteristics of compressive structures. The angular pieces have different sizes, which generally vary from several to tens of centimeters. The largest tectonic angular pieces, with a diameter of up to several to a dozen meters, are wrapped by loose sandy argillaceous materials of fault structures. The fractured zone of the Tongshan Fault shows the downward dragging traces of tectonic angular pieces in hanging-wall rocks, tectonic sandy argillaceous materials, and mineral debris. This finding indicates that the Tongshan Fault was a normal fault in the early stage and the hanging wall once moved downward. The Tongshan Fault zone is relatively flat and straight along the strike and shows completely different lithologies on the two walls. The hanging wall of the fault consists of Middle Ordovician rocks. Most of the ore bodies on the hanging wall are lost, with only the head of the No. 2 ore body and the tail of the No. 1 ore body remaining in the outer contact zone. The footwall consists of Middle Hercynian granodiorite plutons. The No. 3 ore body is visible in the inner contact zone, while the upper half is also lost. The traces that are not visible in the Tongshan Fault include the thermal metamorphism of surrounding rocks near the contact zones; biotite alteration, hornstone alteration, and contamination, which are common in ore bodies. Moreover, no xenoliths are visible in rocks near the contact zones. Various signs indicate that the parts with lost ore bodies have a large scale and a high mineralization level. The strike of ore bodies on the hanging wall of the Tongshan Fault is different from that of the No. 3 ore body on the footwall, and both strikes have an included angle of 30°–35°. Since the fault plane is steep in the east but gentle in the west, the Tongshan Fault is torsional. A comprehensive study of the metallogenic conditions of the Tongshan porphyry deposit, especially of the hydrothermal

alteration and the ore-controlling details of the Tongshan Fault, shows that there still exist ore bodies in the south of the Tongshan mining area, which is concealed on hanging wall of ore-bearing alteration rings. This finding provides reliable evidence for exploring supergiant porphyry copper deposits.

3.3. Intrusive rocks

The frequent tectonic movements in the Duobaoshan mining area were accompanied by multi-stage complex magmatism. The intense magmatism produced multi-stage composite plutons. Major outcrops of magmatic rocks in the Duobaoshan mining area include Hercynian and Yanshanian plutons. The Yanshanian plutons include Middle Yanshanian biotite granites, and the Hercynian plutons include Late Hercynian oligoclase granites and plagiogranites, Middle-Late Hercynian granodiorites, granodiorite porphyries, quartz diorites, and diorites (Du Q, 1980; Figs. 2, 4). Among them, the intrusions closely related to mineralization are the composite plutons composed of Middle-Late Hercynian granodiorites and granodiorite porphyries (Zhao C, 2019), which have whole-rock Rb-Sr isochron ages of 292 Ma and 283 Ma (Du Q, 1988). Regarding the granodiorites, the isotope ages of their amphiboles and biotites and their whole-rock isotope ages are 226–310 Ma (K-Ar and Rb-Sr dating; Zhao YM, 1997). A few scholars determined the U-Pb zircon age to be 480 Ma (Caledonian; Cui G et al., 2008).

Granodiorite plutons: These plutons are cyrtospirifer-shaped on the surface, extend in the NW-SE direction, and have a dip direction of SW and a dip angle of 60°. They cover an area of 9 km^2. When extending downwards to a depth of 500 m, the granodiorite plutons have an enlarged area of 16 km^2 and a triangular morphology. They have a clear contact boundary with their surrounding rocks and all show hornstone and biotite alterations to different degrees. Their major associated veins include hornblende-diorite porphyrites, finely crystalline quartz diorites, and diorite porphyrites. The granodiorite plutons show continuous changes in lithofacies, with the marginal K-feldspar decreasing in quantity and transitioning into plagiogranites.

Granodiorite porphyry plutons: These plutons are mostly exposed in the Dalazi area in the central part of the Duobaoshan porphyry Cu deposit. They intrude into the granodiorite plutons, and the granodiorites in direct contact with the granodiorite porphyry plutons are significantly fractured and have a thermal metamorphic halo with a width of 3 –10 cm, making their contact boundary jagged and complex. The porphyry plutons are exposed on a small scale

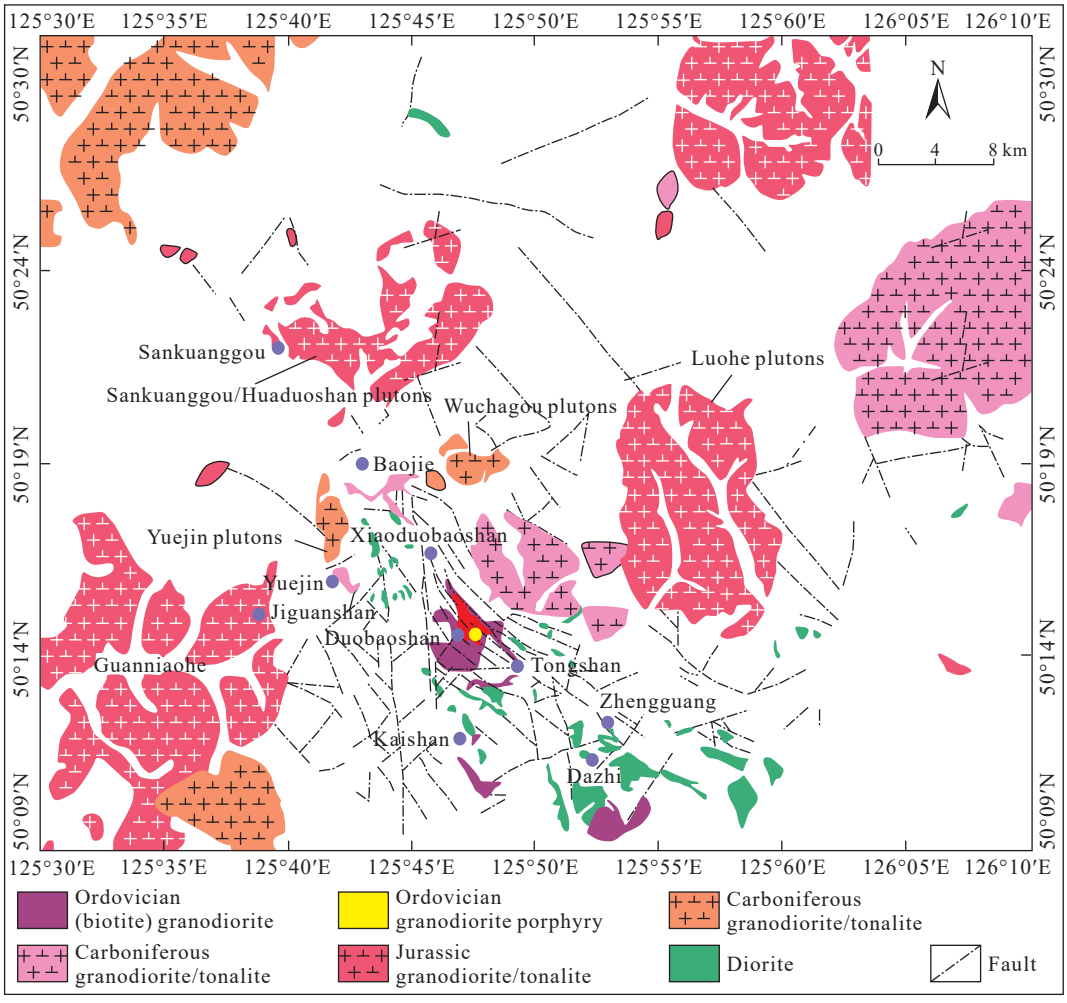

Fig. 4. Distribution map of intrusions and structures in the Duobaoshan mining area (after Cai WY, 2020).

and are mainly divided into two NW-trending lenticular plutons, which have an area of 0.08 km^2 and 0.09 km^2, respectively. The two lenticular plutons have a dip direction of SW and dip angles of 75°–80°, pitch northwestward, and significantly expand downwards, finally merging into a whole. The granodiorite porphyries are partially cut by the late-stage oligoclase granites. Their associated dykes include diorites and finely crystalline diorites. Their rocks are hoary and have porphyritic textures, their matrix has microscopic granitic textures, and their phenocrysts mainly include quartz and plagioclase ones, followed by perthite and biotite ones.

Plagiogranite plutons: They are mainly distributed in the northeast of the mining area, with some small plagiogranite plutons visible at some structural intersections in the central part of the mining area. Their surrounding rocks show significant thermal metamorphism and assimilation and contamination. Their rocks are highly crystallized and show medium-grained textures. They have a regular contact interface with the surrounding rocks and contain no xenoliths of surrounding rocks. The plagiogranite plutons have a small scale and intruded into the mining area after the mineralization of the porphyry copper deposit.

4. Alterations and mineralization

4.1. Ore body characteristics

Ore bodies in this mining area were finally formed after the superposition of multiple times of mineralization (Wang XC, 2007). The ore bodies in the Duobaoshan ore block primarily occur in the NW-trending arcuate schistosity zone. They are generally distributed in the NW direction, with Cu and Mo closely associated. The ore bodies mostly occur in lenticular and banded forms and generally have thicknesses of several meters to tens of meters and extended depths of 100 m or 200 m to 400 m or 500 m. The major ore bodies are surrounded by small banded ore bodies on both sides. Multiple ore bodies usually merge into one ore cluster, and adjacent ore clusters merge into one mineralized zone (Fig. 5). The Duobaoshan ore block is divided into four mineralized zones, among which, the No. 1 mineralized zone lies on the footwall of the porphyry plutons, and the Nos. 2, 3, and 4 mineralized zones are exposed in sequence from northwest to southeast on the hanging wall. Since the ore bodies are mainly controlled by the NW-trending transpressional tectonic belts, they mostly show an en-echelon distribution. The ore bodies generally incline southwestward, with dip angles of 65°–80°. The No. 3 mineralized zone is the dominant one and has favorable metallogenic conditions and a favorable spatial position related to porphyry plutons. This mineralized zone has a thickness of 300–400 m and an extended depth of more than 1000 m. The copper mineralization is relatively uniform and continuous, with a copper grade of generally greater than 0.3%. This mineralized zone gradually pinches out toward the northwest and southeast ends (Fig. 6). The porphyry plutons

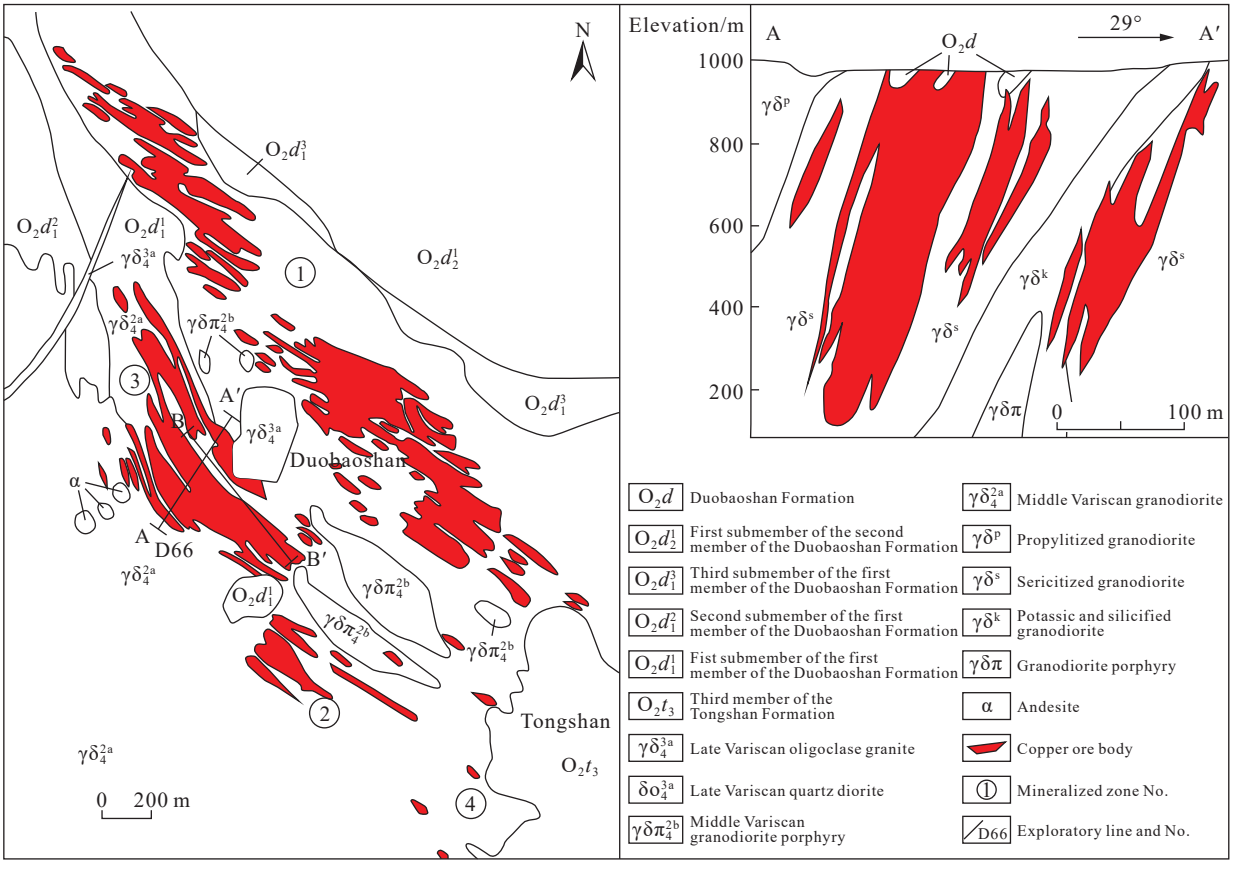

Fig. 5. Distribution map of the ore bodies in the Duobaoshan porphyry Cu deposit and the profile of exploratory line No. 66 in the No. 3 mineralized zone (after Wei H, 2014).

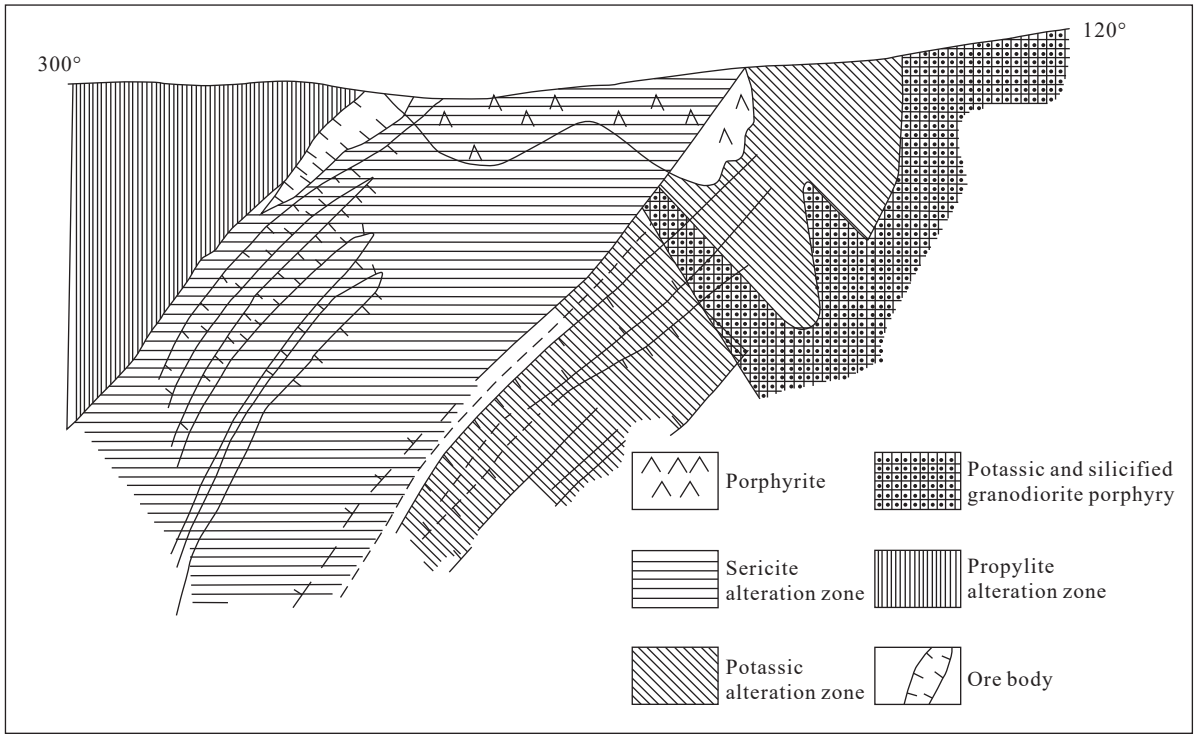

Fig. 6. Longitudinal profile of No. 3 mineralized zone of the Duobaoshan porphyry Cu deposit (after Wu JR, 2012).

tilt up at the southeastern end of the Duobaoshan porphyry Cu deposit, where nearly 1000 m -thick tuffaceous glutenites of the Tongshan Formation are distributed. Since large ore bodies are all distributed at the top of glutenites, the thick and large ore bodies in the study area are inferred to have been completely denuded (Cai WY, 2020).

Oxidation zones and mixed mineralized zones are located in the upper part of the Duobaoshan porphyry Cu deposit, and the oxidation transition zones generally have a depth of 10–35 m. It is difficult to form a secondary enrichment zone due to the north China climate. The copper mineralization related to granodiorites in the Duobaoshan ore block mainly occurs in the inner and outer contact zones between granodiorite plutons and surrounding rocks. Major ore bodies mostly occur in the outer contact zones and extend downward into the plutons. The thick and large ore blocks mostly occur near the top strata, that is, near the edges of the inner contact zones. The known ore bodies show that when the outer contact zones have a mineralization scale with a width of 200 m and a thickness of 50 m, the copper ore bodies in the lower inner contact zones are relatively enlarged and may develop into thick and large ore bodies. The porphyry copper mineralization related to granodiorite porphyry intrusion mainly occurs in the outer contact zones of the porphyry plutons, and the major ore bodies are almost all distributed in the upper part of the periphery of the granodiorite porphyry plutons. The mineralization of the hanging wall of the granodiorite porphyry plutons (southwestern wall) is superior to that of the footwall, and the mineralization of the pitching part (northwest) is superior to that of the tilted part.

In terms of spatial distribution, the ore bodies are all distributed in a ring form around the porphyry plutons. The major ore bodies are mostly distributed in the upper part around the major porphyry plutons, generally 0–500 m away from the latter. The ore bodies within a range of 50–150 m away from the porphyry plutons show the intensest mineralization, high ore grades, and uniform distribution, and their Cu mineralization gradually weakens toward both sides of the porphyry plutons. When the porphyry plutons have a burial depth of greater than 500 m, the ore bodies around the porphyry plutons tend to have a great burial depth. When the porphyry plutons have a great denudation depth, only some ore body branches with a small burial depth remain on the hanging and footwalls of the porphyry plutons. Some dykes tend to occur in the upper part of the porphyry plutons, and the mineralization alteration and mineralization around are generally weak (Fig. 7; Wang XC, 2007; Wei H, 2014; 2014; Cai WY, 2020).

4.2. Characteristics of ore minerals

The ores in the Duobaoshan porphyry Cu deposit can be roughly divided into three simple industrial types, namely the disseminated type, the veinlet-disseminated type, and the veinlet type. Primary ores constitute the main body of the deposit, and copper sulfide ore accounts for 98% of all copper ores. Major ore minerals in the deposit include chalcopyrite, pyrite, bornite, and molybdenite. They are distributed in a certain zoning pattern, with bornite, chalcopyrite, and pyrite occurring in turn from the center to the edge of ore bodies (Feng JX, 2008). Gangue minerals include quartz, plagioclase, and potassium feldspar (Fig. 8). The ores have disseminated, veinlet, and lumpy structures and hypidiomorphic crystalline-granular, metasomatic relict, and exsolution textures. The pyrite mainly has automorphic/hypidiomorphic crystalline-

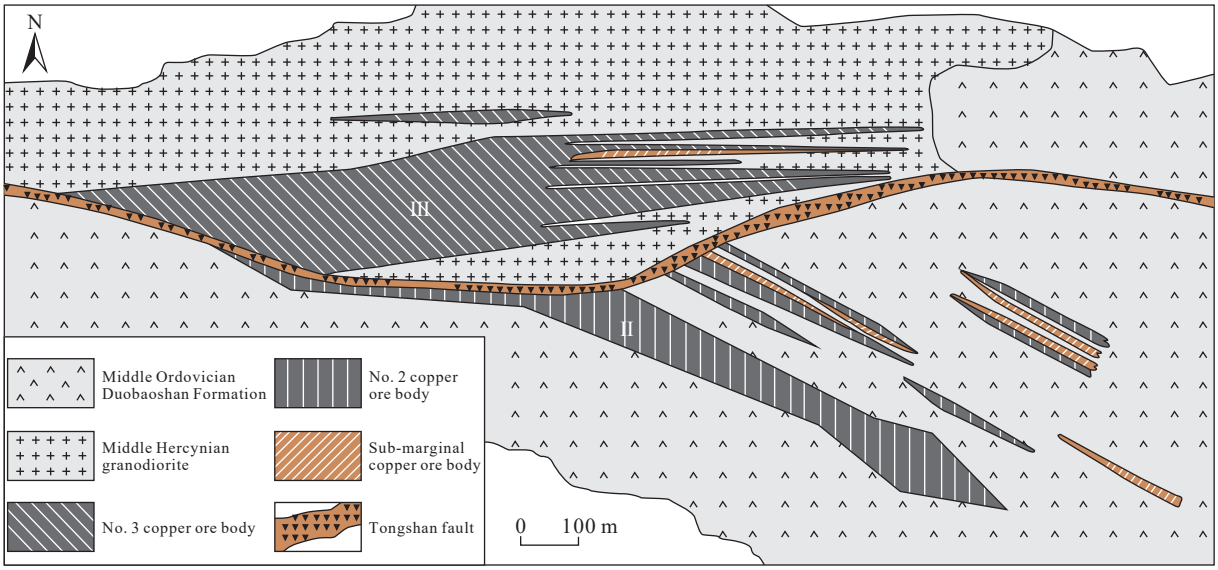

Fig. 7. Two hundred meters long horizontal section of the Duobaoshan porphyry Cu deposit (after Wei H, 2014).

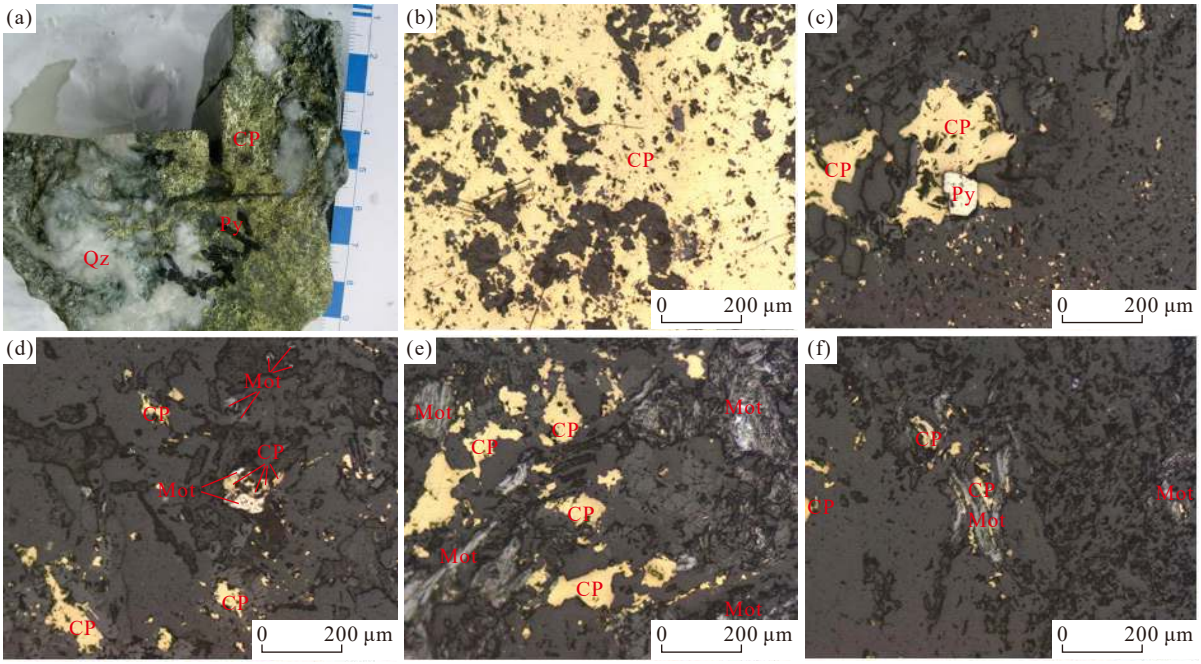

Fig. 8. Field and microscopic photomicrographs of major ore minerals. a–sulphide ore; b–photomicrograph of chalcopyrite mass; c–photomicrograph of chalcopyrite metasomatic pyrite; d–photomicrograph of disseminated chalcopyrite, local chalcopyrite metasomatic pyrite; e–photomicrograph of molybdenite associated with chalcopyrite; f–micrograph of chalcopyrite distributed around molybdenite (after Liu J. et al., 2015). Bn–bornite; Cal–calcite; Ccp–chalcopyrite; Dg–cyanite; Mot–molybdenite; Py–Pyrite; Qtz–quartz; Sp–sphalerite.

granular textures. It was metasomatized by chalcopyrite in a xenomorphic irregular form, forming xenomorphic interstitial, skeleton crystalline, metasomatic stellated, and metasomatic reticulated textures. Chalcopyrite and bornite/sphalerite generally have emulsion /graphic textures, and molybdenite has slightly curved scaly and flaky textures. The ores mainly have a (veinlet) disseminated structure, followed by veinlet, lumpy, and banded structures. In addition, brecciaous ores can be observed locally. The ores are composed mainly of Cu, Mo, Au, Ag, Se, and Ga, which have an average content of 0.46%, 0.015%, 0.16 g/t, 1.22 g/t, 0.0003%, and 0.001%–0.003%, respectively (Han ZX, 2004; Wei H, 2014; Cai WY, 2020).

Major metallic minerals are characterized as follows. (1) Chalcopyrite: It is brassy yellow and has greenish-black streaks and metallic luster visually and is bright yellow under a reflector. It tends to be paragenetic with bornite to form exsolution textures. Chalcopyritization is closely related to quartz-sericite alteration and can be mainly divided into disseminated, veinlet-disseminated, and stockwork types. The chalcopyrite in the Duobaoshan ore block far away from the schistosity zone mostly occurs as disseminated single-grain veinlet aggregates. In the schistosity zone, chalcopyrite and quartz mostly form veinlets and occur along the bedding of the schistosity plane or chalcopyrite is paragenetic with

sericite and quartz and occurs in a xenomorphic granular form in fractured rocks. Besides, a small amount of chalcopyrite is filled in quartz fissures in the form of stockwork aggregates. In the schistosity zone of the Tongshan ore block, the chalcopyrite is mostly filled in quartz fissures in the form of stockwork aggregates and is coarse-grained. By contrast, the chalcopyrite far away from the schistosity zone mainly occurs in disseminated and veinlet forms and is fine-grained. (2) Pyrite: It was formed over a long time. The major mineralization stage is closely related to sericite alteration. The pyrite in the Duobaoshan ore block mostly occurs in the form of disseminated aggregates or forms veinlets with paragenetic quartz, sericite, and chalcopyrite to be filled in the fissures of surrounding rocks. Pyrite widely occurs in the Tongshan ore block and is strongly affected by the schistosity zone. In this ore block, the pyrite far away from the schistosity zone is mostly disseminated and lumpy, has a perform crystalline form, and is accompanied by disseminated chalcopyrite. In contrast, the crystalline form of the pyrite near the schistosity zone is gradually broken. A large amount of paragenetic stockwork chalcopyrite in the schistosity zone filled in fissures of the early fractured pyrite and quartz and was metasomatized. (3) Molybdenite: The aggregates are mostly scaly and flaky or are paragenetic with quartz to form veinlets. Some of it was metasomatized and superposed by late chalcopyrite veinlets with filled fissures. (4) Bornite: It is dark copper red and has a metallic luster. Most of it is wrapped in chalcopyrite grains in the form of latticed and graphic fine crystals, finally forming an exsolution structure. It is paragenetic with chalcopyrite and occurs in disseminated and veinlet forms.

Near the Yanshanian schistosity zone in the Tongshan ore block, quartz is fractured due to tectonic stress, with the fissures filled with xenomorphic veined chalcopyrite. It is inferred that the veined chalcopyrite was formed after Yanshanian shearing and that two-stage chalcopyritization might have occurred in the Duobaoshan porphyry Cu deposit. The Late Hercynian mineralization centers on the NW-trending tectonic schistosity zone. Specifically, in the schistosity zone, chalcopyrite is well-developed and mostly distributed in the form of veinlets along the bedding of the schistosity plane. The mineralization gradually weakens towards both sides of the schistosity zone and mostly occurs in a disseminated form. The Duobaoshan porphyry Cu deposit was transformed again during the Yanshanian. The Tongshan ore block was significantly affected by the Yanshanian shear schistosity. The disseminated metallic minerals and various gangue minerals formed during the Late Hercynian were fractured at different degrees in the Yanshanian schistosity zone. The fissures among these fractured minerals were filled with late chalcopyrite. It is inferred that the chalcopyritization is related to the Yanshanian tectonic hydrothermal process.

4.3. Alteration and zoning of surrounding rocks

The ore bodies in the Duobaoshan porphyry Cu deposit mainly occur in the granodiorites and the lower part of the Ordovician Duobaoshan Formation. Their lithology is dominated by altered andesites and tuffs, mixing with a few granitic aplite veins. The shear and compression by the NW-trending arcuate schistosity zone have caused plutons, sedimentary volcanic rocks, and pyroclastic rocks to be deformed and metamorphosed to varying degrees, forming tuffaceous slates, mylonitized granitic rocks, and foliated andesitic rocks with tabular and flaky structures and lepidoblastic and granoblastic textures. The Yanshanian structures also transformed the Duobaoshan porphyry Cu deposit. As a result, schists and mylonitized rocks were primarily formed by compressional schistositization in the stope. Generally, the surrounding rocks in the mining area show various alterations, which can be divided into two categories, namely the central alterations occurring around porphyry plutons and the zonal alterations distributed along the NW-trending schistosity zone according to their distribution characteristics. Major central alterations include silicification, K-feldspar alteration, sericite alteration, and propylite alteration, while zonal alterations include sericitolite alteration and carbonation. These alterations are almost distributed in a ring pattern around the porphyry plutons. Major linear alterations include linear sericitolite alteration, followed by carbonation. Among them, sericitolite alteration is the most closely related to copper mineralization, followed by sericite alteration and K-feldspar alteration (Fig. 9; Wei H, 2014; Cai WY, 2020). The above-mentioned alterations of surrounding rocks are all distributed in a banded pattern roughly in the NW direction. With the granodiorite porphyries as the alteration center, there exist four alteration zones, namely the quartz core, the potassic alteration zone, the sericite alteration zone, and the propylite alteration zone from inside to outside. Such distribution pattern of the alterations is similar to that of typical porphyry mineralized alteration zones (Sillitoe RH, 2010; Richards JP, 2003; Cooke DR et al., 2005; Wei H, 2014; Hao YJ, 2015; Cai WY, 2020). These alteration zones are characterized as follows.

The quartz core: It consists mainly of strongly silicified granodiorite porphyries. The quartz exhibits metasomatism in the form of irregular veins and stockworks and is filled with porphyry breccias. It shows weak copper mineralization and molybdenum mineralization.

The potassic alteration zone: This zone is composed mainly of silicified K-feldspars and biotitized and silicified granodiorites surrounding the quartz core. The inner zone of the potassic alteration zone primarily shows K-feldspar alteration, while the outer zone is dominated by biotite alteration. This alteration zone is poorly mineralized.

The sericite alteration zone: Major alterations in this zone include sericite alteration, chlorite alteration, epidote alteration, and silicification. This zone is distributed in an elongated ring shape around the potassic alteration zone. According to the mineral assemblages and spatial position, the sericite alteration zone can be further divided into three subzones, namely the sericitolite alteration zone, the chlorite-sericite alteration zone, and the chlorite-epidote-sericite alteration zone from inside to outside. With the sericitolite alteration zone as the center, the schistositization, sericite

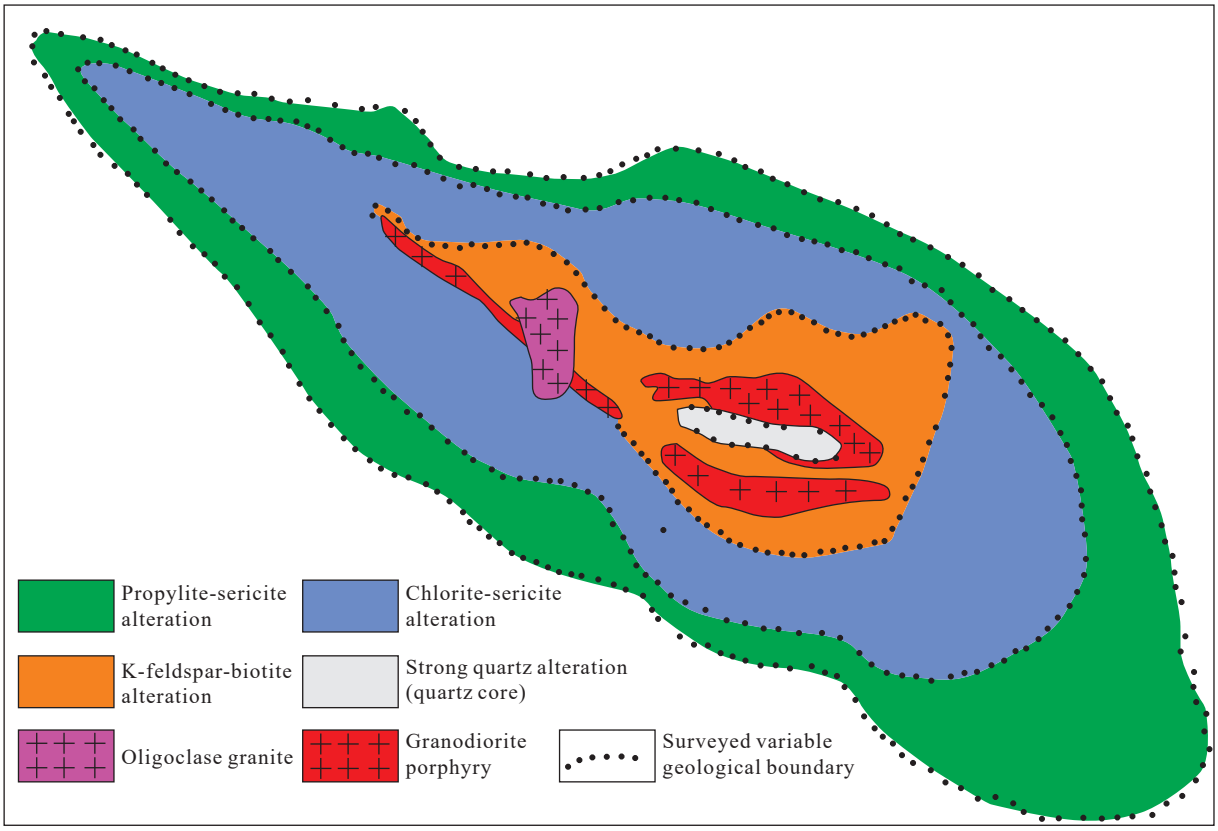

Fig. 9. Schematic diagram of the alterations caused by granodiorite porphyries in the Duobaoshan porphyry Cu deposit and their distribution ranges.

alteration, and copper mineralization gradually weaken toward both sides. This finding indicates that the schistosity zone may provide migration pathways for ore-forming fluids.

The propylite alteration zone: Major alterations in this zone include chlorite and epidote alterations. This zone is distributed in most areas outside the sericite alteration zone and might be the product of the superimposed transformation of multi-stage magmatic-hydrothermal processes. This alteration zone exhibits relatively weak mineralization, with only pyritization discontinuously distributed. In addition, an N-S-extending carbonation zone has developed in the central mining area. This zone is the product of late-stage alterations and is superimposed on early-stage alterations.

4.4. Mineralization periods and mineralization stages

Owing to the relatively high background values of metal elements such as Cu in the Duobaoshan Formation, multi-period and multi-stage magmatic or hydrothermal processes can cause large-scale hydrothermal alteration. Besides, they can induce the migration, enrichment, or depletion of ore-forming elements related to hydrothermal alteration of each stage. According to the temporal and spatial evolution characteristics of the alterations and mineralization, the mineralization of the Duobaoshan porphyry Cu deposit is divided into two periods, namely the Hercynian and the Yanshanian. The Hercynian is the dominant mineralization period of Cu, Mo, and Ag.

The granodiorites and granodiorite porphyries intruded into the NW-trending tectonic belt of the ore field during the Middle-Late Hercynian. The porphyry alteration and mineralization related to these two sets of plutons were formed during the condensation. Major alterations of the granodiorites and granodiorite porphyries include central alterations distributed around porphyry plutons and late-stage linear alterations, with the former consisting of potassic alteration, silicification, planarly distributed propylite alteration, and sericite alteration distributed in the form of a flat ring and the latter comprising sericitolite alteration and carbonation. The alterations and mineralization of this period were controlled by porphyry plutons and NW-trending structures, showing a distribution pattern of a flat ring. According to the interpenetration relationship of hydrothermal veins, mineral assemblages, and the temporal evolution and spatial distribution of alterations and mineralization, major alterations and mineralization of this period can be divided into the following four stages (Wei H, 2014; Hao YJ, 2015; Cai WY, 2020), namely the potassic alteration stage, the molybdenite-chalcopyrite-quartz stage, the chalcopyrite-quartz stage, and the calcite-quartz stage (Table 3).

4.5. Resources and ore chemical composition

The Duobaoshan porphyry Cu deposit consists of four mineralized zones and 215 ore bodies. Among them, ore body No. X in the No. 3 mineralized zone has the largest resource reserves, accounting for more than 78% of the total reserves of the deposit. The No. 3 mineralized zone has total reserves

Table 3. Mineralization stages and mineral formation sequence of the Duobaoshan copper-gold-molybdenum-sliver deposit (after Wei H, 2014; Cai WY, 2020).

Stage / Mineral name	Potassic alteration stage	Molybdenite-chalcopyrite-quartz stage	Chalcopyrite-quartz stage	Calcite-quartz stage
Biotite	———			
Potassium feldspar	———			
Magnetite	- - - -			
Pyrite	- - - -			- - - -
Chlorite	———			
Epidote	———			
Sericite		- - - -	———	
Molybdenite		———	- - - -	
Bornite			———	
Chalcopyrite		- - - -	———	
Sphalerite				
Galena			- - - -	
Quartz	———	———	———	———
Carbonate minerals				———

——— A large amount ——— A small amount - - - - A tiny amount

of ores with grades above minimum production grade of 382.688×10^6 t, which include 1.7797×10^6 of copper (grade: 0.47%), 57400 t of molybdenum (average grade: 0.015%), 71.35 t of associated gold (average grade: 0.149g/t), and 950.87 t of associated silver (average grade: 1.951g/t). The ores contain many types of elements. Cu and Mo are relatively enriched and their grades meet the industrial requirements. Au, Ag, Se, Ni, and Pt group elements have reached the criteria of associated beneficial components. In addition, the Os^{187} content in molybdenite is up to 5.14 g/T. The comprehensive utilization of Au and Ag can be adopted if the heap leaching process is used to extract copper oxide. The ores have very low contents of harmful components, such as arsenic, fluorine, zinc, and magnesium oxide, which cause little effect on copper leaching. Regarding the chemical composition, the oxidized ores consist of 1.3×10^{-6} of Au, 5.5×10^{-6} of Ag, 0.15% of Zn, 0.08% of Pb, 0.03% of Cu, 0.02% of As, 0.23% of Ti, 5.0% of Al, 0.38% of Ca, 0.84% of Mg, 0.04% of Ba, and 2.5% of K. In addition, the ores also contain 0.30% of total carbon and 0.09% of organic carbon, which have a certain impact on Au recovery.

5. Discussion

5.1. Mineralization epoch

At present, the mineralization epoch of the Duobaoshan porphyry Cu deposit is still controversial. Cai WY (2020) determined that the molybdenite in quartz veins and the disseminated molybdenite in the surrounding rocks in the deposit have a model age of 475.7±3.3 Ma to 478.7±4.1 Ma and 476.0±4.2 Ma to 476.6±2.3 Ma, respectively. These two model ages are roughly the same within the error range, with a weighted average of 477.1±1.2 Ma and an isochron age of 477.0±2.8 Ma. This result means that the two types of mineralization were formed in the magmatism of the same period, indicating that the porphyry Cu-Mo mineralization of the Duobaoshan porphyry Cu deposit occurred during the Early Ordovician. In addition, Hao YJ (2015) determined that the disseminated molybdenite in the porphyritic granite veins of the Tongshan deposit has a model age of 229.4±3.5 Ma, implying that the Duobaoshan porphyry Cu deposit was superimposed with Late Triassic Cu-Mo mineralization. Liu J (2012) conducted zircon LA-ICP-MS dating for granodiorite porphyries that are closely related to mineralization in the deposit and obtained a U-Pb age of 474.9±1.8 Ma. Xiang AP (2012) conducted high-precision zircon U-Pb LA-ICP-MS dating for the metallogenic plutons and determined that the metallogenic parent rocks (granodiorite porphyries), host rocks (granodiorites), and the biotite granodiorites around ore bodies have a zircon U-Pb age of 474.8±4.7 Ma, 478.1±4.1 Ma, and 483.9±4.5 Ma, respectively, and that the molybdenite has a weighted-averaged Re-Os isotope model age of 475.1±5.1 Ma. The above metallogenic chronology studies (Table 4) show that the main body of the Duobaoshan porphyry Cu deposit was formed during the Early Ordovician (Fig. 10).

5.2. Ore-forming fluids and mineral sources

5.2.1. Properties of ore-forming fluids

Many previous researchers have studied the ore-forming

Table 4. Chronological data of magmatic rocks and ores in the Duobaoshan porphyry Cu deposit and adjacent areas.

Deposit/area	Rocks/ores	Dated minerals/rocks	Dating method	Age/Ma	Date sources
Duobaoshan	Basalt	Zircon	LA-ICP-MS U-Pb	506±3	Zhao YY et al., 2019a
Duobaoshan	Ultramafic rock	Diamond	LA-ICP-MS U-Pb	497±6	Feng JX et al., 2008
Duobaoshan	Rhyolitic porphyry	Diamond	LA-ICP-MS U-Pb	491±5	Feng JX et al., 2008
Duobaoshan	Granodiorite	Diamond	SHRIMP U-Pb	485±8	Ge WC et al., 2007
Duobaoshan	Andesite	Diamond	LA-ICP-MS U-Pb	485±4	Zhao YY et al., 2019a
Duobaoshan	Biotite granodiorite	Diamond	LA-ICP-MS U-Pb	484±5	Xiang AP et al., 2012
Duobaoshan	Biotite granodiorite	Diamond	LA-ICP-MS U-Pb	484±5	Yu HQ et al., 1996
Duobaoshan	Granodiorite	Diamond	LA-ICP-MS U-Pb	482±4	Zeng QD et al., 2014
Duobaoshan	Granodiorite	Diamond	LA-ICP-MS U-Pb	480±13	Bai LA, 2013
Duobaoshan	Granodiorite	Diamond	SHRIMP U-Pb	480±5	Zhao HL et al., 2012
Duobaoshan	Granodiorite	Diamond	LA-ICP-MS U-Pb	479±2	Cai WY, 2020
Duobaoshan	Granodiorite	Diamond	LA-ICP-MS U-Pb	479±2	Wu G et al., 2015
Duobaoshan	Granodiorite	Diamond	SHRIMP U-Pb	478±5	Cui G et al., 2008
Duobaoshan	Granodiorite	Diamond	LA-ICP-MS U-Pb	478±4	Xiang AP et al., 2012
Duobaoshan	Granodiorite	Diamond	LA-ICP-MS U-Pb	478±4	Yu HQ et al., 1996
Duobaoshan	Granodiorite porphyry	Diamond	SIMS U-Pb	478±3	Zhao YY et al., 2018
Duobaoshan	Granodiorite porphyry	Diamond	LA-ICP-MS U-Pb	477±4	Zeng QD et al., 2014
Duobaoshan	Granodiorite porphyry	Diamond	SIMS U-Pb	476±3	Zhao YY et al., 2018
Duobaoshan	Granodiorite porphyry	Diamond	LA-ICP-MS U-Pb	475±5	Xiang AP et al., 2012
Duobaoshan	Granodiorite porphyry	Diamond	LA-ICP-MS U-Pb	475±5	Yu HQ et al., 1996
Duobaoshan	Granite	Diamond	LA-ICP-MS U-Pb	474±1	Yu HQ et al., 1996
Duobaoshan	Andesite	Diamond	LA-ICP-MS U-Pb	461±3	Yu HQ et al., 1996
Duobaoshan	Basaltic andesite	Diamond	LA-ICP-MS U-Pb	450±2	Wu G et al., 2015
Duobaoshan	Andesite	Diamond	LA-ICP-MS U-Pb	447±2	Wu G et al., 2015
Duobaoshan	Monzodiorite	Diamond	SHRIMP U-Pb	292±7	Zhang FF et al., 2015
Duobaoshan	Tonalite	Diamond	LA-ICP-MS U-Pb	231±3	Zeng QD et al., 2014
Duobaoshan	Tonalite	Diamond	LA-ICP-MS U-Pb	231±2	Hao YJ et al., 2017
Duobaoshan	Tonalite	Diamond	LA-ICP-MS U-Pb	223±3	Zhao YY et al., 2019b
Duobaoshan	Granodiorite	Diamond	LA-ICP-MS U-Pb	128±1	Cai WY, 2020
Duobaoshan	Andesite	Diamond	LA-ICP-MS U-Pb	127±1	Yu HQ et al., 1996
Duobaoshan	Ore	Molybdenite	Re-Os	477.0±2.8	Cai WY, 2020
Duobaoshan	Ore	Chalcopyrite and pyrite	Re-Os	481.6±6.7	Liu J et al., 2012
Duobaoshan	Ore	Molybdenite	Re-Os	485.6±3.7	Liu J et al., 2012
Duobaoshan	Ore	Molybdenite	Re-Os	475.1±5.1	Xiang AP et al., 2012
Duobaoshan	Ore	Molybdenite	Re-Os	477.8±5.7	Zeng QD et al., 2014
Duobaoshan	Ore	Molybdenite	Re-Os	506±14	Zhao YM et al., 1997
Duobaoshan	Ore	Feldspar and sericite	^{40}Ar-^{39}Ar	253-220	Liu J et al., 2012
Tongshan	Tonalite	Diamond	LA-ICP-MS U-Pb	479±2	Cai WY, 2020
Tongshan	Tonalite	Diamond	LA-ICP-MS U-Pb	478±2	Cai WY, 2020
Tongshan	Granodiorite	Diamond	LA-ICP-MS U-Pb	478±3	Hu XL et al., 2017
Tongshan	Granodiorite	Diamond	LA-ICP-MS U-Pb	476±1	Hao YJ et al., 2015
Tongshan	Tonalite	Diamond	LA-ICP-MS U-Pb	472±1	Liu J et al., 2017
Tongshan	Tonalite	Diamond	LA-ICP-MS U-Pb	461±1	Liu J et al., 2015
Tongshan	Porphyritic granite	Diamond	LA-ICP-MS U-Pb	235±3	Hao YJ et al., 2017
Tongshan	Porphyritic granite	Diamond	LA-ICP-MS U-Pb	231±1	Hao YJ et al., 2015
Tongshan	Tonalite	Diamond	LA-ICP-MS U-Pb	214±3	Hu XL et al., 2017
Tongshan	Ore	Molybdenite	Re-Os	476.0±4.5	Cai WY, 2020
Tongshan	Ore	Chalcocite	Re-Os	473±4	Hao YJ et al., 2015
Tongshan	Ore	Chalcocite	Re-Os	473±4	Hao YJ et al., 2014
Tongshan	Ore	Chalcocite	Re-Os	229.4±3.5	Hao YJ et al., 2017
Sankuanggou	Tonalite	Diamond	LA-ICP-MS U-Pb	200-168	Lü PR et al., 2012
Sankuanggou	Granodiorite	Diamond	SHRIMP U-Pb	177±3	Ge WC et al., 2007
Sankuanggou	Granodiorite	Diamond	LA-ICP-MS U-Pb	177±1	Dai M et al., 2017
Sankuanggou	Granodiorite	Diamond	LA-ICP-MS U-Pb	176±1	Hao YJ et al., 2015
Sankuanggou	Biotite granodiorite	Diamond	LA-ICP-MS U-Pb	176±1	Chu SX et al., 2012
Sankuanggou	Granodiorite	Diamond	LA-ICP-MS U-Pb	175±1	Cai WY, 2020

Table 4 (*Continued*)

Deposit/area	Rocks/ores	Dated minerals/rocks	Dating method	Age/Ma	Date sources
Sankuanggou	Ore	Chalcocite	Re-Os	174.1±1.7	Chu SX et al., 2019
Sankuanggou	Ore	Chalcocite	Re-Os	173.7±1.8	Chu SX et al., 2019
Sankuanggou	Ore	Chalcocite	Re-Os	173±6	Hao YJ et al., 2015
Xiaoduobaoshan	Granodiorite	Diamond	LA-ICP-MS U-Pb	233±2	Hao YJ et al., 2017
Xiaoduobaoshan	Granite porphyry	Diamond	LA-ICP-MS U-Pb	227±2	Hao YJ et al., 2017
Xiaoduobaoshan	Granodiorite	Diamond	LA-ICP-MS U-Pb	172±2	Bai LA, 2013
Zhengguang	diorite porphyrite	Diamond	LA-ICP-MS U-Pb	492±5	Wang L et al., 2018
Zhengguang	diorite porphyrite	Diamond	LA-ICP-MS U-Pb	481±5	Wang L et al., 2018
Zhengguang	Diorite	Diamond	LA-ICP-MS U-Pb	481±3	She HQ et al., 2012
Zhengguang	Dacitic porphyry	Diamond	LA-ICP-MS U-Pb	481±3	Che HW et al., 2015
Zhengguang	Dacitic porphyry	Diamond	LA-ICP-MS U-Pb	481±3	Che HW et al., 2015
Zhengguang	Dacitic porphyry	Diamond	LA-ICP-MS U-Pb	480±3	Che HW et al., 2015
Zhengguang	Dacitic porphyry	Diamond	LA-ICP-MS U-Pb	480±2	Wang L et al., 2018
Zhengguang	Monzodiorite	Diamond	LA-ICP-MS U-Pb	479±6	Wang L et al., 2018
Zhengguang	Diorite	Diamond	LA-ICP-MS U-Pb	478±4	Li Y et al., 2016b
Zhengguang	diorite porphyrite	Diamond	LA-ICP-MS U-Pb	477±5	Wang L et al., 2018
Zhengguang	diorite porphyrite	Diamond	LA-ICP-MS U-Pb	477±5	Wang L et al., 2018
Zhengguang	diorite porphyrite	Diamond	LA-ICP-MS U-Pb	469±4	Wang L et al., 2018
Zhengguang	Quartz-mica dioritic porphyry	Diamond	LA-ICP-MS U-Pb	462±2	Gao RZ et al., 2017
Zhengguang	Quartz-mica dioritic porphyry	Diamond	LA-ICP-MS U-Pb	462±2	Yuan MW et al., 2018
Zhengguang	Feldspar porphyry	Diamond	LA-ICP-MS U-Pb	455±1	Song GX et al., 2015
Zhengguang	Diorite	Diamond	LA-ICP-MS U-Pb	440±5	Wang L et al., 2018
Zhengguang	diorite porphyrite	Diamond	LA-ICP-MS U-Pb	436±6	Wang L et al., 2018
Zhengguang	Granodiorite porphyry	Diamond	LA-ICP-MS U-Pb	436±2	Song GX et al., 2015
Zhengguang	diorite porphyrite	Diamond	LA-ICP-MS U-Pb	292±6	Song GX et al., 2015
Zhengguang	Diorite	Diamond	LA-ICP-MS U-Pb	151±1	Li Y et al., 2016b
Zhengguang	Ore	Diamond	Re-Os	506±44	Hao YJ et al., 2016
Zhengguang	Ore	Diamond	Re-Os	474.7±7.9	Cai WY, 2020
Zhengguang	Ore	Diamond	Re-Os	246.0±6.4	Cai WY, 2020
Zhengguang	Ore	Chalcocite	Re-Os	463±24	Li Y et al., 2016b
Sandaowanzi	Syenogranite	Diamond	LA-ICP-MS U-Pb	377±3	Liu J et al., 2017
Sandaowanzi	Syenogranite	Diamond	LA-ICP-MS U-Pb	369±2	Liu J et al., 2017
Sandaowanzi	Granite	Diamond	LA-ICP-MS U-Pb	363±3	Liu J et al., 2017
Sandaowanzi	Trachyandesite	Diamond	LA-ICP-MS U-Pb	313±1	Zhai DG et al., 2015
Sandaowanzi	Monzogranite	Diamond	LA-ICP-MS U-Pb	194±2	Wang L et al., 2018
Sandaowanzi	Monzogranite	Diamond	LA-ICP-MS U-Pb	185±1	Wang L et al., 2018
Sandaowanzi	Monzogranite	Diamond	LA-ICP-MS U-Pb	183±1	Wang L et al., 2018
Sandaowanzi	Monzogranite	Diamond	LA-ICP-MS U-Pb	185±1	Wang L et al., 2018
Sandaowanzi	Granodiorite	Diamond	LA-ICP-MS U-Pb	183±2	Liu J et al., 2017
Sandaowanzi	Monzogranite	Diamond	LA-ICP-MS U-Pb	182±1	Zhai DG et al., 2015
Sandaowanzi	Granodiorite	Diamond	LA-ICP-MS U-Pb	124±1	Liu J et al., 2017
Sandaowanzi	Andesite	Diamond	LA-ICP-MS U-Pb	123±3	Wang L et al., 2018
Sandaowanzi	Andesite	Diamond	LA-ICP-MS U-Pb	122±2	Wang L et al., 2018
Sandaowanzi	Granite porphyry	Diamond	LA-ICP-MS U-Pb	122±1	Wang L et al., 2018
Sandaowanzi	Andesite	Diamond	LA-ICP-MS U-Pb	121±1	Wang L et al., 2018
Sandaowanzi	Andesite	Diamond	LA-ICP-MS U-Pb	121±1	Wang L et al., 2018
Sandaowanzi	Andesite	Diamond	LA-ICP-MS U-Pb	121±1	Wang L et al., 2018
Sandaowanzi	Andesite	Diamond	LA-ICP-MS U-Pb	120±1	Wang L et al., 2018
Sandaowanzi	Andesite	Diamond	LA-ICP-MS U-Pb	120±1	Wang L et al., 2018
Sandaowanzi	Dacite	Diamond	LA-ICP-MS U-Pb	120±1	Wang L et al., 2018
Sandaowanzi	Granodiorite	Diamond	LA-ICP-MS U-Pb	116±1	Liu J et al., 2017
Sandaowanzi	Ore	Quartz	Rb-Sr	121.3±2.6	Zhai DG et al., 2015
Sandaowanzi	Ore	Pyrite	Rb-Sr	119.1±3.9	Zhai DG et al., 2015
Sanfengshan	Gabbro	Diamond	LA-ICP-MS U-Pb	464±8	Li Y, 2016
Huaduoshan	Granodiorite	Diamond	SHRIMP U-Pb	177±3	Ge WC et al., 2007
Huaduoshan	Granodiorite	Diamond	SHRIMP U-Pb	176±3	Ge WC et al., 2007

Table 4 (*Continued*)

Deposit/area	Rocks/ores	Dated minerals/rocks	Dating method	Age/Ma	Date sources
Huaduoshan	Ore	Molybdenite	Re-Os	172.4±2.7	Hao YJ, 2015
Yongxin	Andesite	Diamond	/	114±2	Yuan MW et al., 2018
Huolongmen	Monzogranite	Diamond	SHRIMP U-Pb	351.5±3.5	Li Y, 2016
Huolongmen	Monzogranite	Diamond	LA-ICP-MS U-Pb	323±2	Yuan MW et al., 2018
Yongxin	Diorite	Diamond	/	115±2	Yuan MW et al., 2018
Dachazi	Syenogranite	Diamond	SHRIMP U-Pb	345±3	Dai M et al., 2017
Huolongmen	Monzogranite	Diamond	LA-ICP-MS U-Pb	316±2	Yuan MW et al., 2018
Huolongmen	Granite mylonite	Diamond	SHRIMP U-Pb	310.7±6.5	Hao YJ, 2015
Huolongmen	Monzogranite	Diamond	LA-ICP-MS U-Pb	307±5	Yuan MW et al., 2018
Huolongmen	Syenogranite	Diamond	LA-ICP-MS U-Pb	291±1	Yuan MW et al., 2018
Huolongmen	Syenogranite	Diamond	LA-ICP-MS U-Pb	291±1	Yuan MW et al., 2018
Yikete	Alkali-feldspar Granite	Diamond	SHRIMP U-Pb	309.0±3.0	Hao YJ, 2015
Yikete	Syenogranite	Diamond	SHRIMP U-Pb	299.3±2.8	Hao YJ, 2015
Zhuanghuhe	Finely crystalline granite	Diamond	LA-ICP-MS U-Pb	320±3	Li Y, 2016
Zhuanghuhe	Granite porphyry	Diamond	LA-ICP-MS U-Pb	301±1	Li Y, 2016
Zhuanghuhe	Granite porphyry	Diamond	LA-ICP-MS U-Pb	299±1	Li XY and Zhao YZ, 2018
Zhuanghuhe	Rhyolite	Diamond	LA-ICP-MS U-Pb	292±1	Li XY and Zhao YZ, 2018
Zhuanghuhe	Quartz diorite	Diamond	LA-ICP-MS U-Pb	171±2	Li XY and Zhao YZ, 2018
Zhuanghuhe	Tonalite	Diamond	LA-ICP-MS U-Pb	244±2	Zhao C et al., 2019b
Zhuanghuhe	Granodiorite	Diamond	LA-ICP-MS U-Pb	225±2	Zhao C et al., 2019b
Zhuanghuhe	Granodiorite	Diamond	LA-ICP-MS U-Pb	240±2	Zhao C et al., 2019b
Yuejin	Granodiorite	Zircon	LA-ICP-MS U-Pb	243±2	Zhao C et al., 2019b

fluids of the Duobaoshan porphyry Cu deposit (Wu G et al., 2009; Chu SX et al., 2012; Wei H et al., 2014; Liu J et al., 2010, 2012; Wei H, 2014; Cai WY, 2020), obtaining the following results. Major fluid inclusions include aqueous inclusions, CO_2-rich inclusions, multi-phase daughter crystal-bearing inclusions, and pure CO_2 inclusions. They have a homogeneous temperature range of 245–400°C, 260–300°C, 200–280°C, and 125–170°C in stages I, II, III, and IV, respectively, and salinity of 6%–10% NaCleqv., 1.7%–39%, 0.1%–24.8%, and 0.5%–12.8% in stages I, II, III, and IV, respectively (Fig. 11).

The fluid inclusions mainly contain H_2O and CO_2, and there exist pure CO_2 inclusions. The ore-forming fluids are of the H_2O-CO_2-NaCl type in the early stage and the NaCl-H_2O type in the late stage. These are similar to the fluids of most porphyry deposits. The gas-phase components of the fluid are dominated by H_2O and CO_2, followed by N_2 and CH_4, with the presence of a small amount of Ar, C_2H_6, and H_2S. The liquid phase components primarily include Cl^- and Na^+, followed by SO_4^{2-}, Ca^{2+}, and K^+, with the presence of a trace amount of Mg^{2+} and F^-. The salt compounds in the ore-forming fluids consist mainly of NaCl and bear a small quantity of Ca compounds as well. The NaCl content in the early-stage fluids is higher than that in the late-stage fluids.

This study estimated the minimum trapping pressure of the inclusions formed in major metallogenic stages I, II, and III of the Duobaoshan porphyry Cu deposit. The minimum trapping pressure of stage I was estimated to be 110–160 MPa using the CO_2-H_2O isovolumic cross plot, that of stage II was estimated to be 58–80 MPa based on the CO_2 concentration and that of stage III was estimated to be 5–12 MPa using the depth-temperature diagram of the boiling curves of the NaCl-H_2O-type fluids with different salinities. The corrected ore-forming temperatures of metallogenic stages I, II, and III are 375–650°C, 310–350°C, and 210–290°C, respectively. The minimum ore-forming temperature and pressure of each stage show a gradual downward trend. In addition, as revealed by the data on P-T evolution, the fluids in the potassic alteration and silicification stage were mostly supercritical medium-salinity fluids exsolved from the deep magma chamber. No end member of salinity appeared due to the high pressure and low-level phase separation. During the molybdenum mineralization stage, the decreased temperature and pressure intensified the immiscibility between CO_2 and water, leading to the presence of two end members of fluid salinity and a small quantity of high-salinity inclusions containing halite daughter crystals. The boiling and mixing of fluids during the copper mineralization stage played an important role in the mineralization. Compared with the inclusions in a typical porphyry deposit, the early-stage inclusions of the Duobaoshan porphyry Cu deposit contain fewer high-salinity inclusions, which is mainly related to the Yanshanian transformation and destruction. Inclusions containing halite daughter crystals were only present in stage II instead of the potassic alteration and silicification stage I. This occurred might be related to the immiscibility of CO_2 and H_2O in stage II.

5.2.2. Sources of ore-forming fluids

Wei H (2014) held that the fluid inclusions in the Duobaoshan porphyry Cu deposit had hydrogen isotopic values of −101.5‰–−82.2‰ (range: 19.3‰) and that the ore-forming fluids have oxygen isotopic values of 2.42‰–8.08‰ (range: 5.66‰). The large variation ranges of hydrogen and

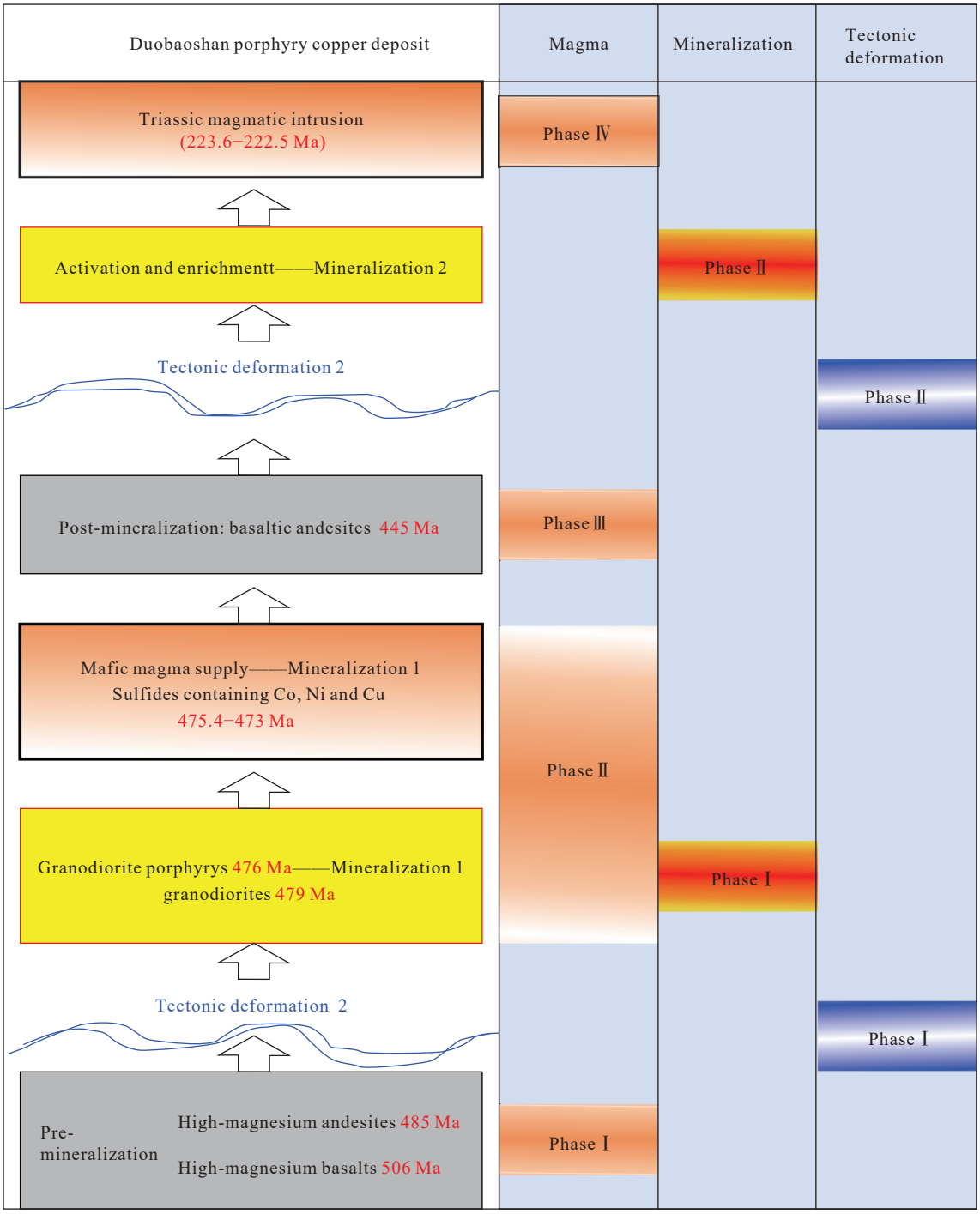

Fig. 10. Time framework of multi-stage magmatic-tectonic mineralization of the Duobaoshan porphyry Cu deposit (after Zhao C, 2019).

oxygen isotopic compositions reflect that the ore-forming hydrothermal fluids of different stages have different properties, suggesting multi-stage mineralization (Fig. 12). The hydrogen and oxygen isotopic compositions of the medium water of each alteration and mineralization stage were between the range of those of magmatic water and meteoric water and their evolution processes approximated to a straight line. The hydrogen and oxygen isotope values of the ore-forming fluids of the early potassic alteration and silicification stage fall under the magmatic water line, and the hydrothermal fluids of this stage were dominated by magmatic water. This result reflects the effects of the water-rock interactions on the hydrothermal fluids in the high-temperature stage. In the stage of sericitolite alteration and copper mineralization, the projection points of hydrogen and oxygen isotope values significantly shifted toward the side of the meteoric water line. This result indicates that much geothermal water was mixed into the altered hydrothermal fluids at this stage. The characteristics described above generally reflect the evolution of ore-bearing hydrothermal fluids from magmatic-hydrothermal fluids to magmatic-hydrothermal fluids mixed with geothermal water.

Cai WY (2020) determined that the quartz has $\delta^{18}O$ values of 9.2‰–12.5‰, the ore-forming fluids had $\delta^{18}O_{H2O}$ values of

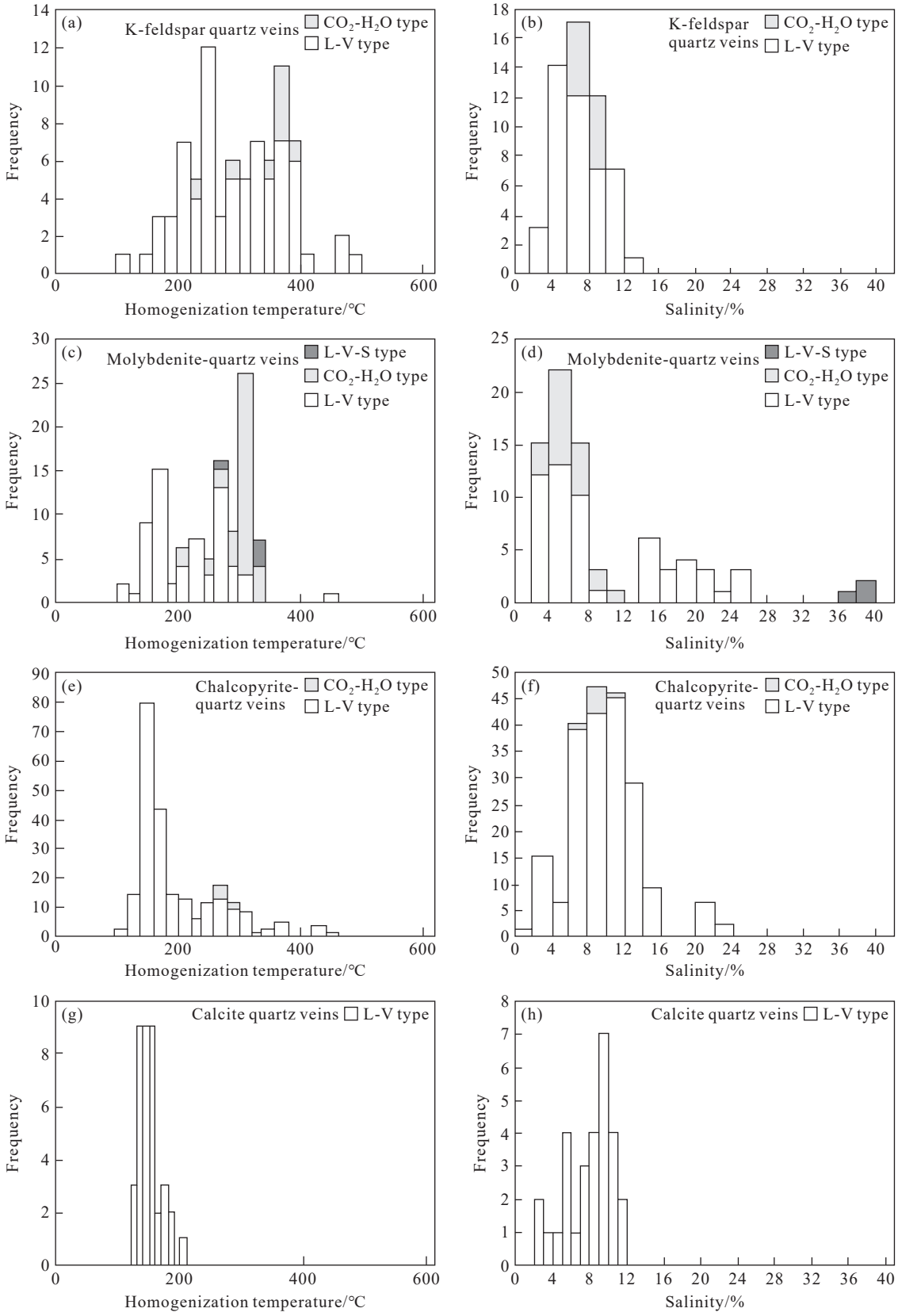

Fig. 11. Homogeneous temperature *vs.* salinity histograms of primary fluid inclusions in quartz veins at different stages of the Duobaoshan porphyry Cu deposit (after Wei H, 2014).

−0.5 ‰ –6.9 ‰, and the fluids have δD values of −111.9‰–−83.4‰ in the Duobaoshan porphyry Cu deposit. Moreover, the fluid inclusions in the quartz of stage I have $\delta^{18}O_{H2O}$ values of 5.8‰–6.1‰, which approximate those of other reported porphyry deposits, reflecting the typical characteristics of a magmatic origin (5.5‰–10‰). However,

their δD values (−89.5‰–−88.4‰) are slightly lower than the hydrogen isotope values (−80 ‰ –−50 ‰) of the primary magmatic water. This occurs possibly due to the degassing of the enclosed system of parent magma or the mixing of meteoric water (Fig. 13). Previous studies show that magma degassing alone can hardly change the δ^{18}O values but the mixing of meteoric water can significantly reduce the δ^{18}O values. In addition, the δD and δ^{18}O values of stage I of the Duobaoshan porphyry Cu deposit are roughly consistent with the fluid characteristics of the potassic alteration stage of typical porphyry deposits. Therefore, it can be inferred that the initial ore-forming fluids of the Duobaoshan porphyry Cu deposit originated from magmatic water. The ore-forming fluids of stages II, III, and IV had lower δ^{18}O values (4.9‰–6.9‰) than those of stage I. However, the ore-forming fluids of stage III had increased δD values (−99.2‰–−83.4‰), which approximate the δD values (−96‰–−88‰) of meteoric water (Du Q et al., 1988). Therefore, the ore-forming fluids of the late mineralization stage originated from meteoric water mixed with magmatic water. As revealed by Wu JR (2012), the quartz fluid inclusions in the Duobaoshan porphyry Cu deposit have $\delta^{18}O_{H2O}$ values of −9.7‰–3.7‰ and δD values

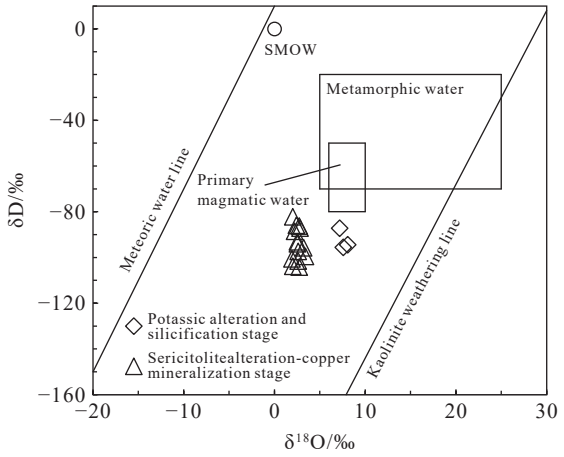

Fig. 12. Hydrogen and oxygen isotopic compositions of the Duobaoshan porphyry Cu deposit (after Wei H, 2014).

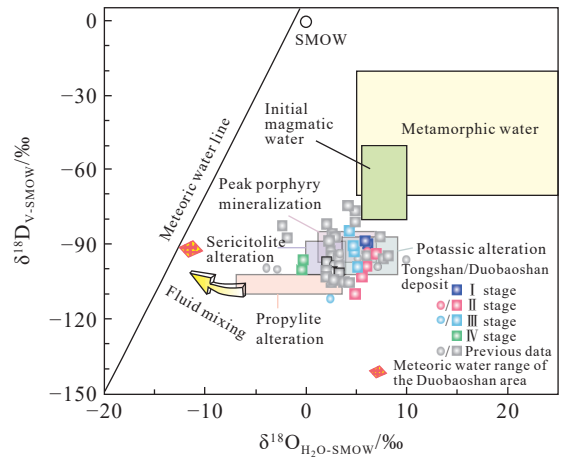

Fig. 13. Hydrogen and oxygen isotopic compositions of the Duobaoshan porphyry Cu deposit (after Cai WY, 2020).

of −120.9 ‰ –−96.7 ‰, and the δD values almost remained unchanged and the $\delta^{18}O_{H2O}$ values gradually decreased as the mineralization proceeded. They also discovered that the hydrothermal calcites have $\delta^{13}C_{PDB}$ values of −3.2‰–−1.8‰ and $\delta^{18}O_{SMOW}$ values of −4.0‰–−10.4‰ and that the $\delta^{13}C_{PDB}$ values almost remained unchanged and the $\delta^{18}O_{SMOW}$ values gradually decreased as the mineralization proceeded. The hydrogen and oxygen isotope data indicate that the ore-forming fluids mainly originated from magma and mantle systems and were also mixed with meteoric water and crust-derived materials.

5.2.3. Sources of ore-forming minerals

(i) Sulfur isotopes (Table 5). The early studies on the sulfur isotopes of the Duobaoshan porphyry Cu deposit (Ma DY, 1984) show that the ore-forming fluids of the deposit have a total sulfur content of −0.75‰–−1.1‰. The sulfur in the ore field originated from the deep crust, and the sulfur isotopes show a certain spatial-temporal distribution pattern. In terms of spatial distribution, ^{32}S is more enriched in areas closer to ore bodies, while ^{34}S is more enriched in areas farther away from ore bodies. In terms of temporal distribution, ^{34}S becomes increasingly enriched from early to late mineralization. Feng JX (2008) also described in detail the spatial distribution of sulfur isotopes in the Duobaoshan porphyry Cu deposit. Feng JX (2008) concluded that the chalcopyrite in the deposit has δ^{34}S values of −4.2‰–1.2‰ and explained the reason why the δ^{34}S values of the sulfur isotopes in the Duobaoshan porphyry copper deposit are low in the central ore bodies and gradually increase toward the surrounding. Wei H (2014) determined that the chalcopyrite in the deposit has δ^{34}S values of −1.6‰–−1.9‰. The previous studies obtained relatively consistent results and all concluded that δ^{34}S values in the Duobaoshan mining area vary in a small range. Therefore, the isotope fractionation effect in the mining area is relatively uniform and not intense n general. Moreover, the chalcopyrite in the deposit has small negative δ^{34}S values, which are close to those of mantle-derived sulfur, indicating that the sulfur in the mining area has the characteristics of mantle-derived sulfur. However, the sulfur in the mining area deviates slightly from the normal mantle-derived sulfur, which is slightly richer in δ^{32}S, indicating that the sulfur in the deposit mainly originated from the mantle and is mixed with a small amount of crust-derived sulfur. Cai WY (2020) determined that sulfur-bearing minerals have δ^{34}S values of −4.7‰–2.5‰ (average: −1.36‰), in which bornite, chalcopyrite, molybdenite, pyrite, and galena have δ^{34}S values of −3.1‰–0.2‰, −4.7‰–−0.2‰, −0.6‰–2.5‰, −2.82‰–1.1‰, and −2.3‰, respectively. Therefore, the Duobaoshan porphyry Cu deposit has roughly the same sulfur isotope values (−5‰–5‰) as most igneous and porphyry deposits in the world. The ores in the deposit have similar δ^{34}S values to granodiorites (−4.5 ‰ –2.6 ‰), granodiorite porphyries (−1.13‰–0.7‰), and Duobaoshan Formation (−2.3‰–3.3‰) in the Duobaoshan porphyry Cu deposit. The sulfur isotopic

Table 5. Sulfur isotopic compositions of ore sulfides in the Duobaoshan porphyry Cu deposit.

Deposit	Tested mineral	$\delta^{34}S_{V-CDT}$/‰	Data sources	Tested mineral	$\delta^{34}S_{V-CDT}$/‰	Data sources
Duobaoshan	Chalcopyrite	−4.7	Bai LA, 2013	Pyrite	−1.39	Feng JX, 2008
Duobaoshan	Pyrite	−0.28	Du Q et al., 1988	Pyrite	1.1	Feng JX, 2008
Duobaoshan	Chalcopyrite	−1.31	Du Q et al., 1988	Pyrite	0.53	Feng JX, 2008
Duobaoshan	Bornite	−1.38	Du Q et al., 1988	Chalcopyrite	−1.5	Feng JX, 2008
Duobaoshan	Galena	−23	Du Q et al., 1988	Chalcopyrite	−1.84	Feng JX, 2008
Duobaoshan	Chalcocite	2.5	Du Q et al., 1988	Chalcopyrite	−1.69	Feng JX, 2008
Duobaoshan	Molybdenite	0.7	Du Q et al., 1988	Chalcopyrite	−1.53	Feng JX, 2008
Duobaoshan	Chalcopyrite	−1.9	Wei H, 2014	Chalcopyrite	−1.7	Feng JX, 2008
Duobaoshan	Chalcopyrite	−1.6	Wei H, 2014	Chalcopyrite	−2.24	Feng JX, 2008
Duobaoshan	Chalcopyrite	−3	Zeng QD et al., 2014	Chalcopyrite	−2.65	Feng JX, 2008
Duobaoshan	Chalcopyrite	−2.9	Zeng QD et al., 2014	Chalcopyrite	−1	Feng JX, 2008
Duobaoshan	Chalcopyrite	−3.3	Zeng QD et al., 2014	Chalcopyrite	−0.2	Feng JX, 2008
Duobaoshan	Chalcopyrite	−2.7	Zeng QD et al., 2014	Chalcopyrite	−0.7	Feng JX, 2008
Duobaoshan	Chalcopyrite	−2.9	Zeng QD et al., 2014	Bornite	−2.2	Feng JX, 2008
Duobaoshan	Bornite	−3.1	Zeng QD et al., 2014	Bornite	−1.7	Feng JX, 2008
Duobaoshan	Chalcopyrite	−3.5	Zeng QD et al., 2014	Bornite	−0.7	Feng JX, 2008
Duobaoshan	Chalcopyrite	−3	Zeng QD et al., 2014	Bornite	−0.2	Feng JX, 2008
Duobaoshan	Chalcopyrite	−0.8	Zeng QD et al., 2014	Bornite	−0.75	Feng JX, 2008
Duobaoshan	Molybdenite	−0.4	Zeng QD et al., 2014	Bornite	−0.6	Feng JX, 2008
Duobaoshan	Molybdenite	−0.6	Zeng QD et al., 2014	Bornite	−0.6	Feng JX, 2008
Duobaoshan	Chalcopyrite	−3.6	This study	Pyrite	−23	Liu J et al., 2017
Duobaoshan	Pyrite	−1.9	This study	Chalcopyrite	−0.7	Liu J et al, 2017
Duobaoshan	Chalcopyrite	−3.5	This study	Pyrite	−0.6	Liu J et al, 2017
Duobaoshan	Pyrite	−1.8	This study	Chalcopyrite	−1.5	Liu J et al, 2017
Duobaoshan	Pyrite	−0.76	Feng JX, 2008	Pyrite	−1.5	Liu J et al, 2017
Duobaoshan	Pyrite	1.1	Feng JX, 2008	Pyrite	−1.2	Liu J et al, 2017
Duobaoshan	Pyrite	−1	Feng JX, 2008	Pyrite	−0.7	Liu J et al, 2017
Duobaoshan	Pyrite	−2.82	Feng JX, 2008	Chalcopyrite	−0.9	Liu J et al, 2017
Tongshan	Pyrite	−1.9	Wei H, 2014	Pyrite	−1.8	Hu XL et al., 2017
Tongshan	Chalcopyrite	−4.1	Wei H, 2014	Chalcopyrite	−2.6	Hu XL et al., 2017
Tongshan	Pyrite	−4.6	Wei H, 2014	Pyrite	−1.1	Hu XL et al., 2017
Tongshan	Chalcopyrite	−1.9	Wei H, 2014	Pyrite	−1.5	Hu XL et al., 2017
Tongshan	Pyrite	−3.4	Wei H, 2014	Pyrite	−1.2	Hu XL et al., 2017
Tongshan	Pyrite	−2.1	Zeng QD et al., 2014	Pyrite	−1.8	Hu XL et al., 2017
Tongshan	Pyrite	−1.9	Zeng QD et al., 2014	Chalcopyrite	−1.9	Wei H, 2014
Tongshan	Pyrite	−1.7	Zeng QD et al., 2014	Pyrite	−1.9	Wei H, 2014
Tongshan	Pyrite	−13	Zeng QD et al., 2014	Chalcopyrite	−4.1	Wei H, 2014
Tongshan	Pyrite	−1.2	Zeng QD et al., 2014	Pyrite	−4.6	Wei H, 2014
Tongshan	Pyrite	−1.1	Zeng QD et al., 2014	Pyrite	−3.4	Wei H, 2014
Tongshan	Pyrite	−1.7	Zeng QD et al., 2014	Pyrite	−0.4	Liu J et al., 2017
Tongshan	Chalcopyrite	−2	Zeng QD et al., 2014	Pyrite	−0.6	Liu J et al., 2017
Tongshan	Chalcopyrite	−1.7	Zeng QD et al., 2014	Pyrite	−0.8	Liu J et al., 2017
Tongshan	Pyrite	−1.1	Hu XL et al., 2017	Pyrite	−1.1	Liu J et al., 2017
Tongshan	Chalcopyrite	−2.6	Hu XL et al., 2017	Pyrite	−13	Liu J et al., 2017
Tongshan	Pyrite	−1.5	Hu XL et al., 2017	Pyrite	−0.7	Liu J et al., 2017
Tongshan	Pyrite	−1.2	Hu XL et al., 2017	Chalcopyrite	−3.6	Cai WY, 2020

composition in the Duobaoshan porphyry Cu deposit varies in a small range overall, indicating that the mining area has a relatively uniform and not intense sulfur isotope fractionation effect (Fig. 14; Feng JX, 2008; Wei H, 2014; Hao YJ, 2015).

Major sulfur isotopes on the Earth originate from mantle-derived sulfur, seawater sulfur, and the reduced sulfur in sediments. Mantle-derived sulfur has $\delta^{34}S$ values of −3‰–3‰, seawater sulfur has a $\delta^{34}S$ value of 20‰, and the reduced sulfur in sediments has large negative sulfur isotope values (Chaussidon M and Lorand JP, 1990). The $\delta^{34}S$ values of the Duobaoshan porphyry Cu deposit are generally similar to those of the mantle-derived sulfur. This finding reflects that the ore sulfur mainly originates from the deep mantle and contains a small amount of reduced sulfur ($\delta^{34}S < 0$) from strata as well.

(ii) Pb isotopes (Table 6). Wei H (2014) determined that the Pb isotopic composition in the Duobaoshan porphyry Cu deposit varies in a small range, with $^{206}Pb/^{204}Pb$ ratios of

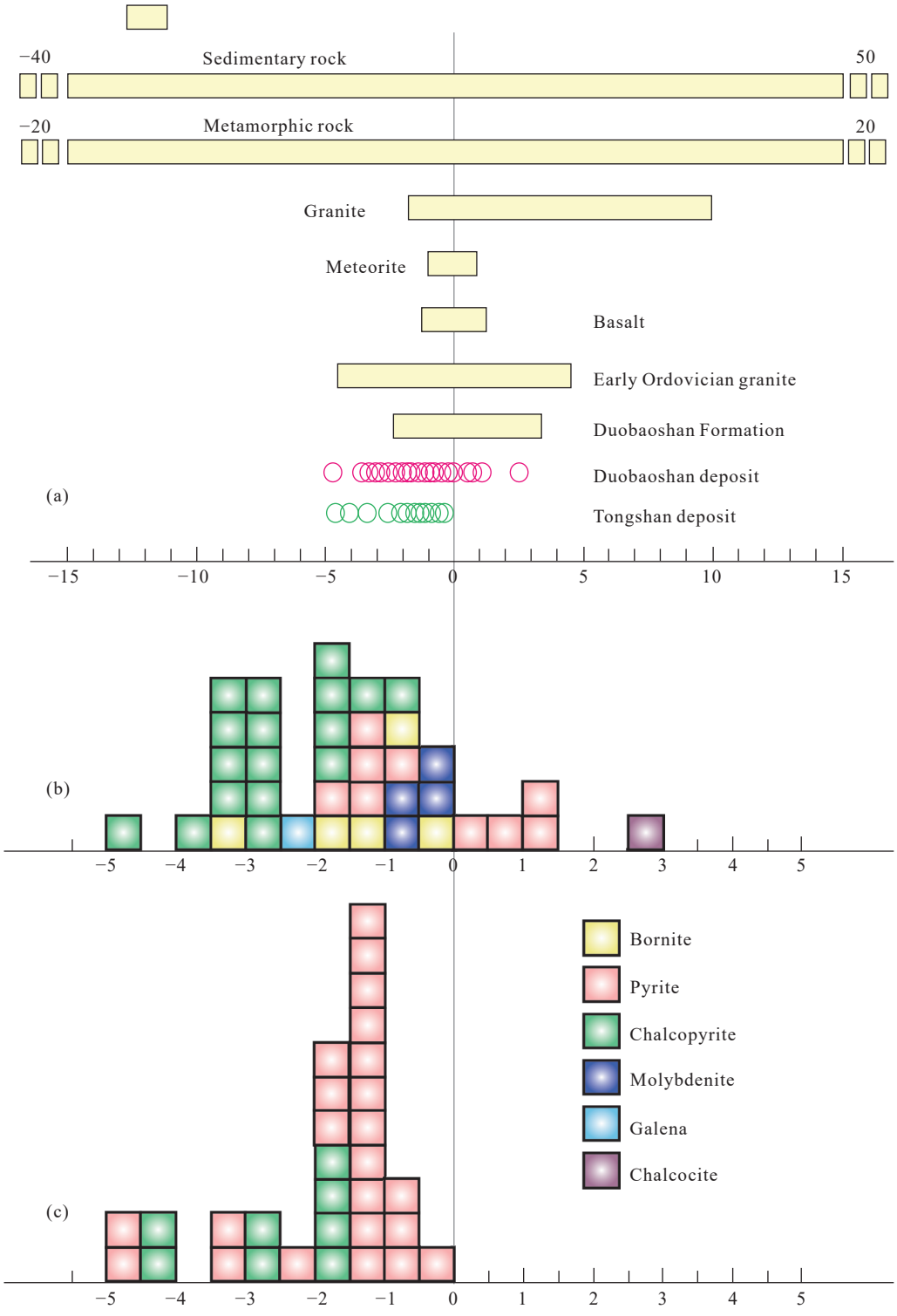

Fig. 14. Distribution diagram (a) and histograms (b−c) of the sulfur isotopic composition in the Duobaoshan porphyry Cu deposit (after Cai WY, 2020).

17.167 –17.464, $^{207}Pb/^{204}Pb$ ratios of 15.235 –15.766, and $^{208}Pb/^{204}Pb$ ratios of 37.269 –38.763 (Table 7, 8). The characteristic μ value of the provenance area of the deposit (7.55) is lower than the normal μ value of the crust (9.58) and close to the μ value (i.e., the $^{238}U/^{204}Pb$ ratio) of the mantle (7.3–8.0). The ω value of the provenance area of the deposit (33.32) is lower than that of the crust (36.50), while the Th/U value (4.38) of the provenance area is higher than the normal Th/U value of the crust (3.8). These results indicate that the ore-forming materials contain mantle-derived components. Additionally, the variation ranges of these data are consistent with those of lead in the gold deposits in the Jiaodong area, both showing the characteristics of lead from the lower crust (Fig. 15). Overall, the lead in the Duobaoshan porphyry Cu deposit mainly originates from the lower crust and also include a small amount of mantle-derived lead.

Table 6. Lead isotopic compositions of ore sulfides in the Duobaoshan porphyry Cu deposit.

Deposit	Tested mineral	$^{206}Pb/^{204}Pb$	σ	$^{207}Pb/^{204}Pb$	2σ	$^{208}Pb/^{204}Pb$	2σ	Data sources
Duobaoshan	Pyrite	17.704	0.003	15.431	0.003	37.314	0.010	Cai WY, 2020
Duobaoshan	Pyrite	17.812	0.003	15.401	0.003	37.426	0.010	Cai WY, 2020
Duobaoshan	Chalcopyrite	17.677	0.003	15.390	0.002	37.156	0.006	Cai WY, 2020
Duobaoshan	Chalcopyrite	17.782	0.003	15.370	0.002	37.241	0.006	Cai WY, 2020
Duobaoshan	Sulfide	17.996	/	15.568	/	37.707	/	Du Q et al., 1988
Duobaoshan	Pyrite	17.201	0.003	15.460	0.003	37.546	0.007	Liu J et al., 2017
Duobaoshan	Chalcopyrite	17.941	0.005	15.454	0.004	37.243	0.009	Liu J et al., 2017
Duobaoshan	Chalcopyrite	17.896	0.002	15.455	0.002	37.319	0.005	Liu J et al., 2017
Duobaoshan	Pyrite	17.887	0.003	15.483	0.002	36.974	0.005	Liu J et al., 2017
Duobaoshan	Chalcopyrite	17.906	0.001	15.461	0.001	37.340	0.002	Liu J et al., 2017
Duobaoshan	Pyrite	17.859	0.003	15.448	0.003	37.331	0.006	Liu J et al., 2017
Duobaoshan	Chalcopyrite	18.037	0.002	15.500	0.005	37.520	0.013	Liu J et al., 2017
Duobaoshan	Pyrite	17.985	0.002	15.475	0.001	37.431	0.003	Liu J et al., 2017
Duobaoshan	Pyrite	17.695	0.001	15.445	0.001	37.265	0.003	Liu J et al., 2017
Duobaoshan	Pyrite	17.840	0.005	15.496	0.004	37.449	0.010	Liu J et al., 2017
Duobaoshan	Chalcopyrite	18.129	0.003	15.507	0.002	37.734	0.005	Liu J et al., 2017
Tongshan	Pyrite	17.827	0.003	15.406	0.002	37.201	0.005	Cai WY, 2020
Tongshan	Pyrite	18.067	0.003	15.551	0.002	37.999	0.005	Liu J et al., 2017
Tongshan	Pyrite	18340	0.004	15.513	0.003	37.682	0.008	Liu J et al., 2017
Tongshan	Pyrite	18.453	0.005	15.525	0.004	37.638	0.01	Liu J et al., 2017
Tongshan	Pyrite	17.951	0.002	15.521	0.001	37.866	0.003	Liu J et al., 2017
Tongshan	Pyrite	17.591	0.002	15.449	0.002	37.28	0.005	Liu J et al., 2017
Tongshan	Pyrite	17.691	0.004	15.485	0.003	37.5	0.008	Liu J et al., 2017
Tongshan	Chalcopyrite	17.682	/	15.48	/	37.402	/	Hu XL et al., 2017
Tongshan	Pyrite	17.725	/	15.471	/	37.395	/	Hu XL et al., 2017
Tongshan	Pyrite	17.71	/	15.479	/	37.425	/	Hu XL et al., 2017
Tongshan	Pyrite	17.703	/	15.475	/	37.409	/	Hu XL et al., 2017
Tongshan	Pyrite	17.798	/	15.495	/	37.52	/	Hu XL et al., 2017

The lead isotopes of the Duobaoshan porphyry Cu deposit determined based on pyrite and chalcopyrite by Cai WY (2020) are distributed linearly between the evolution curves of lead isotopes from the orogenic belt and the lower crust (Zartman RE and Doe BR, 1981). This result means that the lead isotopes of ores in the deposit originate from mixed mantle-derived and crustal materials (Pass HE et al., 2014). Moreover, the lead isotopes of the sulfide ores mostly fall into the range of mantle lead isotopes, with a small amount originating from the lower crust and orogenic belts. This result indicates that the ore-forming materials of the Early Paleozoic Duobaoshan porphyry Cu deposit originated from regional magmatic-volcanic processes and show the characteristics of a mixed crust-mantle source.

(iii) Re-Os isotopes (Table 7). As shown by the molybdenite testing results obtained by Cai WY (2020) and Hao YJ (2015), the molybdenite in the Duobaoshan porphyry Cu deposit has Re content of (121.7–887.6) × 10^{-6}, which is roughly consistent with that of previous studies (Zeng QD et al., 2014; Zhao YM et al., 1997; Liu J et al., 2012; Xiang AP, 2012; Hao YJ et al., 2015). This finding indicates that the ore-forming materials have the characteristics of mantle-derived materials (Mao JW et al., 1999). This conclusion is consistent with the characteristics of a mixed crust-mantle source of ore-forming materials indicated by the sulfur and lead isotopes of sulfide ores.

5.3. Tectonic evolution and metallogenic model

The Duobaoshan ore field enjoys extremely rich mineral resources, which mainly include Cu, Mo, Au, and Fe. The most typical deposits in this ore field include the Duobaoshan porphyry copper (molybdenum) deposit, the Sankuanggou iron-copper deposit, and the veined Zhengguang gold deposit. As revealed by the comparative study (Tables 8, 9), these deposits are all controlled by NW-trending arcuate structures and primarily distributed at the intersection of multiple sets of structures. These characteristics reflect the tectonic framework where these deposits are controlled by the intersection of NW- and NE-trending fault structures and are distributed at the same interval. Moreover, these deposits were all formed in the island arc tectonic setting.

The granodiorites and granodiorite porphyries related to the mineralization of the Duobaoshan porphyry Cu deposit have Rb-Sr isochron ages of 292 Ma and 283 Ma, respectively (Du Q, 1988). Regarding the granodiorites, the isotope ages of their amphiboles and biotites and their whole-rock isotope ages are 226–310 Ma (K-Ar and Rb-Sr dating; Zhao YM, 1997). Therefore, it can be inferred that the Duobaoshan porphyry Cu deposit has a mineralization epoch of the Late Hercynian. The granodiorites related to the mineralization of the Sankuanggou iron-copper deposit have a concordant zircon age and a $^{238}U/^{206}Pb$ weighted average age

Table 7. Re content in molybdenite of the Duobaoshan porphyry Cu deposit.

Deposit	Model age/Ma	Re content/IO*	Data sources
Duobaoshan	476.8±7.3	835.2	Zeng QD et al., 2014
	476.6±7.3	887.6	
	447.9±6.7	614	
	480.2±7.3	121.7	
	478.2±7.3	718.3	
	521±20	567	Zhao YM et al., 1997
	509±5	537.9	
	507±3	303.2	
	482.6±4.3	406.8	Liu J et al., 2012
	479.2±6.6	433	Xiang AP et al., 2012
	483.0±7.3	557.5	
	469.1±6.9	399	
	480.0±7.3	729.4	
	473.1±7.7	353.9	
	472.1±6.7	514.4	
	469.5±7.2	458.6	
	475.7±3.3	282.0	Cai WY, 2020
	477.7±1.8	459.3	
	478.7±4.1	138.3	
	476±4.2	176.5	
	476.6±2.3	325.5	
Tongshan	476.6±6.9	1159	Zeng QD et al., 2014
	505±14	822	Zhao YM et al., 1997
	476±14	497	
	473.0±7.1	151.8	Hao YJ et al., 2015
	471.3±7.5	617.3	
	472.5±7.5	1099	
	475.2±7.6	1650.8	
	471.3±7.4	689.6	
	471.3±6.8	203.7	
	476.6±2.6	405.9	Cai WY, 2020
	477.7±3.9	304.7	
	474.3±6	411.5	
	475±2.9	242.1	
	475.7±3.5	162.5	
	229.4±3.5	312.5	Hao YJ, 2015

of 175.9±1.6 Ma and 175.9±1.1 Ma, respectively (Chu SX, 2012). Therefore, it can be inferred that the Sankuanggou deposit has a mineralization epoch of the Early Yanshanian. The quartz diorite plutons in the Luohe Formation that are the most closely related to the mineralization of the veined Zhengguang gold deposit have a K-Ar age of 182 Ma (Li DR, 2010). Therefore, it can be inferred that the Zhengguang deposit has a mineralization epoch of the Early Yanshanian. From the angle of the mineralization age evolution relationship of the Duobaoshan ore field, the Late Hercynian (about 280 Ma) and the Early Yanshanian (about 175 Ma) are important mineralization periods of porphyry copper-molybdenum and copper-gold in the Duobaoshan ore field, respectively. Therefore, the Duobaoshan area provides metallogenic spaces for both the Paleozoic large porphyry copper-molybdenum and the Mesozoic medium-large copper-gold deposits. Overall, the Duobaoshan ore field experienced multi-stage mineralization featuring long-term evolution, complex internal structures, and strong superposition of various metal elements. As mentioned above, the Duobaoshan ore field lies in the region sandwiched by the Siberian, North China, and paleo-Pacific plates and is in an island arc tectonic setting, creating a favorable tectonic environment and ore-forming material basis for the formation of various deposits in the ore field. This ore field experienced a long-term evolution from the Caledonian to the Yanshanian, during which frequent tectonic and magmatic processes gave birth to the Sankuanggou-Duobaoshan-Zhengguang polymetallic metallogenic belt. Based on the characteristics of strata, structures, plutons, and ore-forming fluids, the multi-stage superimposed mineralization in the Duobaoshan ore field is summarized as follows (Wei H et al., 2014; Hao YJ, 2015; Cai WY, 2020).

5.3.1. Relationship between the Paleo-Asian Ocean subduction and the Duobaoshan arc and the porphyry mineralization

Most researchers hold that the Ordovician magmatism in the Duobaoshan area is associated with the subduction of the Paleo-Asian Ocean (Liu J et al., 2017; Wu G et al., 2015). The latest study shows that the high-Mg# mafic magmatism in the Duobaoshan mining area began during the Middle Cambrian (about 506 Ma) (Zhao C et al., 2019a), implying the initial subduction of the Paleo-Asian Ocean at the end of the Middle Cambrian or an environment of back-arc basin spreading. The porphyry mineralization in the Tongshan and Duobaoshan areas was formed at 485–473 Ma and that in the deep part of the Zhengguang deposit was formed later at about 475 Ma. The Early Ordovician granodiorite (porphyry) and tonalite intruded mainly at 485–477 Ma, which is consistent with the time of the porphyry Cu-Mo-Au mineralization in the Duobaoshan, Tongshan, and Zhengguang areas. As indicated by the whole-rock geochemical and isotopic data, the porphyry ore-forming magmas might be related to the Adakic characteristics of the Early Ordovician magmas. As described earlier, the absence of contemporaneous volcanic rocks may imply a suspension of volcanism, which caused the metallic elements and fluids in the ores to flow toward and accumulate at the roof/apex of magma chambers and created favorable conditions for later mineralization (Richards JP, 2003; Cooke DR et al., 2005; Li XY et al., 2019). The arc magmatism probably ended during the Silurian and was subsequently covered by the continental/neritic (metamorphic) clastics and carbonate rocks of the Niqiuhe Formation. The volcanic rock strata of the Ordovician Duobaoshan and Tongshan formations are composed of sandstones and siltstones interbedded with andesitic porphyrites and tuffaceous siltstones, mixed with marble lens. Among them, the Duobaoshan Formation has high Cu and Au contents, laying a material basis for the Caledonian porphyry Cu-Au mineralization. The Caledonian tectonic movements were mainly reflected in the strong compression and deformation of the strata, forming various fold and fault structures, as well as a transtensional environment and an alternating

Table 8. Geological characteristics of the Duobaoshan porphyry Cu deposit and adjacent areas.

Deposit/ore occurrence	Mineral type	Genetic type	Mineralization epoch	Strata	Pluton	Ore-bearing structure	Ore body characteristics	Data source
Duobaoshan	Cu-Mo-(Au)	Porphyry type	Early Ordovician	Duobaoshan Formation	Granodiorite porphyry	Outer contact tectonic belt	Lenticular or lentil-shaped, attitudes: 310°–330°∠70°–80°	Cai WY, 2020; Hao YJ, 2015; Zeng QD et al., 2014; Liu J et al., 2012; Xiang AP, 2012
Tongshan	Cu-Mo-(Au)	Porphyry type	Early Ordovician and Late Triassic	Duobaoshan Formation	Granodiorite	Inner and outer contact tectonic belts	Stratoid - large-lens-shaped, attitudes: 290°–310°∠ 80°–90°	Cai WY, 2020; Hao YJ et al., 2014, 2015, 2017
Zhengguang	Au	Intermediate-sulfidation type	Early Ordovician and Late Triassic	Duobaoshan Formation	Diorite	Structurally fractured zone	Veined and stockwork, mainly in the NE trending	Cai WY, 2020
Sankuanggou	Fe-Cu	Skarn type	Early-Middle Jurassic	Duobaoshan Formation	Granodiorite	Contact zone structure	Lenticular or lentil-shaped, NE- and NW-trending, dip directions and angles greatly changing	Cai WY, 2020; Chu SX et al., 2012; Hao YJ et al., 2015; Deng K et al., 2018; Chu SX et al., 2019
Xiaoduobao-shan	Fe-Cu	Skarn type	Early-Middle Jurassic	Duobaoshan Formation	Granodiorite	Contact zone structure	Irregularly lenticular or lentil-shaped, strike: 300°–320°, dip angel: SW	Cai WY, 2020; Bai LA, 2013
Yubaoshan	Fe-Cu	Skarn type	Jurassic	Duobaoshan Formation	Tonalite	Contact zone structure	Veined or lenticular, NW-trending (300°–320°)	Hao YJ, 2015
Huaduoshan	Cu-Mo	Cryptoexplosive breccia type	Jurassic	/	Granodiorite	Cryptoexplosive breccias as ore-controlling structures	Five Mo ore bodies, one Cu ore body, one Au ore body, veined, NW-trending	Cai WY, 2020
Baojie	Cu	Magmatic-hydrothermal type?	?	Duobaoshan Formation	Diorite and andesite	Structural intersection	Four mineralized bodies, NW- and nearly EW-trending	Zhao GJ, 2007
Daye	Fe	Submarine hydrothermal exhalative sedimentation type	?	Duobaoshan Formation	Diorite	/	Nearly EW-trending	Hao YJ, 2015
Zhuanghuhe	Sb-Au	Hydrothermal vein type	Jurassic?	Duobaoshan and Luohe formations	Granite porphyry, (quartz) diorite	Sructurally fractured zone	NW-trending, banded, lenticular	Li XY et al., 2018
Erdaokan	Ag-Pb-Zn	?	Early-Late Carboniferous	Nichouhe Formation	Diorite	Breccias as ore-controlling structures	NW-trending, two ore bodies	Yuan MW et al., 2018
Yuejin	Cu-Mo	Porphyry type	?	Duobaoshan and Bashilixiaohe formations	Granodiorite	Tectonic fracture alteration zone	Small lenticular ore bodies, strikes: 290°–300°	Cai WY, 2020
Xiaogushan	Cu	Magmatic-hydrothermal type?	?	Duobaoshan Formation	Granodiorite	Contact zone	NW-trending	Cai WY, 2020
Xiaopingshan	Cu-Mo	Magmatic-hydrothermal type?	?	Duobaoshan Formation	Granodiorite	Contact zone and schistosity zone	Nine mineralized zones, NW-trending	Hao YJ, 2015
Zhenzishan	Mo	Magmatic-hydrothermal type?	?	Nichenghe Formation	Granite porphyry	Contact zone	Three copper mineralized bodies	Hao YJ, 2015
Jiguanshan	Cu-Mo	Porphyry type	?	Duobaoshan Formation	Granodiorite	Inner and outer contact zone structures	Veinlet ore bodies, attitudes: 290°–300°	Cai WY, 2020

Note: ? represents that the character of the genetic type or mineralization epoch is uncertain and disputed.

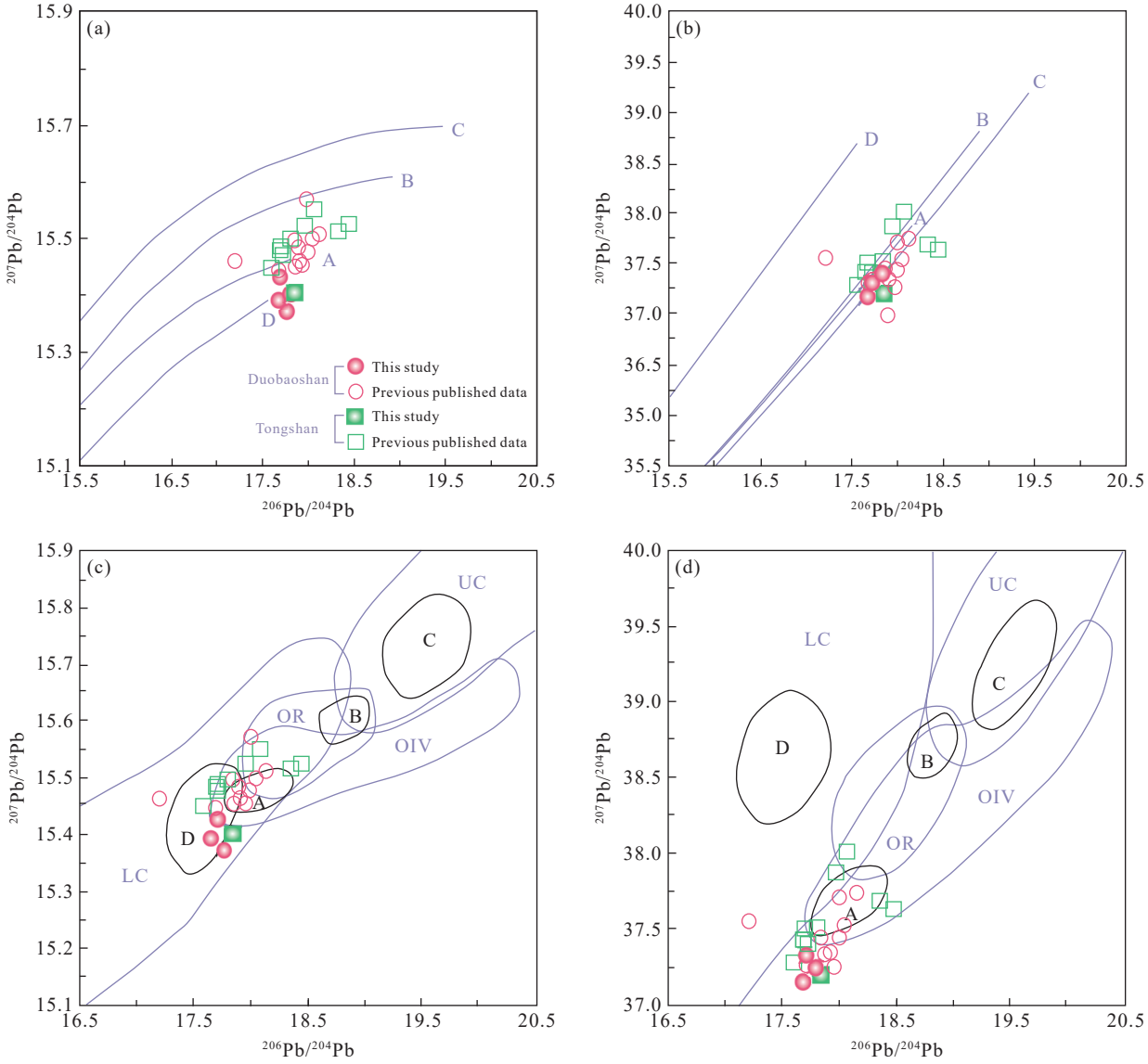

Fig. 15. Lead isotope growth curves (a, b) and tectonic environment discrimination diagram (c, d) of the Duobaoshan porphyry Cu deposit (after Cai WY, 2020). A–mantle; B–orogenic belt; C–upper crust; D–lower crust; LC–lower crust; UC–upper crust; OIV–oceanic volcanic rocks; OR–orogenic belt.

compressional-tensional tectonic environment in the NW direction. Finally, the NW-trending arcuate Duobaoshan-Luohe tectonic belt was formed. Under the combined effects of strata, structures, and magmatic rocks, porphyry deposits including the typical Duobaoshan and Tongshan deposits were formed during the Caledonian. The NW-trending arcuate tectonic belt, which was formed by the NW- and NWW-trending schistosity zones and compressive-tensional structures, control the occurrence of most ore bodies in the Duobaoshan and Tongshan deposits. Accordingly, most of the ore bodies show a NW-trending en-echelon distribution. The Duobaoshan Formation is the main layer rich in the element Cu. From the center of the ore bodies outwards, the copper geochemical anomaly field varies from orebodies, then to a strongly decreased field, then to an increased field, and finally to decreased field. Both the Duobaoshan and Tongshan Cu-Mo-(Au) deposits occur in the increased field within the decreased field. The decreased field of element Cu is distributed in the NW direction, which is consistent with the strike of the granodiorites (porphyries) and ore bodies. This result indicates that the Duobaoshan Formation provided a large number of copper materials for mineralization. The granodiorite (porphyry) plutons related to the mineralization of the Duobaoshan porphyry Cu deposit mainly have zircon U-Pb ages of 485–474 Ma (Cai WY, 2020; Ge WC et al., 2007; Zhao C et al., 2018, 2019a; Xiang AP et al., 2012; She HQ et al., 2012; Zeng QD et al., 2014; Bai LA, 2013; Zhao HL et al., 2012; Wu G et al., 2015; Cui G et al., 2008), and their metallogenic ages also fall in the same range (determined by molybdenite Re-Os dating; Cai WY, 2020; Liu J et al., 2012; Zeng QD et al., 2014; Xiang AP et al., 2012). The tonalite plutons related to the mineralization of the Tongshan deposit have zircon U-Pb ages of 479–472 Ma (Cai WY, 2020; Hu XL et al., 2017; Hao YJ et al., 2015; Liu J et al., 2017), which is consistent with the metallogenic ages of 476–473 Ma (determined by molybdenite Re-Os dating; Cai

Table 9. Comparison between the Duobaoshan porphyry Cu deposit and typical porphyry Cu deposits in the world.

Deposit type	Typical porphyry copper deposits	Duobaoshan porphyry copper deposit
Tectonic setting	Convergent plate margins; island arc or continental arc environment formed by oceanic crust subduction; continental collision environment or intracontinental environment	Volcanic-magmatic arc setting
Mineralization epoch	Dominated by the Mesozoic and the Cenozoic, followed by the Paleozoic, and earlier mineralization epochs with a very small number of deposits	Early Paleozoic and Caledonian
Properties of porphyry plutons	Dominated by the intermediate-acid calc-alkaline magma series, with a small amount of high-K calc-alkaline rock series. Lithology mostly comprises quartz dioritic, quartz monzonitic, granodioritic, and granitic porphyry plutons or porphyroid intrusions	High-K calc-alkaline rock series
Surrounding rock properties	Salic rocks, carbonate rocks, and intermediate-acid volcanic rocks	Andesitic pyroclastic strata of the Ordovician Duobaoshan and Tongshan formations
Magmatic rocks	Small-scale intrusive bodies and multi-stage intrusion, with magmatic rocks before, during, and after mineralization mostly occurring	Contemporaneous and homologous Duobaoshan granodiorite-granodiorite porphyry composite plutons; the exposed granodiorite porphyries formed during the mineralization epoch covering an area of only 0.17 km^2
Hydrothermal alterations	Potassic alteration, silicification, sericitolite alteration, argillization, and propylite alteration	Biotite alteration, silicification, K-feldspar alteration, Na-feldspar alteration, sericite alteration, sericitolite alteration, chlorite alteration, epidote alteration, propylite alteration, and occasionally visible clay alteration
Mineralization properties	Mineralization mainly occurs in potassium silicate alteration zones or the sericite alteration zones; the ore minerals mainly include chalcopyrite, followed by a small amount of bornite and chalcocite. Most mineralization occurs in various veins with fractures	Copper mineralization is the most closely related to potassic alteration – silicification and sericite alteration; molybdenum mineralization is closely related to silicification
Data source	Zhao C et al., 2019a; Cai WY, 2020	Du Q et al., 1988

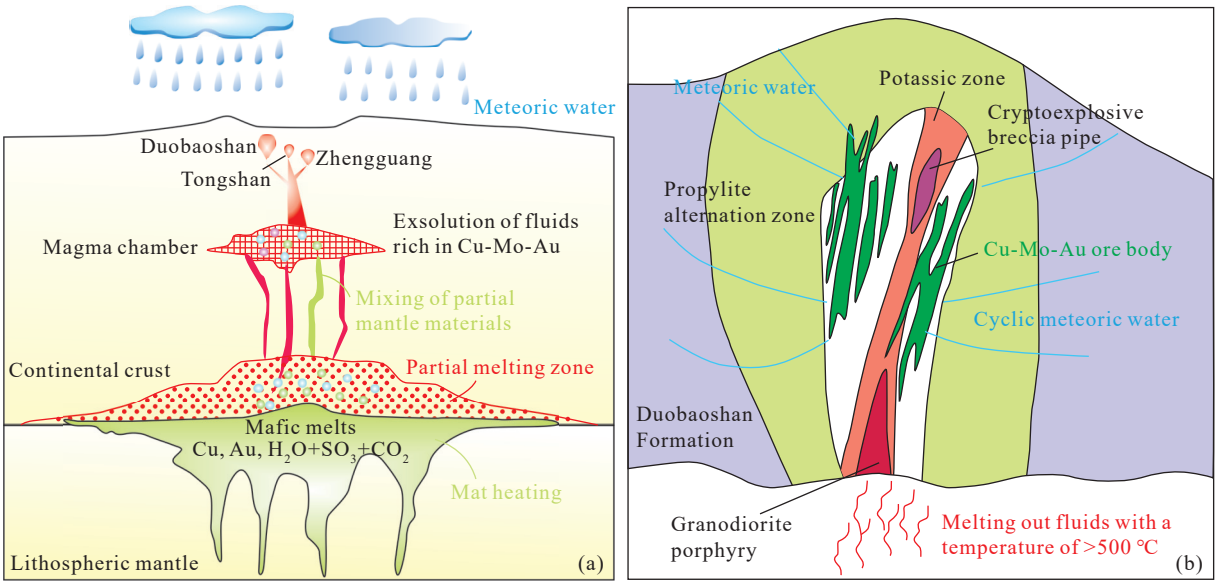

Fig. 16. Schematic diagram of Caledonian porphyry Cu-Mo-Au mineralization in the Duobaoshan porphyry Cu deposit (after Cai WY, 2020).

WY, 2020; Hao YJ et al., 2014, 2015, 2017). Therefore, the Duobaoshan and Tongshan deposits were formed by the same Early Ordovician tectonic-magmatic-hydrothermal processes. As indicated by the S-Pb isotopes of the ores in the Duobaoshan and Tongshan deposits, the ore-forming materials were mainly derived from magmas, might be mixed with a small amount of reduced S ($\delta^{34}S < 0$) from the strata, and have the characteristics of a mixed crust-mantle source. The high Re content in molybdenites also indicated the contribution of mantle materials to the ore-forming materials. The Cu-Mu-(Au) ore-forming hydrothermal fluids had a hydrochemical type of NaCl-H_2O-CO_2, medium-high temperatures, and medium-high salinities overall. The significant immiscibility of the ore-forming fluids is considered the main mechanism for the precipitation of ore-forming materials in the Duobaoshan porphyry Cu deposit (Cai WY, 2020; Wu G et al., 2009; Liu J et al., 2010; Wei H et al., 2011, 2013). The ore-forming fluids in the early stage were magmatic water and those in the late stage gradually transitioned to the mixed hydrothermal liquids of meteoric water and magmatic water, which were H_2O-NaCl hydrothermal liquids with medium-low temperatures and low salinities. As indicated by these findings and previous research results, the temperature and salinity of the ore-

forming fluids and the ore-forming pressure all decreased gradually. The Tongshan and Duobaoshan deposits have similar geographical locations, as well as consistent ore-forming material sources and ore-forming fluid characteristics and sources. Both deposits are typical porphyry deposits and the product of Early Ordovician magmatism. Based on the petrogeochemical characteristics determined by previous researchers, it can be inferred that the Duobaoshan deposit was formed in the initial subduction environment of the Early Ordovician Paleo-Asian Ocean plate. All these characteristics jointly constitute the Caledonian porphyry Cu-Mo-(Au) mineralization (Fig. 16).

5.3.2. Southward subduction of the Mongol-Okhotsk Ocean and the superimposed mineralization of deposits

The Mesozoic magmatism in the western part of Northeast China (especially during the Triassic and the Early Jurassic) is generally interpreted to be associated with the subduction of the Mongol-Okhotsk Ocean (Tang J et al., 2015, 2016; Li Y et al., 2017, 2018). During the Permian-Jurassic/Early Cretaceous, the Mongol-Okhotsk Ocean was located between the Siberian and Amurian plates that had been merged (Kravchinsky VA et al., 2002; Cogné JP et al., 2005). The Triassic magmatism (244 –239 Ma, 235 –231 Ma, and 227 –223 Ma) in the Duobaoshan deposit, the Au mineralization (about 246.0 Ma) in the Zhengguang deposit, and the Cu-Mo mineralization (about 229.4 Ma) in the Tongshan deposit (Hao YJ et al., 2017) were all occurred in a setting where the Mongol-Okhotsk Ocean the was subducted southward/southeastward relative to the Amurian Plate. By contrast, the magmatism in the late stage of the Late Triassic (about 214 Ma) in the Tongshan deposit occurred under a more complex tectonic setting (Hu XL et al., 2017), which is supposed to be the result of the dual effects of both the Mongol-Okhotsk Ocean and the Paleo-Pacific Ocean. The subduction of the Mongol-Okhotsk Ocean could have lasted until the late stage of the Late Triassic (Li Y et al., 2017, 2018). The Late Triassic Raohe gabbros (216±5 Ma) and Heilongjiang blueschists (210 –180 Ma) were found in the Paleo-Pacific accretionary terrane in Northeast China and the Russian Far East (Zhou JB et al., 2014). Accordingly, the westward/northwestward subduction of the Paleo-Pacific Ocean might have begun in the Late Triassic. The Jurassic and Cretaceous tectonic patterns in the Duobaoshan area were jointly affected by the closure of the Mongol-Okhotsk Ocean and the subduction of the Paleo-Pacific Ocean. The tectonic influence of the former gradually changed from subduction-related compression to syn/post-collision extension. In contrast, the tectonic influence of the subduction of the Paleo-Pacific Ocean changed from subduction arc-related compression to back-arc extension (or vanished gradually), with the subduction front gradually retreating eastward due to terrain accretion. The Au-(Cu-Mo) mineralization mainly includes the Au-(Cu-Mo) mineralization of the Indosinian Zhengguang epithermal copper deposit and the superimposed Triassic Cu-Mo mineralization in the Tongshan deposit. The Au-(Cu-Mo) mineralization is related to the southward subduction of the Mongol-Okhotsk Ocean. Porphyry mineralization occurs in the deep part of the Zhengguang gold deposit, and the ores have veinlet-disseminated structures. The shallow part of the Zhengguang deposit shows typical intermediate-sulfidation epithermal mineralization, with the ore bodies mostly occurring in a veined form under the control of NE-, NNE-, and NW-trending faults. As shown by studies of the Re-Os isotopic dating, the deep porphyry mineralization occurred during the Early Ordovician (about 474 Ma), which is roughly consistent with the emplacement age of the diorites in the area (478 Ma; Li Y et al., 2016b). The presence of veinlet-disseminated mineralization indicates that there is a genetic relationship between diorites and Au mineralization at this stage. The epithermal Au mineralization occurred during the Middle Triassic (about 246 Ma; Cai WY, 2020). No Triassic pluton has been found in the Zhengguang mining area. However, the presence of the quartz diorites (230 Ma) in the Duobaoshan deposit and the porphyritic granites (235 Ma) in the Tongshan deposit, it can be inferred that the Triassic plutons related to late-stage Au mineralization might be concealed in the deep part of the Zhengguang mining area. Previous studies have revealed that Late Jurassic dioritic porphyrites (about 151 Ma) exist in the Zhengguang mining area and are cut through by gold-bearing veins. This finding implies that the Zhengguang deposit might be superimposed with certain Late Jurassic Au mineralization. Therefore, the Zhengguang gold deposit was formed by the superposition of Caledonian, Indosinian, and late Yanshanian tectonic movements. Moreover, deep porphyry mineralization occurred in the early stage, and dominant epithermal mineralization occurred in the late stage, both resulting from magmatic-tectonic-hydrothermal processes. The sulfur isotopic composition across the Zhengguang gold deposit varies greatly, with $\delta^{34}S$ values dominated by −12.1‰–−1.5‰ (−3.9‰ on average), significantly negatively deviating from meteorite sulfur. This result indicates that the ore-forming minerals originate from deep magmas and the Duobaoshan Formation. The Pb isotope data fall near the mantle growth curve and tend to migrate to the crust (Wu ZY et al., 2006), indicating the characteristics of a mixed crust-mantle source. As indicated by research on fluid inclusions and isotopes, the ore-forming fluids were the mixture of magmatic water and meteoric water (dominant), showed the characteristics of a mixed crude-mantle source, and were low-temperature and low-salinity fluids. As the mineralization proceeded, the ore-forming fluids were continuously mixed with meteoric water, causing the temperature and salinity to decrease, which is the main mechanism for sulfide precipitation (Che HW, 2016). In summary, the ore-forming fluids of the Zhengguang epithermal gold deposit were dominated by meteoric water, the ore-forming materials were mainly sourced from deep magmas and the Duobaoshan Formation, and mineralization occurred during the Middle Triassic (Fig. 17).

5.3.3. Constraints of the composite action of the Mesozoic multi-stage tectonic systems on regional polymetallic mineralization

The Early-Middle Jurassic magmatism (178 –168 Ma) in the Duobaoshan area occurred in the same epoch as the

magmatic discontinuity (175–165 Ma) in the northeast of the Amurian Plate (Eerguna Block; Tsui WSR, 2018). The magmatic discontinuity was formed by the continent-continent collision between the Siberian and Amurian plates. This view has been verified by the formation of the pre-collision continental arc-related porphyry copper deposit (Wunugetu Mountain: 181–177 Ma; Chen ZG et al., 2011; Wang YH et al., 2015; Zhang FF et al., 2015) and the post-collision-related epithermal silver-lead-zircon deposit (Jiawula; Dai M et al., 2017; Niu SD et al., 2017). During the Early-Middle Jurassic, Northeast China might have experienced the superposition of the subduction and compression of the Paleo-Pacific Ocean in addition to the collision between the Siberian and Amurian plates. As indicated by the granodiorite-tonalite assemblages aged 178 –168 Ma in the study area and their geochemical characteristics, the Duobaoshan area was in a continental arc setting during the Early-Middle Jurassic and accreted to the Eurasian continental margin (170–137 Ma) a little earlier than the Raohe complex (the Nadanhada accretionary terrane;

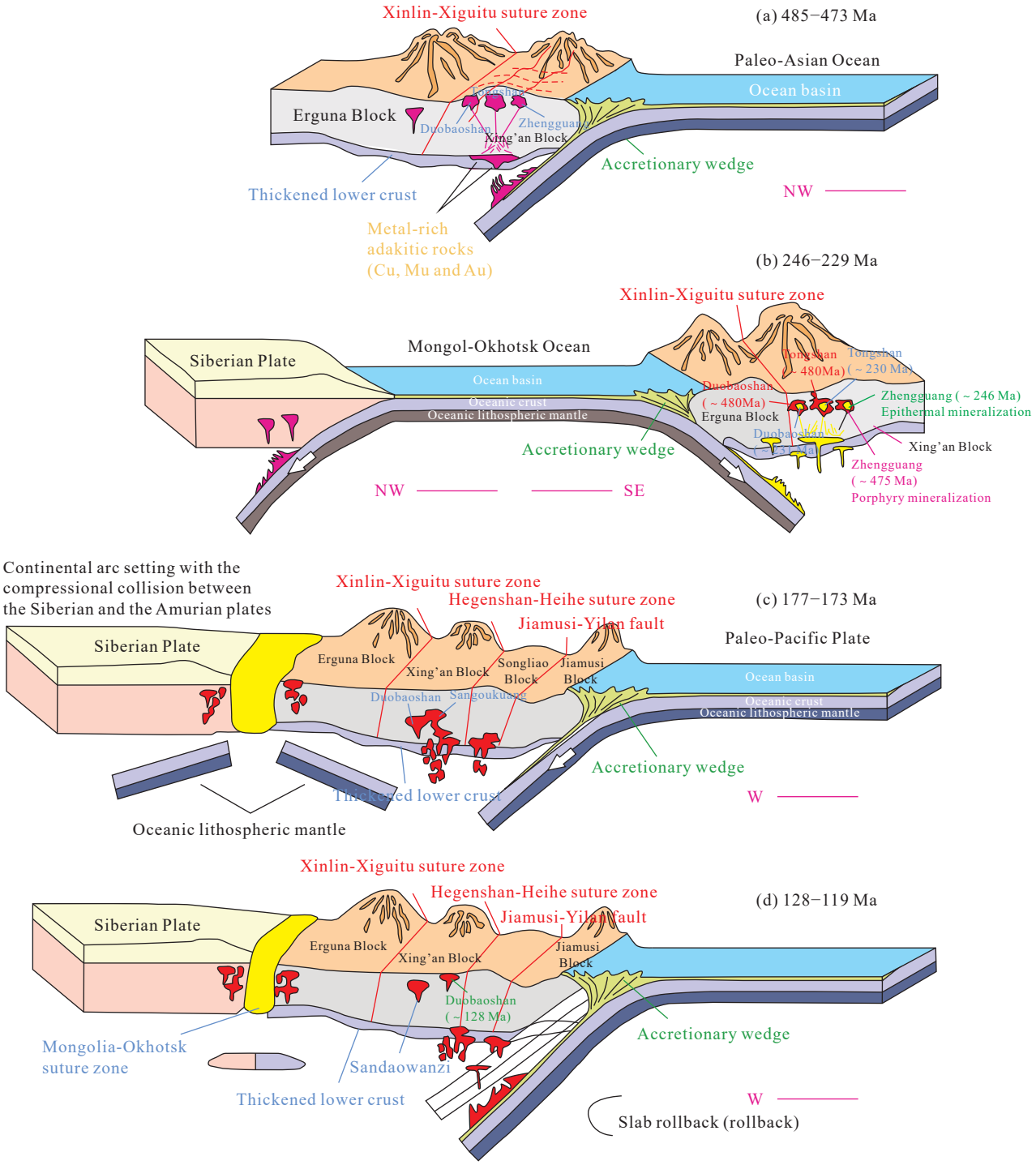

Fig. 17. Schematic diagram of Early Paleozoic–Mesozoic tectonic evolution and mineralization of the Duobaoshan porphyry Cu deposit (after Cai WY, 2020).

Zhou JB et al., 2014). Therefore, the authors of this study hold that the continental arc environment of the compressional collision between the Siberian and Amurian plates created favorable metallogenic conditions for the Duobaoshan area. The compressional collision is similar to the flat-slab subduction or the instantaneous compression caused by the subduction of the aseismic ridge or oceanic island/plateau, except that the stress was from the opposite direction. This led to the skarn mineralization in the Xiaoduobaoshan and Sankuanggou areas. The accretion of the Raohe complex (170–137 Ma) and the Sikhote-Alin terrane (130–123 Ma; Kruk et al., 2014) and the eastward rollback of the subduction front caused the Duobaoshan area to be gradually beyond the influencing reach of the Paleo-Pacific Ocean subduction. This explains the magmatic discontinuity in the Duobaoshan area during the Middle-Late Jurassic (168–152 Ma). During the Late Jurassic, the magmatism in the study area (about 151 Ma) (Li Y et al., 2016b) and the periphery was mainly in the extensional tectonic environment due to the collapse caused by post-collision gravitational instability and/or the long-range back-arc extensional effect of the Paleo-Pacific Ocean subduction. This opinion can be verified by the presence of the porphyry molybdenum deposits (150 –146 Ma) related to the intracontinental extension environment in the Daheishan area (Hu XL et al., 2014). During the Early Cretaceous, magmatism in the study area further weakened and only occurred in the Dubaoshan deposit (128–127 Ma; Cai WY, 2020; She HQ et al., 2012). By contrast, magmatism associated with epithermal gold mineralization (Sandaowanzi: 122–119 Ma; Zhai DG et al., 2015; Yongxin: 119–114 Ma; Yuan MW et al., 2018) was widely developed in the periphery. A-type granites and bimodal magmatism (130–90 Ma) are widely developed in the southeast of the Songnen-Jiamusi block (Sun MD et al., 2018). This finding indicates that Northeast China was in the process of subduction slab rollback of the Paleo-Pacific Ocean during the Early Cretaceous. The slab rollback made the Duobaoshan area to be further away from the continental arc. Moreover, regional magmatism/mineralization was relatively developed and mainly distributed around crustal faults in the Duobaoshan area. For instance, the Yongxin, Sandaowanzi, and Daxingtun deposits mainly occur near the Nenjiang fault. The weak Early Cretaceous magmatism in the Duobaoshan area possibly also because large faults or other inter-arc structures far away from the crust hindered magmas from intruding the surface. The Sankuanggou iron-copper deposit is a typical skarn deposit, where the ore bodies mainly occur near the contact zones between granodiorites and the Duobaoshan Formation. About 3/4 of the ore bodies in the Duobaoshan area are mainly controlled by NW-trending secondary faults or interlayer fracture zones, and the remaining 1/4 are controlled by NE-trending ones. The granodiorite plutons of the Sankuanggou skarn deposit have zircon U-Pb ages of 177–175 Ma (Cai WY, 2020; Ge WC et al., 2007; Chu SX et al., 2012; Hao YJ et al., 2015; Deng K et al., 2018), which is slightly older than the Re-Os metallogenic age of molybdenites (174 –173 Ma) revealed by previous studies (Hao YJ et al., 2015; Chu SX et al., 2019). Therefore, the Sankuanggou deposit is the product of the same tectonic-magmatic-hydrothermal processes during the Early Jurassic. The sulfur isotopic composition of the Sankuanggou skarn iron-copper deposit varies greatly but generally shows a tower-like distribution pattern. This result indicates relatively uniform sulfur sources overall and that the sulfur mostly originated from deep magmas, with a very small part possibly derived from strata. The results of the Pb isotope analysis indicate that the ore-forming materials mainly originated from a mixed crust-mantle source, which can be also verified by the high Re content in molybdenites (Hao YJ, 2015; Chu SX et al., 2019). Detailed studies of the lithography and micro thermography of fluid inclusions show that the ore-forming fluids of the Sankuanggou iron-copper deposit were a high-temperature and high-salinity fluid system. In the early mineralization stage, magmatic-hydrothermal fluids reacted strongly with the surrounding rocks, forming massive metallic minerals, such as skarn minerals, magnetites, and hematites. In the quartz-sulfide mineralization stage, the decline in the temperature and salinity of ore-forming fluids, together with the meteoric water mixing, induced the boiling or immiscibility of ore-forming fluids, which led to massive chalcopyrite precipitation (Lu HZ et al., 2004; Chen YJ et al., 2007; Li N et al., 2007; Wang Y et al., 2009).

5.4. Prospecting models

As indicated by the detailed analysis of the Duobaoshan porphyry Cu deposit and the understanding of the ore-controlling geological factors, ore-bearing conditions, and mineralization of the Duobaoshan mining area mentioned above, as well as previous exploration results and the discovery of ore bodies (Zhao YY et al., 1997; Wei H, 2014), favorable metallogenic conditions in the study area are as follows: (1) In terms of strata, the Duobaoshan Formation is composed of andesites and tuffs interbedded with purple sandstones, glutenites, and a small number of impure carbonate rocks. As summarized above, the ore-hosting horizons and material sources of the deposits or ore occurrences developing in the NW-trending arcuate tectonic belt of the Duobaoshan ore field are basically all related to the Middle Ordovician Duobaoshan Formation. For the Duobaoshan porphyry Cu deposit, the Duobaoshan Formation also serves as the pathway for the ore-forming hydrothermal fluids and caprocks; (2) in terms of magmatic rocks, the magmatism in the Duobaoshan ore field had long been unstable, triggering deep magmas repeatedly, and exhibited inherited activities along the NW-trending tectonic belt. Both Early Caledonian extrusive rocks and Late Hercynian and Yanshanian intrusions occur in the ore field. Almost every magmatic cycle reflects the evolution process from intermediate rocks to intermediate-acid rocks and then to acid rocks. The Duobaoshan, Sankuanggou, and Zhengguang deposits are all related to the magmatic-hydrothermal fluids to some extent. Therefore, large-scale dense granitic plutons, stocks, intermediate-mafic veins, and other strongly active small plutons are all favorable ore-bearing zones. The volcanic rock zone with intense tectonism also has the potential for mineralization; (3) in terms of tectonic setting, the Duobaoshan porphyry Cu-Au-Mo-Ag deposit is located in

a continental-margin island arc environment related to subduction and in the secondary structures of deep-rooted faults. Concerning deposit distribution, the deposits are strictly controlled by the NW-trending arcuate tectonic belt, and especially, the parts with superimposed multiple sets of structures are more favorable to mineralization. Therefore, much attention should be paid to zones where Caledonian, Hercynian, and Yanshanian structures are superimposed, such as the zone with superimposed NW-trending structures (including the curved turning parts), the Late Hercynian schistosity zone, and the intersection of NE- and NW-trending tectonic belts; (4) in terms of surrounding rock alteration, typical alterations related to mineralization occur in all the deposits in the Duobaoshan ore field, such as the skarnization in the Sankuanggou iron-copper deposit, the sericite and sericitolite alterations in the Duobaoshan and Tongshan deposits, and the silicification and sericite alteration of the Zhengguang gold deposit. These alterations can be regarded as indicators of the mineralization of the Duobaoshan ore field. In addition, enough attention should also be paid to other extensive surrounding rock alterations, such as potassic and epidote alterations; (5) in terms of geophysics and geochemistry, major prospecting indicators in the geophysical and geochemical exploration contour maps mainly include parts with a local reduction in the positive anomalies of ΔT magnetic field, ΔTd positive magnetic field area, parts with a local reduction in the positive Bouguer gravity anomalies, parts with distortion of the Bouguer gravity anomaly contours, local negative anomaly zones of residual positive gravity anomalies, and the concentration centers of geochemical anomalies of elements Cu, Au, and Sb. They are almost all located in the NW-trending arcuate tectonic belt. Since the Cu and Mo background values are generally high in the Duobaoshan ore field, Cu and Mo are also possibly enriched outside the arcuate tectonic belt. On this basis, the quantitative prospecting model of the Duobaoshan ore field is summarized as follows (Fig. 18).

Regional geological prospecting indicators (x_1, x_2) (Table 10): Deposits in the ore field lie on the east side of the Nenjiang deep-rooted fault (x_1), which has important controlling effects on the formation of deposits. The NE-trending tectonic line of the Da Hinggan Mountains is nearly orthogonal to the NW-trending tectonic line of the ore field. Such a tectonic line pattern forms the NW-trending arcuate metallogenic tectonic belt (x_2). Ore field-scale geological prospecting indicators (x_3, x_4, x_5): The ore body tops are mostly located in the first member of the Duobaoshan Formation (x_3), which serves as a shielding layer and is a metallogenic formation indicator. The homologous gas-liquid activities after the formation of granodiorite porphyries formed deposits. Therefore, porphyry plutons (x_4) are the magmatic rock-related prospecting indicators. The Duobaoshan deposit is located at the intersection of the NW-trending arcuate tectonic belt and the NE-trending fault (x_5). Deposit-scale geological prospecting indicators (x6, x7, x8, x9, x10, x11): The main ore zone is located on the hanging wall of the porphyry plutons (x_6), and the ore bodies are 0 –500 m away from the porphyry plutons. The optimal

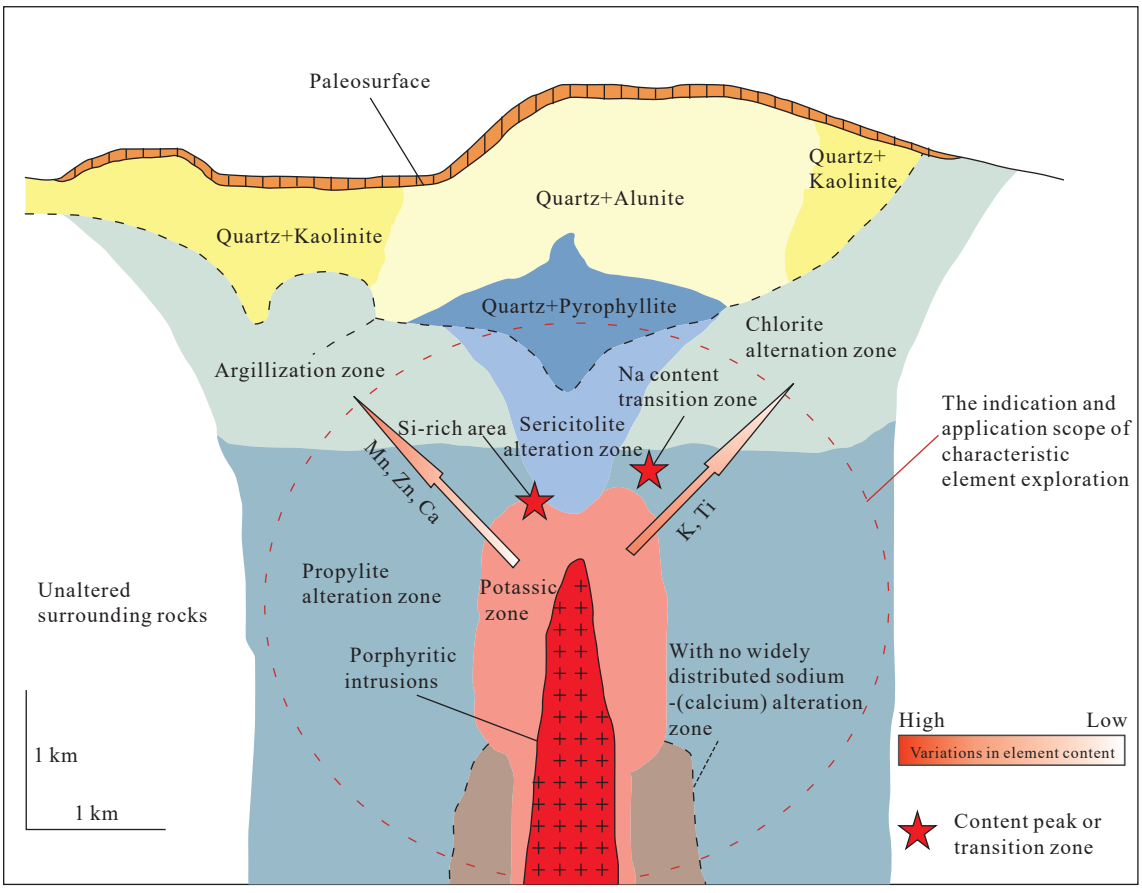

Fig. 18. Prospecting model of the Duobaoshan porphyry Cu deposit (after Zhao YY et al., 1997).

mineralization position is at the distance of 50−150 m from the porphyry plutons (x_7), with subzones of porphyry, chalcopyrite, pyrite, and sphalerite spreading in turn from the center of the ore belt outwards (x_8). The surrounding rock alterations are distributed in an elliptical pattern and consist of the quartz core, the potassic alteration and silicification zone, the sericitolite alteration zone (major occurring part of orebodies), and the propylite alteration zone from the porphyry plutons outwards (x_9). The major mineralization stages of the deposits include the mineralization stages of quartz, carbonate-chalcopyrite, bornite, molybdenite, and pyrite after the magmatic gas-liquid stage (x_{10}). Moreover, the deposits have a multi-stage transformation - homologous hydrothermal mineralization model (x_{11}).

Regional geophysical prospecting indicators (x_{12}, x_{13}, x_{14}) (Table 10): The Duobaoshan ore field is located at the intersection of the gentle slope, gentle uplift, and gentle depression zones and lies in the part where the nose-shaped bulging part of the gentle uplift plunges toward the gentle depression (x_{12}). The 1∶1000000 aeromagnetic ΔT contour plan shows that the ore field is located in the NE-extending positive field with a strength of 100–200 nT (x_{13}). The 1∶1000000 Bouguer gravity anomaly map shows that the ore field is located at the parts with distortion of the NE-trending Bouguer gravity anomaly contours, with field strength greater than 10×10^{-5} m/s^2 (x_{14}). Ore field-scale geophysical prospecting indicators of the (x_{15}, x_{16}, x_{17}): The known deposits are located in a complex field area (x_{15}). The areal induced-polarization (IP) anomaly results indicate that more than 5% of IP anomalies exist near the known deposits (x_{16}). The 1∶200000 Bouguer gravity map shows that the known deposits lie in a NW-trending gradient zone (x_{17}). Deposit-scale geophysical prospecting indicators (x_{18}, x_{19}, x_{20}): The ore bodies fall in or near the local anomalies with a strength greater than 50 nT (x_{18}). The high-precision magnetic survey anomalies correspond well to the ore bodies (x_{19}). The exposed No. 3 ore belt shows significant IP anomalies, and the concealed No. 4 orebody exhibits significant apparent polarizability anomalies (x_{20}).

Regional geochemical prospecting indicators (x_{21}, x_{22}) (Table 10): The 1∶1000000 stream sediment geochemical map shows that the Duobaoshan ore field is located at the intersection of the NE-trending Fe, Ni, Co, Ti, Cr, and V anomaly zone and the NW-trending Fe, Ni, and Co anomaly zone (x_{21}), at the intersection of NE-, NW-, and SN-trending high background value zones of Cu, and in the high background value zones of Mo, Au, Ag, As, and Sb (x_{22}). Ore-field-scale geochemical prospecting indicators (x_{23}, x_{24}, x_{25}): The deposits in the Duobaoshan ore field lie in the high background value zones of Cu, Mo, Au, Ag, and Zn (x_{23}). They are also distributed in the high background value zones surrounded by low background value zones (x_{24}). The deposits have a large comprehensive anomaly area, and their element associations are dominated by Cu, Mo, Au, and Ag (x_{25}). Deposit-scale geochemical prospecting indicators (x_{26}, x_{27}, x_{28}): The horizontal zoning of elements in the deposits (from inside to outside) is from Cu, Mo, Au, Ag, Bi, W, K_2O, and Na_2O to Pb, Zn, As, and Sb (x_{26}). Sb is a remote indicator element, Ag and As are the near-deposit indicator elements, Cu, Zn, Pb, Au, and Mo are the indicator elements of ore bodies, and Bi and W are the indicator elements of ore body tails (x_{27}). Indicators for the denudation depth of ore bodies: ore body front: Sb > 3.0, AS > 25.0, Na_2O > 4.0, Sb/Bi > 10, As/W > 40.0, Sb × 10^4/Cu > 300.0, Pb × 10^3/Cu > 7.0, Zn/Mo > 25.0, Pb/Mo > 3.0, (As+Sb) × 10^3/Cu > 290.0, (Pb+Zn+Mn)/(Au+A g) > 18.0; ore body head: Pb > 10.0; ore body center: K_2O/Na_2O > 2.4, Cu/W > 550; ore body tail: K_2O > 5.0, Bi > 4.0, W > 40.0, W/Ag > 90.0, (W+B i) × 10^2/(As+Sb) > 900.0, (W+Mo)/(Au+Ag) > 7.0 (x_{28}). In summary, according to the different understandings of various prospecting stages, different prospecting models have been proposed as follows.

6. Conclusions

(i) Multiple adjacent deposits in the Duobaoshan area, which were previously thought to be independent, are actually supergiant porphyry Cu-Au-Mo-Ag deposits. They have proven resources of Cu, Mo, Au, and Ag of 2.28×10^6 t, 80×10^3 t, 73 t, and 1046 t, respectively, ranking first among the copper deposits in China and 33rd in terms of reserves.

(ii) The Duobaoshan porphyry Cu-Au-Mo-Ag deposit exhibits multi-stage mineralization featuring long-term evolution, complex internal structures, and strong superposition of various metal elements. This deposit was formed by the superposition of Caledonian, Indosinian, and Late Yanshanian tectonic movements. Moreover, deep porphyry mineralization occurred in the early stage, and dominant epithermal mineralization occurred in the late stage. Therefore, the Duobaoshan deposit is the product of magmatic-tectonic-hydrothermal processes.

(iii) The ore-forming fluids of the Duobaoshan copper-gold-molybdenum-sliver deposit were initially sourced from magmatic water and then from the mixture of meteoric water and magmatic water at the late mineralization stage. The ore-forming fluids experienced three stages. The ore-forming fluids of stage I had a fluid type of H_2O-CO_2-NaCl, an ore-forming temperature of 375–650°C, and ore-forming pressure of 110–160 MPa. The ore-forming fluids of stage II had a fluid type of H_2O-CO_2-NaCl, an ore-forming temperature of 310–350°C, and ore-forming pressure of 58–80 MPa. The ore-forming fluids of stage III had a fluid type of NaCl-H_2O, an ore-forming temperature of 210–290°C, and ore-forming pressure of 5–12 MPa. The Cu-Au-Mo-Ag mineralization mainly occurred at stages I and II, with the ore-forming materials having a mixed crust-mantle source.

Table 10. Prospecting models of the Duobaoshan porphyry Cu deposit (after Zhao YY et al., 1997).

Regional prospecting model A	A = A' (x_1, x_2, x_{12}, x_{13}, x_{14}, x_{21}, x_{22})
Ore-field-scale prospecting model B	B = B' (x_3, x_4, x_5, x_{15}, x_{16}, x_{17}, x_{23}, x_{24}, x_{25})
Deposit-scale prospecting model C	C = C' (x_6, x_7, x_8, x_9, x_{10}, x_{11}, x_{18}, x_{19}, x_{20}, x_{26}, x_{27}, x_{28})
Integrated prospecting model M	M = F (A, B, C)

(iv) The Duobaoshan porphyry Cu-Au-Mo-Ag deposit lies in an area sandwiched by the Siberian, North China, and paleo-Pacific plates. It was formed in an island arc tectonic setting and was controlled by the NW-trending arcuate tectonic belt. The ore bodies are primarily distributed at the intersection of multiple sets of structures. This deposit experienced a long-term evolution from the Caledonian to the Yanshanian, during which frequent tectonic and magmatic processes gave birth to the Sankuanggou-Duobaoshan-Zhengguang polymetallic metallogenic belt. This deposit features multi-stage superimposed mineralization.

(v) The Duobaoshan porphyry Cu-Au-Mo-Ag deposit was formed in the initial subduction environment of the Paleo-Asian Ocean plate during the Early Ordovician. It was affected by the closure of the Mongol-Okhotsk Ocean during the Triassic-Jurassic and was superimposed by the Paleo-Pacific Ocean subduction and compression during the Jurassic-Cretaceous. The mineralization includes the Caledonian porphyry Cu-Mo-(Au) mineralization, the Indosinian porphyry-epithermal Au-Cu mineralization, and the Yanshanian hydrothermal-skarn Au-Cu-Fe-Pb-Zn mineralization in sequence.

(vi) Major prospecting models of the Duobaoshan copper-gold-molybdenum-sliver deposit include the rock assemblages of andesites and tuffs interbedded with purple sandstones, glutenites, and a small number of impure carbonate rocks in the Duobaoshan Formation; volcanic rock zones with intense multi-stage tectonism; zones with superimposed Caledonian, Hercynian, and Yanshanian structures; surrounding rock alterations, such as skarnization, sericite alteration, sericitolite alteration, silicification, potassic alteration, and epidote alteration; parts with a local reduction in the positive anomalies of the ΔT magnetic field, ΔTd positive magnetic field area, parts with local reduction in the positive anomalies of Bouguer gravity, parts with distortion of the Bouguer gravity anomaly contours, local negative anomaly zones of residual positive gravity anomalies, and the concentration centers of geochemical anomalies of elements Cu, Au, and Sb.

CRediT authorship contribution statement

Sen Zhang designed the conceptualization, presented the idea, and wrote the manuscript with input from all authors. Nan Ju contributed to the investigation, data curation, and visualization. Guo-bin Zhang carried out the sample preparation and formal analysis. Bao-shan Liu supervised the findings of this work. All authors discussed the results and contributed to the final manuscript.

Declaration of competing interest

The authors declare no conflicts of interest.

Acknowledgment

The author would like to extend their sincere gratitude to Researcher De-ming Sha for proofreading this paper and putting forward valuable suggestions and to Researcher Zi-guo Hao for advising them to prepare this paper and offering precious comments for revision. This study was jointly funded by the National Scientific and Technological Basic Resources Investigation Program (2022FY101800), a project of the National Natural Science Foundation of China (42102087), a project of the China Postdoctoral Science Foundation (2022M712966), and a major project of the Ministry of Science and Technology of the People's Republic of China (2021QZKK0304).

References

Bai LA. 2013. Study on Metallogenic Mechanism and Resource Forecast of Hydrothermal Cu Deposits in the Central and North of the Great Xing'an Range, NE China. Changchun, Jilin University, Ph. D thesis, 1–132 (in Chinese with English abstract).

Bai LA, Sun JG, Zhang Y, Han SJ, Yang FC, Men LJ, Gu AL, Zhao KQ. 2012. Genetic type, mineralization epoch and geodynamical setting of endogenous copper deposits in the Great Xing'an Range. Acta Petrologica Sinica, 28(02), 468–482 (in Chinese with English abstract).

Cai WY. 2020. Metallogenesis of Copper-molybdenum-gold Polymetallic in the Duobaoshan Orefield, Heilongjiang Province. Changchun, Jilin University, Ph. D thesis, 1–223 (in Chinese with English abstract).

Chaussidon M, Lorand JP. 1990. Sulphur isotope composition of orogenic spinel lherzolite massifs from Ariege (North-Eastern Pyrenees, France): An ion microprobe study. Geochimicaet Cosmochimica Acta, 54, 2835–2846. doi: 10.1016/0016-7037(90)90018-G.

Che HW. 2016. Study on Geological Features and Ore-forming Mechanisms of the Zhengguang Au Deposit in Northern Great Xing'an Range. Beijing, China University of Geosciences (Beijing), Master thesis, 1–77 (in Chinese with English abstract).

Che HW, Zhou ZH, Ma XH, Ouyang HG, Liu J. 2015. Geochemical characteristics, zircons U-Pb ages and Hf isotopic composition of the dacite porphyry from Zhengguang Au deposit in Northern Great Xing'an Range. Acta Geologica Sinica, 89(8), 1417–1436 (in Chinese with English abstract).

Chen YJ, NI P, Fan HR, Pirajno F, Lai Y, Su WC, Zhang H. 2007. Diagnostic fluid inclusions of different types hydrothermal gold deposits. Acta Petrologica Sinica, 23(9), 2085–2108 (in Chinese with English abstract). doi: 10.3321/j.issn:1000-4734.2007.z1.080.

Chen ZG, Zhang LC, Wan B, Wu HY, Cleven N. 2011. Geochronology and geochemistry of the Wunugetushan porphyry Cu-Mo deposit in NE China, and their geological significance. Ore Geology Reviews, 43, 92–105. doi: 10.1016/j.oregeorev.2011.08.007.

Chu SX, Liu JM, Xu JH, Wei H, Chai H, Tong KY. 2012. Zircon U-Pb dating, petrogenesis and tectonic significance of the granodiorite in the Sankuanggou skarn Fe-Cu deposit, Heilongjiang Province. Acta Petrologica Sinica, 28(2), 433–450 (in Chinese with English abstract).

Chu SX, Zeng QD, Liu JM, Wang YB. 2019. Early–Middle Jurassic magmatism and skarn-porphyry mineralization in NE China: Geochronological and geochemical constraints from the Sankuanggou skarn Fe-Cu-(Mo) deposit, and tectonic implications. Journal of Geochemical Exploration, 200, 84–103. doi: 10.1016/j.gexplo.2019.01.013.

Cogné JP, Kravchinsky VA, Halim N, Hankard F. 2005. Late Jurassic–Early Cretaceous closure of the Mongol-Okhotsk Ocean demonstrated by new Mesozoic palaeomagnetic results from the Trans-Ba¨ıkal area (SESiberia). Geophysical Journal of the Royal Astronomical Society, 163(2), 813–832. doi: 10.1111/j.1365-246X.2005.02782.x.

Cooke DR, Hollings P, Walsh JL. 2005. Giant porphyry deposits: Characteristics, distribution, and tectonic controls. Economic Geology, 100, 801–818. doi: 10.2113/100.5.801.

Cui G, Wang JY, Zhang JX, Cui G. 2008. U-Pb SHRIMP dating of zircons from Duobaoshan granodiorite in Heilongjiang and its geological significance. World Geology, 27(4), 387–394 (in Chinese with English abstract). doi: 10.3969/j.issn.1004-5589.2008.04.006.

Dai M, Yan GS, Liu C, Deng JF. 2017. Southward subduction of the Mongolia –Okhotsk Ocean: Insights from Early –Middle Triassic intrusive rocks from the Jiawula–Tsagenbulagen area in NE China. Geological Journal, 55(1), 967–993.

Deng K, Li QG, Chen YJ, Zhang C, Zhu XF, Xu QW. 2018. Geochronology, geochemistry and Sr-Nd-Pb-Hf isotopes of the Early Jurassic granodiorite from the Sankuanggou intrusion, Heilongjiang Province, Northeastern China: Petrogenesis and geodynamic implications. Lithos, 296, 113–128. doi: 10.1016/j.lithos.2017.10.016.

Du Q. 1980. Alteration and mineralization characteristics of Duobaoshan porphyry copper deposit. Acta Geologica Sinica, 59(4), 310–323 (in Chinese with English abstract).

Du Q, Zhao YM, Lu BG. 1988. Duobaoshan Porphyry Cu (Mo) Deposit. Beijing, Geological Publishing House, 1–344 (in Chinese).

Fan SW. 2020. Characteristics and Genesis of Sb-Au Mineralization in Zhuanghuhe Area, Heihe County, Heilongjiang Province. Changchun, Jilin University, Master thesis, 1 –68 (in Chinese with English abstract).

Feng JX. 2008. Distribution character of sulfur isotope in the Duobaoshan copper deposit. Geology and Exploration, 44(1), 46–49 (in Chinese with English abstract).

Gao RZ, Xue CJ, Lü XB, Zhao XB, Yang YS, Li CC. 2017. Genesis of the Zhengguang gold deposit in the Duobaoshan ore field, Heilongjiang Province, NE China: Constraints from geology, geochronology and S-Pb isotopic compositions. Ore Geology Reviews, 84, 202–217. doi: 10.1016/j.oregeorev.2016.12.031.

Ge WC, Wu FY, Zhou CY, Zhang JH. 2007a. Metallogenic age and geodynamic significance of porphyry Cu, Mo deposits in the eastern segment of Xingmeng orogenic belt. Chinese Science Bulletin, 52(20), 2407–2417 (in Chinese with English abstract). doi: 10.3321/j.issn:0023-074x.2007.20.012.

Ge WC, Wu FY, Zhou C, Zhang JH. 2007b. Porphyry Cu-Mo deposits in the eastern Xing'an-Mongolian Orogenic Belt: Mineralization ages and their geodynamic implications. Chinese Science Bulletin, 52(24), 3416–3427. doi: 10.1007/s11434-007-0466-8.

Han ZX, Xu YQ, Zheng QD. 2004. Metallogenic series and evolution of important metallic and non-metallic minerals in Heilongjiang Province. Harbin, Heilongjiang Provincial People 's Publishing House, 1–241 (in Chinese).

Hao YJ. 2015. Mineralization and Metallogenic Regularity of Duobaoshan Ore Concentration Area in Heilongjiang Province, Northeast China. Changchun, Jilin University, Ph. D thesis, 1 –199 (in Chinese with English abstract).

Hao YJ, Ren YS, Duan MX, Tong KY, Chen C, Li C. 2014. Re-Os isotopic dating of the molybdenite from the Tongshan porphyry Cu-Mo deposit in Heilongjiang Province, NE China. Acta Geologica Sinica (English Edition), 88, 522–523. doi: 10.1111/1755-6724.12374_14.

Hao YJ, Ren YS, Duan MX, Tong KY, Chen C, Yang C, Li C. 2015. Metallogenic events and tectonic setting of the Duobaoshan ore field in Heilongjiang Province, NE China. Journal of Asian Earth Sciences, 97, 442–458. doi: 10.1016/j.jseaes.2014.08.007.

Hao YJ, Ren YS, Duan MX, Zhao X, Yang Q, Tong KY, Li C. 2016. Mineralization time and tectonic setting of the Zhengguang Au deposit in the Duobaoshan ore field, Heilongjiang Province, NE China. Arabian Journal of Geosciences, 9(15), 1–20. doi: 10.1007/s12517-016-2666-5.

Hao YJ, Ren YS, Duan MX, Zhao HL, Tong KY, Sun ZM. 2017. Tectonic setting of Triassic magmatic and metallogenic event in the Duobaoshan mineralization area of Heilongjiang Province, NE China. Geological Journal, 52(1), 67–91. doi: 10.1002/gj.2732.

Heilongjiang Bureau of Geology and Mineral Resources, 1993. Regional Geology of Heilongjiang Province. Beijing, Geological Publishing House, 1–734 (in Chinese).

Hu XL, Yao SZ, Ding ZJ, He MC. 2017. Early Paleozoic magmatism and metallogeny in Northeast China: A record from the Tongshan porphyry Cu deposit. Mineralium Deposita, 52(1), 85–103. doi: 10.1007/s00126-016-0653-0.

Hu XL, Yao SZ, He MC, Ding ZJ, Chen B. 2014. Geochemistry, U-Pb geochronology and Hf isotope studies of the Daheishan porphyry Mo deposit in Heilongjiang Province, NE China. Resource Geology, 64(2), 102–116. doi: 10.1111/rge.12031.

Kravchinsky VA, Cogné JP, Harbert WP, Kuzmin, MI. 2002. Evolution of the Mongol –Okhotsk Ocean as constrained by new palaeomagnetic data from the Mongol–Okhotsk suture zone, Siberia. Geophysical Journal of the Royal Astronomical Society, 148, 34–57. doi: 10.1046/j.1365-246x.2002.01557.x.

Kruk NN, Simanenko VP, Gvozdev VI, Golozubov VV, Kovach VP, Serov PI, Kholodnov VV, Moskalenko EY, Kuibida ML. 2014. Early Cretaceous granitoids of the Samarkaterrane (Sikhote-Alin '): Geochemistry and sources of melts. Russian Geology and Geophysics, 55(2), 216–236. doi: 10.1016/j.rgg.2014.01.007.

Li DR, Lü FL, Liu SY, Lü J. 2011. Geological features and prospecting orientation of the Sankuanggou Cu-Mo-Au deposit in Nenjiang County, Heilongjiang Province. Geology in China, 38(2), 415–426 (in Chinese with English abstract). doi: 10.3969/j.issn.1000-3657.2011.02.016.

Li DR, Zhu CL, Lu J, Cui G. 2010. Structural-magmatic mineralization of Sankuanggou-Duobaoshan metallogenic belt, Heilongjiang. China Mining Magazine, 19(S1), 142–146 (in Chinese with English abstract).

Li N, Chen YJ, Zhang H, Zhao TP, Deng XH, Wang Y, Ni ZY. 2007. Molybdenum deposits in East Qinling. Earth Science Frontiers, (5), 186–198 (in Chinese with English abstract).

Li XY, Gao QZ, Song H, Song H, Chi GX, Lai CK. 2019. Discriminating ore fertile and barren granites using zircon Ce and Eu anomalies–Perspective from late Mesozoic (Yanshanian) granites in South China. Ore Geology Reviews, 113, 103105. doi: 10.1016/j.oregeorev.2019.103105.

Li Y. 2016. The Study of The Main Rock and Typical Deposits in The North of Duobaoshan District, Heilongjiang Provice. Beijing, China University of Geosciences (Beijing), Master thesis, 1 –104 (in Chinese with English abstract).

Li Y, Zeng H, Qiao ZJ, Wang ZD, Zhao YY, Fu JJ, Chen L, Yang B. 2016a. Ore characteristics of the Sankuanggou iron copper ore deposit in Nenjiang County, Heilongjiang Province, and their significance. Acta Petrologicaet Mineralogica, 35(1), 97–110 (in Chinese with English abstract). doi: 10.3969/j.issn.1000-6524.2016.01.007.

Li Y, Fu JJ, Zhao YY, Zeng H. 2016b. Chronological characteristics and metallogenic significance of Zhengguang gold deposit, Heilongjiang Province, China. Acta Geologica Sinica, 90(1), 151–162 (in Chinese with English abstract). doi: 10.3969/j.issn.0001-5717.2016.01.010.

Li Y, Xu WL, Tang J, Pei FP, Wang F, Sun CY. 2018. Geochronology and geochemistry of Mesozoic intrusive rocks in the Xing'an Massif of NE China: Implications for the evolution and spatial extent of the Mongol –Okhotsk tectonic regime. Lithos, 304, 57–73. doi: 10.1016/j.lithos.2018.02.001.

Li Y, Xu WL, Wang F, Tang J, Sun CY, Wang ZJ. 2017. Early–Middle Ordovician volcanism along the eastern margin of the Xing 'an Massif, Northeast China: Constraints on the suture location between the Xing 'an and Songnen –Zhangguangcai Range massifs. International Geology Review, 60(16), 2046–2062. doi: 10.1080/00206814.2017.1402378.

Li ZT, Wang XJ, Wang HB, Wu G. 2008. Geology of the Sankuanggou gold-bearing iron-copper deposit in. Geology and Resources, 17(3), 170–174 (in Chinese with English abstract). doi: 10.3969/j.issn.1671-

1947.2008.03.003.

Liu J, Li Y, Zhou ZH, OuYang HG. 2017. The Ordovician igneous rocks with high Sr/Y at the Tongshan porphyry copper deposit, satellite of the Duobaoshan deposit, and their metallogenic role. Ore Geology Reviews, 86, 600–614. doi: 10.1016/j.oregeorev.2017.02.036.

Liu J, Wu G, Li Y, Zhu MT, Zhong W. 2012. Re –Os sulfide (chalcopyrite, pyrite and molybdenite) systematics and fluid inclusion study of the Duobaoshan porphyry Cu (Mo) deposit, Heilongjiang Province, China. Journal of Asian Earth Sciences, 49, 300–312. doi: 10.1016/j.jseaes.2011.10.014.

Liu J, Wu G, Zhong W, Zhu MT. 2010. Fluid inclusion study of the Duobaoshan porphyry Cu(Mo) deposit, Heilongjiang Province. Acta Petrologica Sinica, 26(5), 1450–1464 (in Chinese with English abstract).

Liu J, Zhou ZH, He ZF, Ouyang HG. 2015. Zircon U-Pb dating and geochemistry of ore-bearing tonalite in Tongshan copper deposit, Heilongjiang Province. Mineral Deposits, 34(2), 289–308 (in Chinese with English abstract). doi: 10.16111/j.0258-7106.2015.02.006.

Lu HZ, Fan HR, Ni P, Ou GX, Shen K, Zhang WH. 2004. Fluid Inclusions. Beijing, Science Press, 1–487 (in Chinese).

Lü PR, LI DR, Peng YW, Zhang MY. 2012. S-Pb isotopic characteristics of ore sulfides and U-Pb dating of zircon from the Sankuanggou skarn-type Cu-Fe-Mo deposit in Heilongjiang Province. Geology in China, 39(3), 717–728 (in Chinese with English abstract). doi: 10.3969/j.issn.1000-3657.2012.03.013.

Ma DY. 1984. Isotopic geological characteristics of Duobaoshan Copper deposit. Mineral Deposits, 3(1), 47–57 (in Chinese with English abstract).

Mao JW, Zhang ZC, Zhang ZH. 1999. Re-Os isotopic dating of molybdenites in the Xiaoliugou W(Mo) deposit in the northern Qilian mountains and its geological significance. Geochimicaet Cosmochimica Acta, 63(11 –12), 1815 –1818. doi: 10.1111/1755-6724.12378_42.

Niu SD, Li SR, Huizenga JM, Santosh M, Zhang DH, Zeng YJ, Li ZD, Zhao WB. 2017. Zircon U-Pb geochronology and geochemistry of the intrusions associated with the Jiawula Ag-Pb-Zn deposit in the Great Xing 'an Range, NE China and their implications for mineralization. Ore Geology Reviews, 86, 35–54. doi: 10.1016/j.oregeorev.2017.02.007.

Pass HE, Cooke DR, Davidson G, Mass R, Dipple G, Rees C, Ferreira L, Taylor C, Deyell C. 2014. Isotope geochemistry of the Northeast Zone, Mount Polley alkalic Cu-Au-Ag porphyry deposit, British Columbia: A case for carbonate assimilation. Economic Geology, 109, 859–890. doi: 10.2113/econgeo.109.4.859.

Richards JP. 2003. Tectono-magmatic precursors for porphyry Cu–(Mo–Au) deposit formation. Economic Geology, 98, 1515–1533. doi: 10.2113/98.8.1515.

She HQ, Li JW, Xiang AP, Guan JD, Yang YC, Zhang DQ, Tan G, Zhang B. 2012. U-Pb ages of the zircons from primary rocks in middle-northern Daxinganling and its implications to geotectonic evolution. Acta Petrologica Sinica, 28(2), 571–594 (in Chinese with English abstract).

Sillitoe RH. 2010. Porphyry copper systems. Economic Geology 105, 3–41. doi: 10.2113/gsecongeo.105.1.3.

Song GX, Cook NJ, Wang L, Qin KZ, Ciobanu CL, Li GM. 2019. Gold behavior in intermediate sulfidation epithermal systems: A case study from the Zhengguang gold deposit, Heilongjiang Province, NE China. Ore Geology Reviews, 106, 446–462. doi: 10.1016/j.oregeorev.2019.02.001.

Song GX, Qin KZ, Wang L, Guo JH, Li ZZ, Tong KY, Zou XY, Li GM. 2015. Type, zircon U-Pb age and Paleo-volcano edifice of Zhengguang gold deposit in Duobaoshan orefield in Heilongjiang Province, NE-China. Acta Petrologica Sinica, 31(8), 2402–2416 (in Chinese with English abstract).

Sun MD, Chen HL, Milan LA. 2018. Continental arc and back-arc migration in Eastern NE China: New constraints on Cretaceous Paleo-Pacific subduction and rollback. tectonics, 37(10), 3893–3915. doi: 10.1029/2018TC005170.

Tan CY, Wang GH, Li YS. 2010. New progress and significance on the mineral exploration in Duobaoshan mineralization area, Heilongjiang, China. Geological Bulletin of China, 29(Z1), 436–445 (in Chinese with English abstract). doi: 10.3969/j.issn.1671-2552.2010.02.031.

Tang J, Xu WL, Wang F, Zhao S, Li Y. 2015. Geochronology, geochemistry, and deformation history of Late Jurassic –Early Cretaceous intrusive rocks in the Erguna Massif, NE China: Constraints on the late Mesozoic tectonic evolution of the Mongol –Okhotsk suture belt. Tectonophysics, 658, 91–110. doi: 10.1016/j.tecto.2015.07.012.

Tang J, Xu WL, Wang F, Zhao S, Wang W. 2016. Early Mesozoic southward subduction history of the Mongol–Okhotsk oceanic plate: evidence from geochronology and geochemistry of Early Mesozoic intrusive rocks in the Erguna Massif, NE China. Gondwana Research, 31, 218–240. doi: 10.1016/j.gr.2014.12.010.

Tang WH. 2020. Characteristics and Genesis of Copper-Molybdenum Mineralization in Huaduoshan area, Nenjiang County, Heilongjiang Province. Changchun, Jilin University, Master thesis, 1 –87 (in Chinese with English abstract).

Tsui WSR. 2018. Late Permian-early Cretaceous Igneous Events in the Erguna Massif, NE China: Constraints on the Timing of Closure of the Mongol-Okhotsk Ocean. Hong Kong, University of Hong Kong, Master thesis, 1–96.

Wang L, Qin KZ, Song GX, Pang XY, Li ZZ, Zhao C, Jin LY, Zou XY, Li GM. 2018. Volcanic-subvolcanic rocks and tectonic setting of the Zhengguang intermediate sulfidation epithermal Au-Zn deposit, eastern Central Asian Orogenic Belt, NE China. Journal of Asian Earth Sciences, 165, 328–351. doi: 10.1016/j.jseaes.2018.07.023.

Wang XC, Wang XL, Wang Lin, Liu JY, Xia B, Deng J, Xu XM. 2007. Metallogeny and reformation of the Duobaoshan superlarge porphyry copper deposit in Heilongjiang. Chinese Journal of Geology (Scientia Geologica Sinica), 42(1), 124–133 (in Chinese with English abstract).

Wang Y, Chen YJ, MA HW, Xu YL. 2009. Study on ore geology and fluid inclusions of the Tangjiaping Mo deposit, Shangcheng County, Henan Province. Acta Petrologica Sinica, 25(02), 468–480 (in Chinese with English abstract).

Wang YH, Zhao CB, Zhang FF, Liu JJ, Wang JP, Peng RM, Liu B. 2015. SIMS zircon U–Pb and molybdenite Re–Os geochronology, Hf isotope, and whole-rock geochemistry of the Wunugetushan porphyry Cu-Mo deposit and granitoids in NE China and their geological significance. Gondwana Research, 28, 1228–1245. doi: 10.1016/j.gr.2014.10.001.

Wei H. 2014. Fluid Mineralization and Prospect Evaluation of the Duobaoshan Porphyry Cu (Mo) Deposit, Heilongjiang. Beijing, University of Science and Technology Beijing, Ph. D thesis, 1–155 (in Chinese with English abstract).

Wei H, Xu JH, Zeng QD. 2013. Fluid inclusion study on the Duobaoshan porphyry copper deposit, Heilongjiang, China. Mineralogical Magazine, 77(2), 200.

Wei H, Xu JH, Zeng QD, Wang YH, Liu JM, Chu SX. 2011. Fluid evoluton of alteration and mineralization at the Duobaoshan porphyry Cu (Mo) deposit Heilongjiang Province. Acta Petrologica Sinica, 27(05), 1361–1374 (in Chinese with English abstract).

Wu G, Chen YH, Sun FY, Liu J, Wang GR, Xu B. 2015. Geochronology, geochemistry, and Sr–Nd–Hf isotopes of the early Paleozoic igneous rocks in the Duobaoshan area, NE China, and their geological significance. Journal of Asian Earth Sciences, 97, 229–250. doi: 10.1016/j.jseaes.2014.07.031.

Wu G, Liu J, Zhong W, Zhu MG, Mi M, Wan Q. 2009. Fluid inclusion study of the Tongshan porphyry copper deposit, Heilongjiang province, China. Acta Petrologica Sinica, 25(11), 2995–3006 (in Chinese with English abstract).

Wu JR. 2012. Ore Fluids and Stable Isotope Geochemistry of the

Duobaoshan Prophyry Cu Deposit, Heilongjiang Province. Beijing, China University of Geosciences (Beijing), Master thesis, 1–55 (in Chinese with English abstract).

Wu ZY, Sun YC, Wang BQ. 2006. Geology and geochemistry of Zhengguang gold deposit, Heilongjiang Province. Geology and Exploration, 42(1), 38–42 (in Chinese with English abstract). doi: 10.3969/j.issn.0495-5331.2006.01.009.

Xiang AP, Yang YC, Li GT, She HQ, Guan JD, Li JW, Guo ZJ. 2012. Diagenetic and metallogenic ages of Duobaoshan porphyry Cu-Mo deposit in Heilongjiang Province. Mineral Deposits, 31(6), 1237–1248 (in Chinese with English abstract). doi: 10.3969/j.issn.0258-7106.2012.06.009.

Xu WL, Wang F, Pei FP, Meng E, Tang J, Xu MJ, Wang W. 2013. Mesozoic tectonic regimes and regional ore-forming background in NE China: Constraints from spatial and temporal variations of Mesozoic volcanic rockassociations. Acta Petrologica Sinica, 29(02), 339–353 (in Chinese with English abstract).

Yin BC, Ran QC. 1997. Metallogenic tectonic environment of Duobaoshan superlarge copper deposit. Acta Mineralogica Sinica, (2), 220–224 (in Chinese with English abstract).

Yuan MW, Li SR, Li CL, Santosh M, Alam M, Zeng YJ. 2018. Geochemical and isotopic composition of auriferous pyrite from the Yongxin gold deposit, Central Asian Orogenic Belt: Implication for ore genesis. Ore Geology Reviews, 93, 255–267. doi: 10.1016/j.oregeorev.2018.01.002.

Yu JJ, Xu ZG, Xu FS. 1996. Tectonic setting of Ordovician volcanic rocks in Northwestern Xiaoxing'anling, Heilongjiang Province. Acta Geoscientica Sinica, 17(1), 54–64 (in Chinese with English abstract).

Zartman RE, Doe BR. 1981. Plumbotectonics –the model. Tectonophysics, 75, 135–162. doi: 10.1016/0040-1951(81)90213-4.

Zeng QD, Liu JM, Chu SX, Wang YB, Sun Y, Duan XX, Zhou LL, Qu WJ. 2014. Re –Os and U –Pb geochronology of the Duobaoshan porphyry Cu–Mo–(Au) deposit, northeast China, and its geological significance. Journal of Asian Earth Sciences, 79, 895–909. doi: 10.1016/j.jseaes.2013.02.007.

Zhai DG, Liu JJ, Ripley EM, Wang JP. 2015. Geochronological and He–Ar–S isotopic constraints on the origin of the Sandaowanzi gold-telluride deposit, northeastern China. Lithos, 212, 338–352. doi: 10.1016/j.lithos.2014.11.017.

Zhang FF, Wang YH, Liu JJ, Wang JP, Zhao CB, Song ZW. 2015. Origin of the Wunugetushan porphyry Cu –Mo deposit, Inner Mongolia, NE China: Constraints from geology, geochronology, geochemistry, and isotopic compositions. Journal of Asian Earth Sciences, 117, 208–224. doi: 10.1016/j.jseaes.2015.12.018.

Zhao C. 2019. Research on the Mineralogical Characteristics of Metallic Mineral and Mineralization of Longtougou Gold Deposit , Shanyang, Shanxi Province. Beijing, China University of Geosciences (Beijing), Master thesis, 1–48 (in Chinese with English abstract).

Zhao C, Qin KZ, Song GX, Li GM. 2019a. Switch of geodynamic setting from the Paleo-Asian Ocean to the Mongol-Okhotsk Ocean: Evidence from granitoids in the Duobaoshan ore field, Heilongjiang Province, Northeast China. Lithos, 336, 202–220. doi: 10.1016/j.lithos.2019.04.006.

Zhao C, Qin KZ, Song GX, Li GM, Li ZZ. 2019b. Early Palaeozoic high-Mg basalt-andesite suite in the Duobaoshan Porphyry Cu deposit, NE China: Constraints on petrogenesis, mineralization, and tectonic setting. Gondwana Research, 71, 91–116. doi: 10.1016/j.gr.2019.01.015.

Zhao C, Qin KZ, Song GX, Li GM, Li ZZ, Pang XY, Wang L. 2018. Petrogenesis and tectonic setting of ore-related porphyry in the Duobaoshan Cu deposit within the eastern Central Asian Orogenic Belt, Heilongjiang Province, NE China. Journal of Asian Earth Sciences, 165, 352–370. doi: 10.1016/j.jseaes.2018.07.002.

Zhao GJ, Hou YS, Cheng FQ. 2007. Geological characteristics and genisis of Zhengguang gold feposit in Heihe city of Heilongjiang Province. Nonferrous Metals Engineering, 59(3), 91–94 (in Chinese with English abstract). doi: 10.3969/j.issn.2095-1744.2007.03.023.

Zhao HL, Zhu CY, Liu HY, Liu BS. 2012. Zircon Shrimp U-Pb dating and its tectonic implications of the granodiorite in Duobaoshan copper deposit, Heilongjiang Province. Geology and Resources, 21(5), 421–424 (in Chinese with English abstract). doi: 10.3969/j.issn.1671-1947.2012.05.001.

Zhao YM, Bi CS, Zou XQ, Sun YL, Du AD, Zhao YM. 1997. Rhenium-osmium isotopic ages of molybdenite in Duobaoshan and Tongshan large porphyry copper (molybdenum) deposits, Heilongjiang Province. Acta Geoscientica Sinica, 18(1), 61–67 (in Chinese with English abstract).

Zhao YY, Li DC, Cheng ZJ. 1994. Study on surrounding rock alteration characteristics of Anaodaba porphyry Cu-Ag-Snpolymetallic deposit, Inner Mongolia. Jilin Geology, 13(2), 57–62 (in Chinese with English abstract).

Zhao YY, Zhang DQ. 1997. Metallogenic Regularity and Prospective Evaluation of Copper Polymetallic Deposits in Daxing'anling and Its Adjacent Areas. Beijing, Seismological Press, 1–318(in Chinese).

Zhao YY, Zhao GJ. 1995. Geochemical characteristics of rare earth elements and genetic model of Duobaoshan copper deposit in Heilongjiang Province. Jilin Geology, 14(2), 71–78 (in Chinese with English abstract).

Zhou JB, Cao JL, Wilde SA, Cao JL, Zhao G, Zhang JJ. 2014. Paleo-Pacific subduction-accretion: Evidence from Geochemical and U-Pb zircon dating of the Nadanhada accretionary complex, NE China. Tectonics, 33, 2444–2466. doi: 10.1002/2014TC003637.